



Spring 2001

Petrology and Geochemistry of Mafic Lavas near Glacier Peak, North Cascades, Washington

Dylan D. (Dylan Douglas) Taylor
Western Washington University

Follow this and additional works at: <https://cedar.wwu.edu/wwuet>



Part of the [Geology Commons](#)

Recommended Citation

Taylor, Dylan D. (Dylan Douglas), "Petrology and Geochemistry of Mafic Lavas near Glacier Peak, North Cascades, Washington" (2001). *WWU Graduate School Collection*. 815.
<https://cedar.wwu.edu/wwuet/815>

This Masters Thesis is brought to you for free and open access by the WWU Graduate and Undergraduate Scholarship at Western CEDAR. It has been accepted for inclusion in WWU Graduate School Collection by an authorized administrator of Western CEDAR. For more information, please contact westerncedar@wwu.edu.

PETROLOGY AND GEOCHEMISTRY OF MAFIC LAVAS
NEAR GLACIER PEAK, NORTH CASCADES, WASHINGTON

BY
Dylan D. Taylor

Accepted in Partial Completion
Of the Requirements for the Degree
Master of Science

Moheb A. Ghali, Dean of Graduate School

ADVISORY COMMITTEE

Chair, Dr. Susan M. DeBari

Dr. R. Scott Babcock

Dr. Thomas W. Sisson

MASTER'S THESIS

In presenting this thesis in partial fulfillment of the requirements for a master's degree at Western Washington University, I agree that the Library shall make its copies freely available for inspection. I further agree that extensive copying of this thesis is allowable only for scholarly purposes. It is understood, however, that any copying or publication of this thesis for commercial purposes, or for financial gain, shall not be allowed without my written permission.

Signature _____

Date 5-21-01

MASTER'S THESIS

In presenting this thesis in partial fulfillment of the requirements for a master's degree at Western Washington University, I grant to Western Washington University the non-exclusive royalty-free right to archive, reproduce, distribute, and display the thesis in any and all forms, including electronic format, via any digital library mechanisms maintained by WWU.

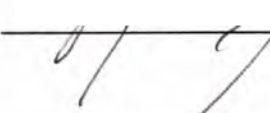
I represent and warrant this is my original work and does not infringe or violate any rights of others. I warrant that I have obtained written permissions from the owner of any third party copyrighted material included in these files.

I acknowledge that I retain ownership rights to the copyright of this work, including but not limited to the right to use all or part of this work in future works, such as articles or books.

Library users are granted permission for individual, research and non-commercial reproduction of this work for educational purposes only. Any further digital posting of this document requires specific permission from the author.

Any copying or publication of this thesis for commercial purposes, or for financial gain, is not allowed without my written permission.

Name: Dylan Taylor

Signature: 

Date: 5-25-2018

PETROLOGY AND GEOCHEMISTRY OF MAFIC
LAVAS NEAR GLACIER PEAK, NORTH CASCADES,
WASHINGTON

A Thesis
Presented to the Faculty of
Western Washington University

In Partial Fulfillment
of the Requirements for the Degree
Master of Science

By
Dylan D. Taylor
May, 2001

ABSTRACT

Major element, trace element, and mineral compositions have been determined for four Quaternary mafic monogenetic cinder cones and flows south of Glacier Peak, a dacitic stratovolcano in the northern Cascade arc. The flows are the Whitechuck basalt, and the basaltic andesites of Indian Pass, Lightning Creek, and Dishpan Gap. Whitechuck has high concentrations of Al_2O_3 (≥ 18 wt.%) and low concentrations of K_2O (≤ 0.45 wt.%) and shares similar trace element characteristics with high alumina olivine tholeiites reported in the central and southern Cascades. The three basaltic andesites are calc-alkaline. Indian Pass and Lightning Creek have primitive compositions, with $\text{Mg}\#$ [$100 \cdot \text{Mg}/(\text{Mg} + \text{Fe}^*)$] > 65 , $\text{Cr} > 200$ ppm, and $\text{Ni} > 100$ ppm. Most samples have olivine in equilibrium with bulk rock compositions. Rb and Sr are relatively low in most flows, especially at Whitechuck and Dishpan Gap. Sr and La decrease with increasing SiO_2 in the Lightning Creek and Dishpan Gap cinder cones, indicating possible mixing with a Sr and La-poor felsic component represented by the most evolved Glacier Peak dacites. Petrographic observations of disequilibrium textures such as xenocrysts, xenoliths, quenched glass inclusions, and strongly-zoned phenocrysts in these two flows also indicate possible melting. All flows are enriched in large ion lithophile elements and light rare earth elements relative to high field strength elements, showing that the mantle beneath Glacier Peak has been fluxed by a hydrous subduction component. Ba/Nb ratios (~ 40 -110) are highest for the three basaltic andesites, indicating that they had the greatest amount of subduction component enrichment. Nb and Ta abundances are highest at Indian Pass (Nb ≈ 7 ppm) and lowest at Whitechuck (Nb = ~ 2 -3), indicating that Indian Pass and the other two basaltic andesites were produced by relatively low degree hydrous

melts of depleted mantle. In comparison, the Whitechuck basalts were produced by relatively dry (<1% H₂O) slightly higher degree melting of a more depleted mantle (similar to NMORB) source. Of the three mantle-domains inferred beneath the Cascades, only a MORB-like mantle and a subduction-fluxed depleted mantle are represented beneath the Glacier Peak region. No OIB-like mantle domain is thus far represented in the Cascades north of the Mt. Rainier region.

ACKNOWLEDGMENTS

Sometimes I think that if you really want to know who wrote a paper, just look in the acknowledgements. Could this be true? If the final copy of this thesis represents the whole, then the whole represents the sum of all its parts; namely, the contributions from all the wonderful people who helped me finish this project.

My appreciation goes out to:

My committee,

Thank you Sue, for being there every step of the way, through sickness, health, crying babies, etc...., There always seemed to be something in my mailbox, just when I needed it. Also, thanks for loaning me your husband and dog on good powder days.

Thank you Tom, for being a long-distance advisor extraordinaire and provider of much data. Your depth of knowledge of the subject material gave me the confidence to realize that I actually have something interesting to say.

Thank you Scott, for being there for my last minute frantic needs for revisions and technical help. Your contributions helped make the final product much more correct and scientifically respectable.

The Geology department at Western,

Thanks especially to Vicki and Chris, for putting up with my absent-mindedness, and for bailing me out whenever I misplaced my office keys, and George Mustoe (who would get anything done around here if it weren't for him?), for many things, including not throwing my rocks away when I forgot about them in the basement for months at a time.

Scott Kuehner,

For great suggestions, countless hours of help, and for keeping the University of Washington microprobe running smoothly.

To the organizations that made this project possible:

This project was funded in part by a grant from the Geological Society of America (1999), The Western Washington University Bureau for Faculty Research (1999), The Western Washington University Geology Department, The Sigma Xi GIAR award for scientific research (1999/2000), and the Cascade Volcano Observatory's Jack Kleinman Grant for Volcanological Research (2000). Thanks also to the U.S. Geological Survey Volcanic Hazards Team (via Tom Sisson) for performing analytical work and thus greatly increasing the size of the available data set.

And last but not least, the friends and colleagues who helped out in a pinch and gave constant support and encouragement,

My parents, for giving love and support through the entire endeavor.

Kristi Pikiewicz – thanks Kristi for being my best friend!

Jeff Laub, Jeff Snyder, Steve Schindler, and Rachel Derycx, who helped in the field and carried heavy rocks for miles and miles... Ingrid Enschede and Tina Woolston for cleaning up after me when I was in a zombie state... And for everyone else that I have forgotten to mention, Thank you!!!

TABLE OF CONTENTS

ABSTRACT.....	iv
ACKNOWLEDGEMENTS.....	vi
LIST OF FIGURES.....	ix
LIST OF TABLES.....	x
INTRODUCTION.....	1
TECTONIC SETTING.....	6
GEOLOGIC SETTING.....	7
METHODS.....	13
<i>Microprobe</i>	13
<i>Whole rock chemistry</i>	13
RESULTS.....	29
<i>Petrography</i>	29
<i>Mineral Chemistry</i>	32
<i>Olivine</i>	32
<i>Pyroxene</i>	32
<i>Plagioclase</i>	36
<i>Oxides</i>	37
<i>Whole Rock Geochemistry</i>	39
<i>Major-element Chemistry</i>	39
<i>Trace-element Chemistry</i>	45
DISCUSSION.....	55
<i>Geothermometry of mafic lavas</i>	55
<i>Evaluation of Primitive Characteristics</i>	57
<i>Crustal effects on lava chemistry</i>	62
<i>Mantle Characteristics beneath the Glacier Peak Region</i>	71
CONCLUSIONS.....	79
REFERENCES.....	81
APPENDIX Sample locations (latitude and longitude).....	85

LIST OF FIGURES

Figure 1. Map of the Cascade arc showing location of study area, primitive lavas, and large volcanic centers.	4
Figure 2. Regional map of Glacier Peak and surrounding mafic flows.....	5
Figure 3. Photographs from the Whitechuck cinder cone.....	8
Figure 4. Photographs from the Lightning Creek flow.....	9
Figure 5. Photographs from the Indian Pass cinder cone.....	10
Figure 6. Photograph from the Dishpan Gap cinder cone.....	11
Figure 7. Pyroxene ternary diagram.....	34
Figure 8. Electron microprobe photomicrograph of disequilibrium relationship between orthopyroxene and clinopyroxene in Lightning Creek.	35
Figure 9. Variation diagram of K_2O vs. CaO for plagioclase phenocrysts.....	38
Figure 10. K_2O vs. SiO_2 variation diagram to discriminate between Low-K and Medium-K volcanic rocks.....	40
Figure 11. FeO/MgO vs. SiO_2 variation diagram to discriminate between calc-alkaline and tholeiitic lavas.....	41
Figure 12. Major-element oxide variation diagrams.....	42
Figure 13. $Mg\#$ vs. SiO_2 variation diagram.....	44
Figure 14. Ni and Cr vs. SiO_2 variation diagrams.....	46
Figure 15. Sr , Rb , and Zr vs. SiO_2 variation diagrams.....	47
Figure 16. Primitive mantle-normalized incompatible element diagram.....	49
Figure 17. Ba vs. Nb , Th vs. Nb , Ba/Nb vs. Nb/Zr and Ba/Zr vs. Nb/Zr variation diagrams.....	51
Figure 18. Chondrite-normalized rare earth element diagram.....	52
Figure 19. Ba/La vs. $(La/Sm)_N$ variation diagram.....	54
Figure 20. Molar $Fe/Mg^{olivine}$ vs. Molar $Fe/Mg^{whole\ rock}$ variation diagram.....	60

Figure 21. Mg# ^{olivine} vs. bulk rock MgO wt.% variation diagram.....	61
Figure 22. Fractional crystallization model using variation diagram of La vs. Sr.....	66
Figure 23. Magma mixing model: measured Lightning Creek and Dishpan Gap major-elements for hybrid magma plotted against predicted major-element concentrations....	68
Figure 24. Magma mixing model: measured Lightning Creek and Dishpan Gap trace-elements for hybrid magma plotted against predicted trace-element concentrations.....	69
Figure 25. Average Whitechuck basalt-normalized incompatible element diagram.....	75

LIST OF TABLES

Table 1. Olivine chemistry data.	15
Table 2. Pyroxene chemistry data.....	17
Table 3. Plagioclase chemistry data.....	19
Table 4. Fe-Ti oxide chemistry data.....	21
Table 5. Cr-spinel chemistry data.....	22
Table 6. Results of wholerock geochemistry of the four mafic flows and the Glacier Peak dacites.....	23
Table 7. Petrographic summary of the mafic flows.....	31
Table 8a. Results from Fe-Ti oxide thermometry calculations.....	56
Table 8b. Results from olivine-liquid thermometry calculations.....	56

INTRODUCTION

Primitive magmas from arc settings provide a rare window into processes occurring in the mantle wedge beneath the arc. These magmas are common in the southern Cascades but become notably rare north of Mt. Rainier. Previous studies in the Cascades have used primitive lavas from several regions to elucidate processes influencing partial melting in the mantle wedge. This thesis presents mineral and whole rock geochemistry of four Late Pleistocene to Early Holocene mafic lava centers between five and ten km south of Glacier Peak. These include the calc-alkaline Indian Pass, Lightning Creek, and Dishpan Gap basaltic andesites, and the fractionated Whitechuck high alumina olivine tholeiite (HAOT). All flows are located along the Pacific Crest.

There are four goals to this petrologic and geochemical study: 1) assess the primitiveness of the four lavas; 2) determine what (if any) effect the crust had on the composition of the lavas; 3) calculate the temperatures at which Fe-Ti oxides and olivine phenocrysts last equilibrated; 4) discern the nature of melting processes and mantle source characteristics beneath the Glacier Peak region. New major and trace-element data for 46 samples of mafic lavas and 11 samples from the Glacier Peak dacites are presented and represent the first modern geochemical study of arc lavas from this segment of the Cascade arc.

The four flows discussed in this thesis can be placed in a regional context with other primitive and near primitive lavas that occur elsewhere in the Cascades. Bacon et al. (1997) recognized three end-member primitive magma types occurring in the Cascades from the Lassen Volcanic Field northward to Mount Rainier (Figure 1), and have correlated these three end-members with three implied mantle components. These

include a depleted mantle domain, a subduction component, and an intraplate mantle domain.

Members of the first magma type are known as high alumina olivine tholeiites (HAOT), high alumina basalts (HAB), or low-K olivine tholeiites (LKOT). They typically have mid-oceanic ridge basalt-like (MORB-like) chemical compositions that are depleted in light rare earth elements (REE) and may be slightly enriched in large ion lithophile elements (LILE) relative to high field strength elements (HFSE) (i.e. Ba/Nb ~10-35). HAOT are thought to represent fairly anhydrous melts of depleted mantle. HAOT occur from Northern California to Southern Washington (Leeman et al. 1990; Bacon et al. 1997; Conrey et al. 1997), as well as east of the Cascades.

The second magma type, the calc-alkaline basalts (CAB), are the most common. These magmas are ubiquitous throughout the Cascades, and have trace-element concentrations typical of arc magmas: high LILE/HFSE ratios (i.e. Ba/Nb ~30-100), higher K and Fe/Mg, and lower Al than MORB-like magmas (Leeman et al. 1990; Bacon et al. 1997; Borg et al. 1997; Conrey et al. 1997; Reiners et al. 2000).

Members of the third magma type have compositions similar to ocean island basalt (OIB). These magmas are characterized by significant enrichment in incompatible elements (LILE, LREE) without depletion of Nb or Ta (i.e. Ba/Nb ~10-17). They occur towards the back-arc of the southern Washington (e.g., Simcoe) and Oregon Cascades (Leeman et al. 1990; Bacon et al. 1997; Borg et al. 1997; Conrey et al. 1997).

Leeman et al. (1990) originally proposed that these three magma types were produced by mixed melts from depleted and enriched mantle domains, without any significant contributions from subducted sediment or a modern H₂O flux. Subsequent

studies by Sisson and Layne (1993), Baker et al. (1994), Bacon et al. (1997), Borg et al. (1997), and Reiners et al. (2000) expanded the primitive lava data set and revealed that subduction fluids significantly influence magma composition. As previously noted, the three end-member magma types are produced by varying contributions of primitive mantle, a modern subduction component, and intraplate mantle (Bacon et al. 1997). Under this assumption, the upper mantle beneath the Cascades to the south of Mt. Rainier is inferred to be uniformly hot but heterogeneous with respect to the locations of upwelling primitive mantle, intraplate mantle, and subduction metasomatized mantle. Understanding primitive magmatism is made more complicated by the addition of several other small but significant components that can affect the composition of the magma. These include subducted sediment, subducted oceanic lithosphere, and continental crust (summarized by Borg et al. 1997).

In contrast to these models, Reiners et al. (2000) investigated the compositional distinction between CAB and OIB-like magmas immediately north of Mt. Rainier and suggested that separate mantle source domains are not required to produce the two magmas. Instead, CAB and OIB-like compositional distinctions are a function of both the added subduction component and degree of melting. MORB-like magmas (HAOT or LKOT) can also be produced from this model in two ways: 1) low degree melts of cold depleted mantle with variable addition of a subduction component or 2) high degree melts of hot mantle with little subduction component.

Mafic lavas from south of Glacier Peak can be used to assess the mantle characteristics beneath the region in light of the models discussed above. This thesis uses field studies, thin section petrography, major and trace element geochemistry and

microprobe analysis to understand the petrogenesis of the lavas and to elucidate characteristics of their source region. in order to discuss the petrogenesis of these lavas and to elucidate characteristics of their source region.

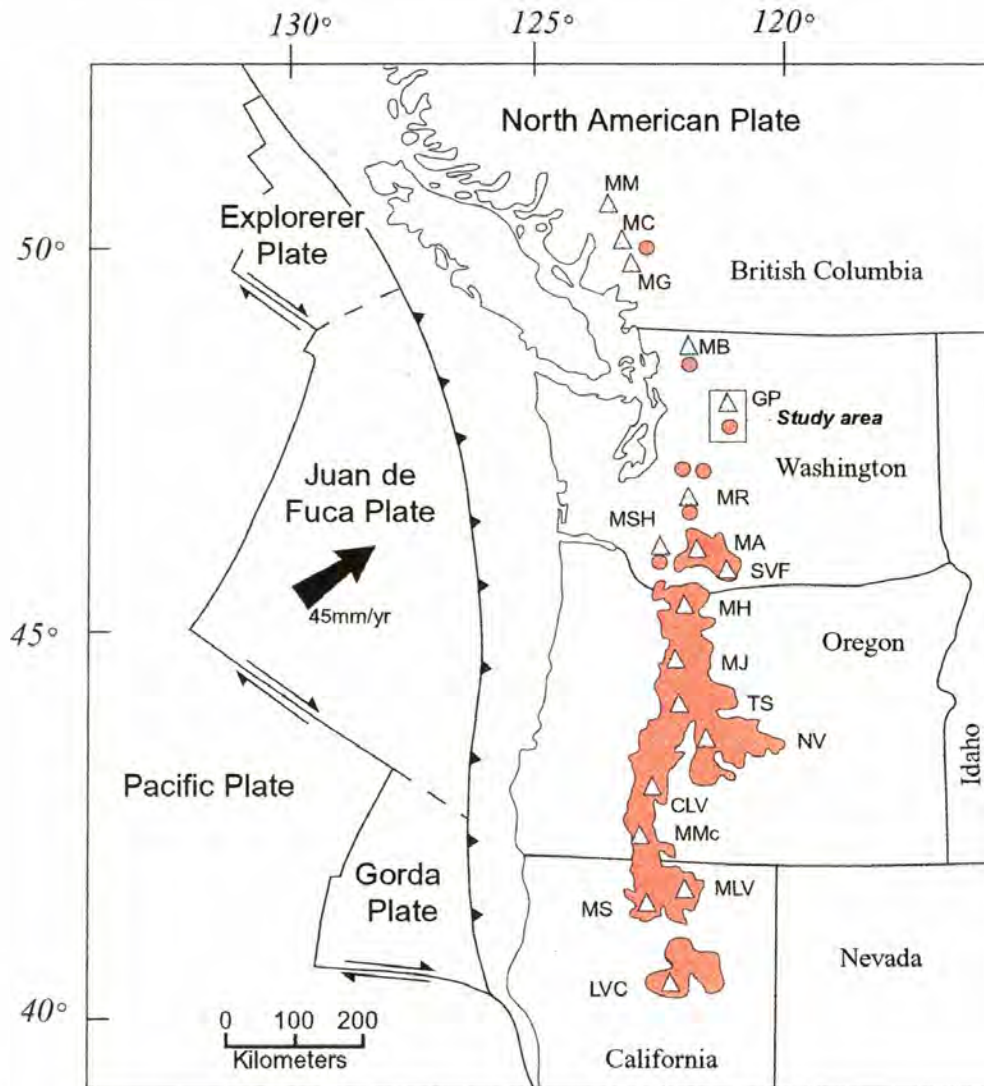


Fig. 1. Tectonic setting of the Cascade range and subduction zone modified from Borg et al. (1997). Small centers of mafic lavas are shown as filled circles, larger regions of mafic lavas are shown as filled regions, and major stratovolcanoes are shown as triangles; data from McBirney, (1968), Borg et al. (1997), Green and Harry (1999), and Reiners et al. (2000). Letters refer to major volcanoes and volcanic fields: MM, Meager Mountain; MC, Mount Cayley; MG, Mount Garibaldi; MB, Mount Baker; GP, Glacier Peak; MR, Mount Rainier; MSH; Mount St. Helens; MA, Mount Adams; SVF, Simcoe Volcanic Field; MH, Mount Hood; MJ, Mount Jefferson; TS, Three Sisters; NV, Newberry Volcano; CLV, Crater Lake Volcano; MMc, Mount McLoughlin; MLV, Medicine Lake Volcano; MS, Mount Shasta; LVC, Lassen Volcanic Center.

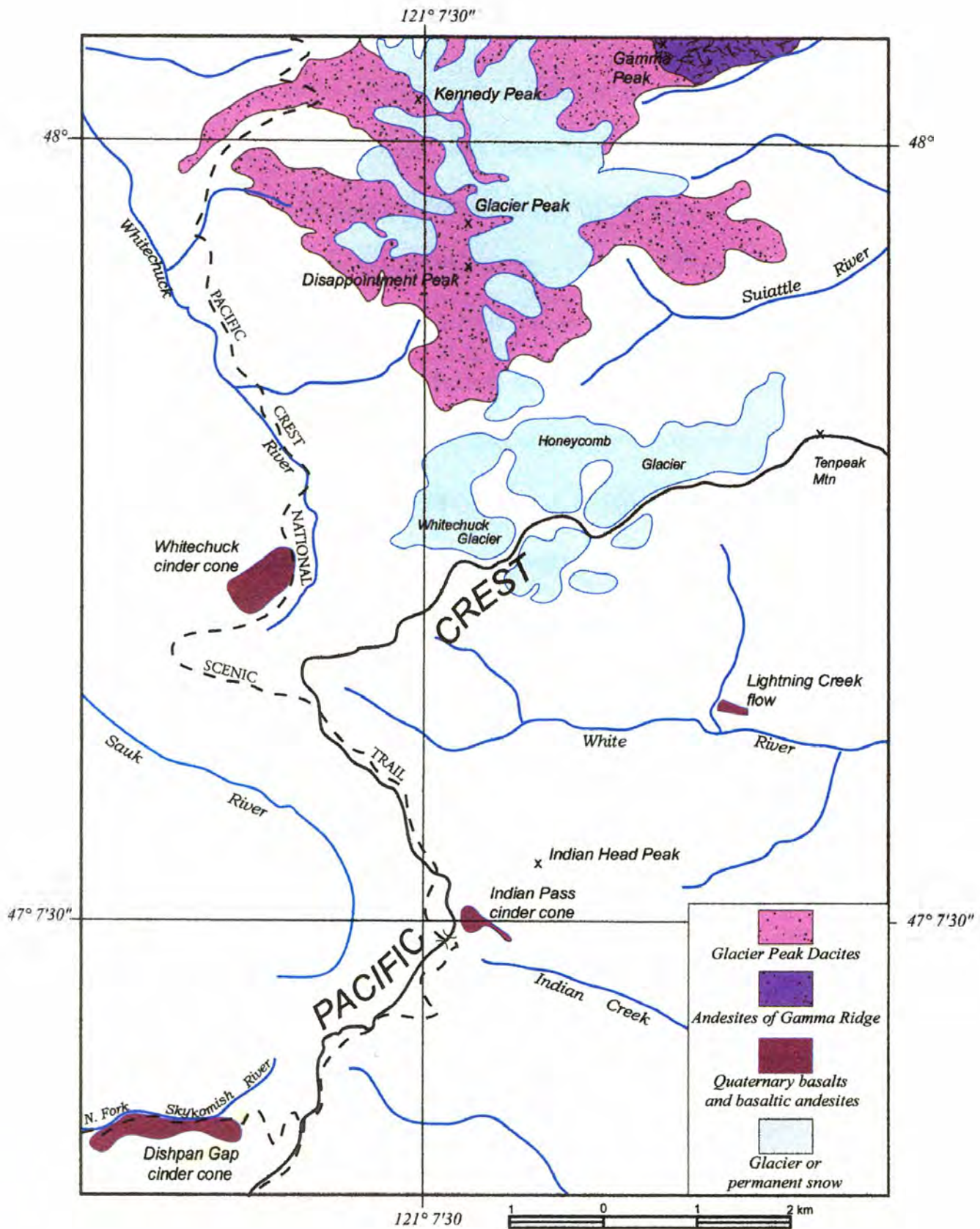


Fig. 2 Simplified geologic map of Glacier Peak and four surrounding mafic flows. Location data for Glacier Peak dacites and older Gamma Ridge flows from Tabor and Crowder (1969).

TECTONIC SETTING

Glacier Peak is the southernmost member of the Garibaldi belt segment of the Cascade arc described by Green and Harry (1999). The easternmost volcano in Washington, it lies approximately 400 miles east of the Cascadia trench where the Juan de Fuca plate is subducting beneath the western margin of North America (Fig. 1). The crust beneath the Cascade Range is estimated to be 40-46 km thick (Mooney and Weaver, 1989). Below parts of the Cascade arc, the slab is steeply dipping (approximately 45°) (Michaelson and Weaver, 1986), and converges obliquely with North America at 45mm/yr (N50°E) (Riddihough, 1984). A gap of approximately 130 km separates the mafic flows near Glacier Peak with the next occurring young mafic lavas to the south: the Quaternary Three Sisters and Pliocene Dalles Lake basalts immediately north of Mt. Rainier (Reiners, 2000; Luedke and Smith, 1992). As yet there is no uniformly accepted explanation for the significant decrease in basalt vent distributions north of the southern Washington Cascades. Green and Harry (1999) postulate that volcanic gaps in the northern Cascades (from Mt. Rainier northwards) result from changes in the geometry of the downgoing slab. Conrey et al. (1997) suggest that voluminous basalt flows in the southern Cascades result from a rift that has been propagating northward from southern Oregon for the last 7-8 Ma. The northern terminus of the rift is thought to lie near Mt. Adams.

GEOLOGIC SETTING

Glacier Peak and the surrounding mafic lavas were studied and mapped by Ford (1957), Crowder et al. (1966), Tabor and Crowder (1969), Beget (1982; 1983), and Crowder et al. (1993) (Fig. 2). These workers concluded that Glacier Peak is a dacitic stratovolcano that has been erupting since the mid- to late Pleistocene (<700 ka). Mafic volcanism in the region is characterized by monogenetic cinder cones and flows that are distributed between four and 10 km south of Glacier Peak (Fig 2). Tabor and Crowder (1969) also mapped a significant number of mafic and intermediate dikes in the area, but their age and relationship to the mafic flows is unknown. The four major mafic vents are mapped as the Whitechuck, Indian Pass, and Dishpan Gap cinder cones, and the Lightning Creek flow (Fig. 2). All are calc-alkaline olivine basalts or basaltic andesites except for the Whitechuck cinder cone, which, for the purposes of this thesis, is termed fractionated high alumina olivine tholeiite (HAOT)(*c.f.* Bacon 1990; Bacon et al. 1997; Borg et al. 1997).

The Whitechuck cinder cone is a small (<100m in height, <1km in diameter) pile of fresh basalt consisting of hyaloclastic breccia interbedded with two thin (≤ 2 -meter) pahoehoe flows of olivine basalt (Fig. 3). The entire cone is overlain by ropy blocks and bombs except for the summit, which is buried by up to several meters of oxidized scoria. Beget (1981) found pumice lapilli from Glacier Peak on parts of the cone, possibly indicating that it is older than 11,000 years.

The Lightning Creek flow is a valley-clinging erosional remnant of a thick (>25 m) basaltic andesite flow (Fig. 4a) which at one time probably covered much of the floor of the White River valley (Tabor and Crowder, 1969)(Fig. 2). Irregular splayed and non-



Fig. 3. Whitechuck cinder cone. A) Summit of Whitechuck cinder cone with oxidized scoria. B) Lowest dense flow in Whitechuck cinder cone. 90cm yellow ice axe for scale.

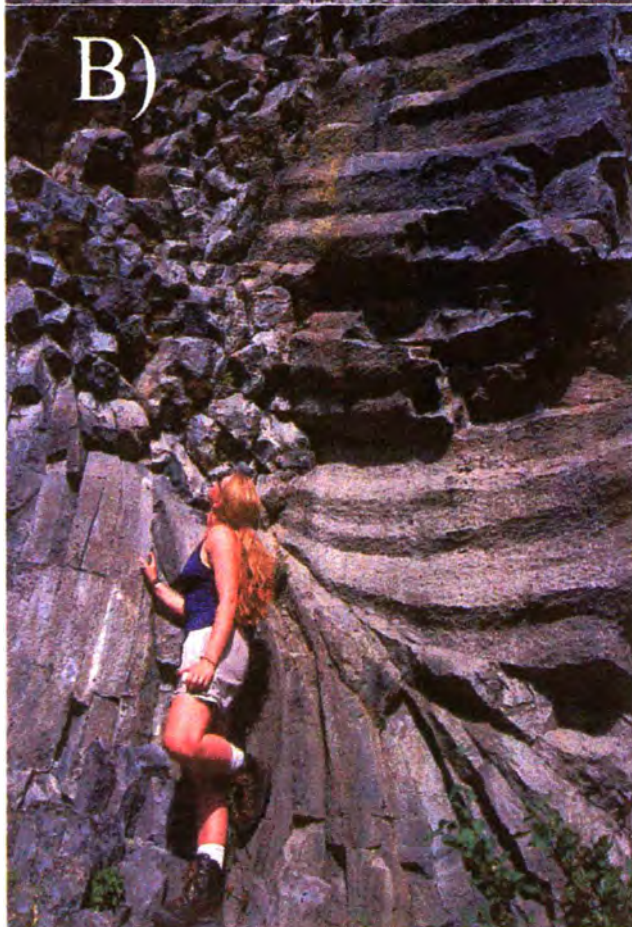


Figure 4. Lightning Creek basaltic andesite flow. A) The flow rests at the base of the White River Valley and exhibits a 20-30 m collonade capped by a 20-30 m entablature. B) Photo taken 100m to the right of A) showing closeup of irregular columnar jointing. The well developed splayed joint orientation could be due to ice-marginal cooling or an intraflow fracture.

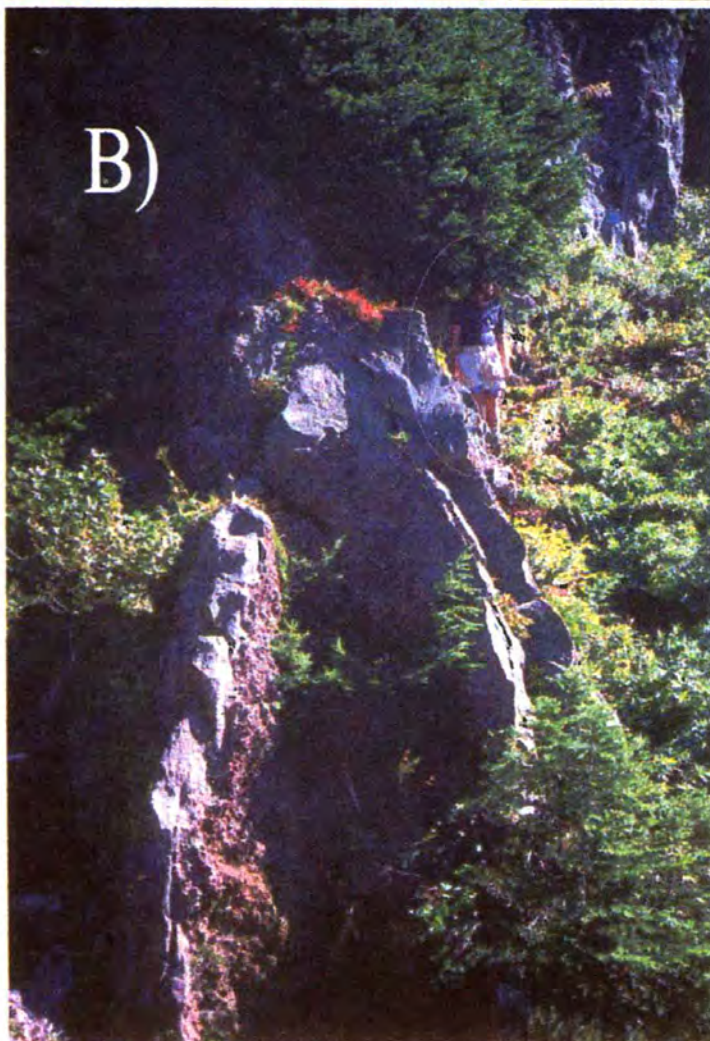
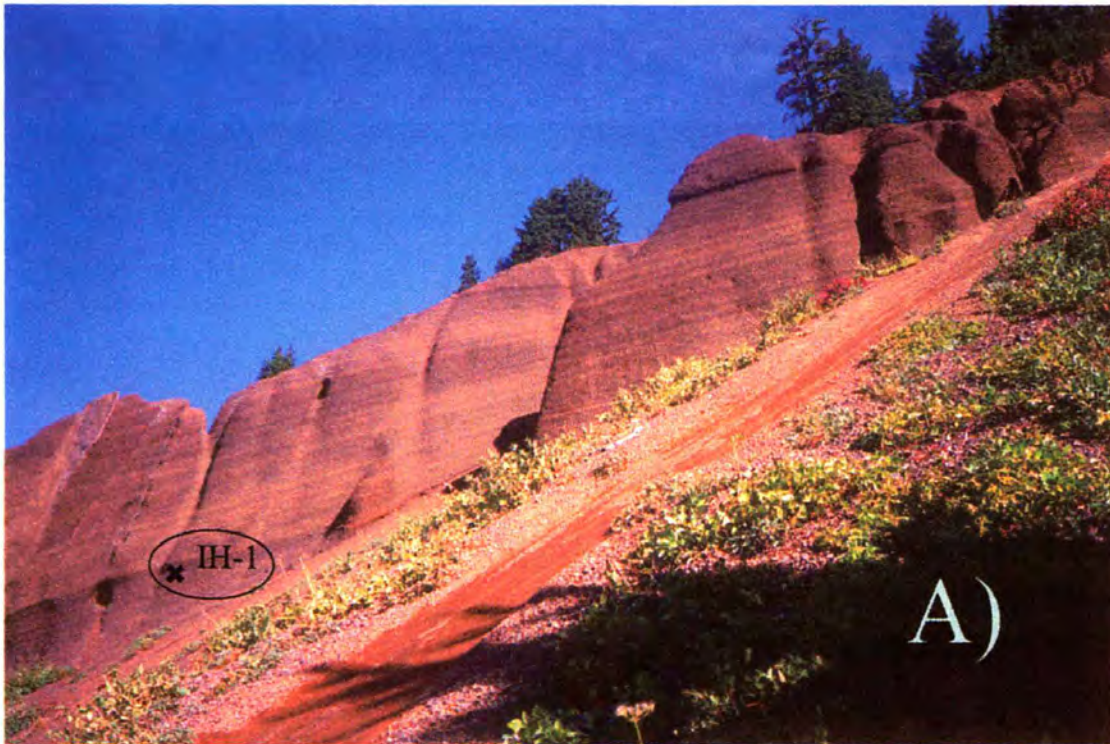


Fig. 5. Indian Pass Cinder Cone. A) Stratified beds of scoriaceous lapilli at the cinder cone. Sample IH-1 (marked on photo) was collected from a coarse, darker layer. B) Basaltic andesite dike feeding the Indian Pass cinder cone. Person (circled) for scale. The photo shows the range in thickness for the feeder dike, i.e. 3-9 m over a length of approximately one km.



Fig. 6. Terminus of the Dishpan Gap basaltic andesite flow. The cinder cone (not pictured) is just west of the Pacific Crest (Fig. 2). The flow runs 2-3 km downvalley from the cinder cone and is completely tree-covered except for the streambed pictured here.

vertical columnar jointing (Fig. 4b) could be the result of intraflow fracturing or ice-marginal cooling (T.W. Sisson, pers. comm. 2001; Lescinsky and Sisson 1998), which suggests that the White River Valley may have been glaciated at the time of volcanism. The relative age and source location of the Lightning Creek flow is unknown.

The Indian Pass cinder cone is a heavily dissected deposit of steeply dipping beds of oxidized scoriaceous bombs and lapilli (Fig. 5). The deposits of the cone comprise a small area of hillside no more than 200-300 m on a side. The cinder cone is fed by a nearby east-west trending feeder dike (3-10 m thick) composed of olivine basalt and basaltic andesite. Tabor et al. (1993) suggested that the cinder cone is Pleistocene in age based on the level of erosion.

The Dishpan Gap cinder cone is a small cone (tree cover makes size hard to estimate) on the Pacific Crest (Fig. 2) with a 7 km long flow of basaltic andesite issuing west down the north fork of the Skykomish River (Fig. 6). The flow conforms to relatively recent post-glacial topography and is dissected by streams on both sides. The cinder cone has undergone significant erosion. Based on these observations, Tabor et al. (1993) inferred the maximum age of the Dishpan Gap cinder cone to be Late Pleistocene.

These Quaternary volcanic rocks rest unconformably on rugged crystalline basement terrain composed of the Miocene Cloudy Pass pluton, the Cretaceous Tenpeak pluton east of the crest and Cretaceous Chiwaukum Schist to the west (Crowder et al., 1966; Tabor and Crowder 1969; Tabor et al. 1993).

METHODS

Microprobe

Compositions of olivine, pyroxene, plagioclase, and oxide mineral phases for the four mafic flows were obtained at the University of Washington using a 4-spectrometer JEOL 733 electron microprobe. A common set of natural and synthetic minerals were used as standards, and all data are ZAF-corrected using the methods of Bence and Albee (1968) and Armstrong (1988). A beam current of 10nA (nano-amps) was used for feldspar and oxide analyses, a current of 15nA was used for olivine and pyroxene analyses. Accelerating voltage was set at 15kV. A beam diameter of $<1\mu\text{m}$ was used for all mineral analyses except for plagioclase, which was analyzed with a beam diameter of $3\mu\text{m}$. Representative mineral chemistry from microprobe analyses of eleven polished thin sections (three from each calc-alkaline flow, two from Whitechuck) is reported for olivine (Table 1), pyroxene (Table 2), plagioclase (Table 3), Fe-Ti oxides (Table 4), and Cr-spinel (Table 5).

Whole Rock Geochemistry

Samples were collected primarily from dense flows and also from pyroclastic deposits (Whitechuck and Indian Pass cinder cones) or feeder dikes (Indian Pass). Ten samples from the Glacier Peak dacites were analyzed for comparison. Samples were chosen based on size, freshness, and a minimum amount of weathering.

Major-element analyses were obtained for 38 samples by wavelength-dispersion X-Ray Fluorescence (XRF) analysis at the U.S. Geological Survey at Lakewood, Colorado. All samples analyzed by the USGS were ground in an alumina shatterbox.

Eighteen samples were analyzed by XRF at the Washington State University GeoAnalytical Lab in Pullman, Washington. Major-element oxides are normalized to 100% on a volatile free basis with all iron as FeO*. Results for all samples are shown in Table 6.

Trace-element analyses for Ni, Cr, Sc, V, Ba, Rb, Sr, Zr, Y, Nb, Ga, Cu, Zn, Pb, La, Ce, and Th were obtained on all samples by XRF analysis at both locations. No significant interlaboratory biases were noted for major or trace elements; however, Pb, La, and Th are measured close to or below their detection limits. Samples were analyzed for additional elements (including REE) at the Washington State University GeoAnalytical Lab by Inductively Coupled Plasma Mass Spectrometry (ICP-MS) (18 samples) and by the U.S. Geological Survey using Instrumental Neutron Activation Analysis (INAA) (37 samples). Laboratory preparation and analytical methods for XRF (Johnson et al. 1999) and ICP-MS analyses are available from the WSU GeoAnalytical Laboratory upon request. Analytical techniques and precision for INAA are described by Baedeker and McKown (1987).

Table 1. Olivine mineral chemistry.

Label	WC-8 olivine 1	WC-8 olivine 1rim	WC-8 olivine 2core	WC-8 olivine 2rim	WC-8 olivine 3core	WC-8 olivine 3rim	WC-8 olivine 4core	WC-8 olivine 4rim	WC-8 olivine 4mid	WC-11 olivine 1core	WC-11 olivine 1rim	WC-11 olivine 2core 2mid	WC-11 olivine 2rim
SiO ₂	38.02	37.61	39.62	38.93	39.41	38.26	39.50	37.74	38.88	37.98	36.95	38.05	37.76
FeO	21.44	22.34	14.78	16.93	13.73	20.29	13.75	21.17	16.59	22.34	26.11	21.50	24.78
MnO	0.41	0.42	0.23	0.28	0.21	0.38	0.20	0.38	0.25	0.35	0.39	0.32	0.38
NiO	0.08	0.07	0.18	0.15	0.13	0.10	0.15	0.09	0.09	0.03	0.00	0.01	0.00
MgO	39.86	38.39	45.73	43.69	46.71	40.96	46.64	39.63	44.43	39.49	35.65	39.62	37.21
CaO	0.22	0.33	0.16	0.18	0.19	0.25	0.19	0.26	0.16	0.15	0.16	0.15	0.14
Total	100.03	99.16	100.70	100.17	100.38	100.23	100.43	99.27	100.39	100.33	99.27	99.65	100.27
Mg#	76.82	75.38	84.64	82.14	85.84	78.26	85.81	76.94	82.68	75.91	70.88	76.65	72.80

Label	WC-11 olivine 3	WC-11 olivine 4core	WC-11 olivine 4rim	LC-4, olivine 1core	LC-4, olivine 1rim	LC-4, olivine 2core	LC-4, olivine 2rim	LC-4, olivine 3core	LC-4, olivine 3rim	LC-6 olivine 1core	LC-6 olivine 1rim	LC-6 olivine 2core	LC-6 olivine 2rim
SiO ₂	36.95	39.00	36.49	40.03	38.78	39.97	38.65	39.94	38.04	37.33	36.01	39.95	38.81
FeO	28.10	14.23	28.44	10.40	17.99	11.76	19.36	12.51	21.27	24.21	26.35	10.47	14.32
MnO	0.44	0.23	0.52	0.15	0.27	0.16	0.25	0.17	0.33	0.43	0.46	0.17	0.22
NiO	0.02	0.09	0.07	0.35	0.22	0.29	0.14	0.40	0.17	0.15	0.14	0.38	0.23
MgO	34.66	45.60	33.75	49.63	42.90	47.97	41.50	47.67	40.30	37.14	36.11	48.77	45.57
CaO	0.23	0.21	0.27	0.17	0.17	0.18	0.19	0.15	0.15	0.17	0.17	0.15	0.14
Total	100.40	99.38	99.55	100.74	100.32	100.33	100.11	100.84	100.25	99.43	99.24	99.89	99.30
Mg#	68.74	85.08	67.90	89.48	80.96	87.91	79.25	87.16	77.15	73.22	70.95	89.25	85.01

Label	LC-6 olivine 3core	LC-6 olivine 3mid	LC-6 olivine 3rim	LC-6 olivine 4core	LC-6 olivine 4rim	LC-6 olivine 5core	LC-6 olivine 5rim	LC-12 olivine 1core	LC-12 olivine 1rim	LC-12 olivine 2core	LC-12 olivine 2rim	LC-12 olivine 3core	LC-12 olivine 3rim
SiO ₂	38.54	38.30	37.55	37.17	39.20	38.27	36.72	39.68	37.54	39.25	37.63	39.56	37.50
FeO	16.20	18.11	21.24	25.77	11.34	13.98	24.36	11.64	22.30	13.13	20.96	10.10	21.37
MnO	0.22	0.26	0.34	0.46	0.18	0.24	0.42	0.18	0.40	0.22	0.36	0.18	0.35
NiO	0.25	0.22	0.20	0.17	0.25	0.23	0.19	0.31	0.21	0.19	0.15	0.21	0.19
MgO	44.10	42.84	40.15	35.83	48.24	46.07	37.48	47.98	38.91	46.70	40.33	49.28	39.89
CaO	0.16	0.16	0.14	0.16	0.16	0.17	0.14	0.18	0.15	0.22	0.18	0.15	0.17
Total	99.46	99.89	99.63	99.56	99.37	98.96	99.31	99.96	99.52	99.76	99.61	99.62	99.46
Mg#	82.91	80.83	77.11	71.25	88.35	85.46	73.28	88.02	75.66	86.37	77.42	89.69	76.89

All Fe as FeO.

Samples without "core" or "rim" designations are groundmass grains

Microprobe work completed at the University of Washington, Seattle, Washington.

Table 1. (cont.) Olivine mineral chemistry.

Label	LC-12 olivine 4core	LC-12 olivine 4rim	IP-3 olivine 1core	IP-3 olivine 2core	IP-3 olivine 2rim	IP-3 olivine 3	IP-8 olivine 1core	IP-8 olivine 2core	IP-8 olivine 2mid	IP-8 olivine 2rim	IP-8 olivine 3core	IP-8 olivine 3rim	IP-8 olivine 4core	IP-8 olivine 4rim
Pt#	44	45	50	52	53	54	66	67	68	69	70	71	72	73
SiO ₂	39.26	37.82	39.55	40.00	38.66	38.79	38.11	39.62	39.38	38.67	39.80	38.98	39.52	38.05
FeO	12.87	20.77	11.15	11.83	14.26	12.61	20.95	12.43	15.14	17.99	11.73	16.54	13.04	19.63
MnO	0.21	0.34	0.17	0.18	0.25	0.20	0.43	0.19	0.25	0.3231	0.16	0.33	0.17	0.39
NiO	0.23	0.19	0.36	0.34	0.20	0.27	0.09	0.26	0.22	0.2134	0.23	0.22	0.29	0.19
MgO	46.81	40.79	46.65	46.81	45.68	47.07	40.32	47.51	45.39	42.89	47.98	44.14	47.14	41.21
CaO	0.19	0.14	0.36	0.18	0.20	0.15	0.13	0.18	0.16	0.1344	0.13	0.13	0.15	0.14
Total	99.57	100.04	98.24	99.34	99.24	99.09	100.02	100.18	100.53	100.22	100.14	100.36	100.32	99.61
Mg#	86.63	77.78	88.18	87.59	85.09	86.93	77.43	87.20	84.23	80.95	87.94	82.62	86.57	78.91

Label	IP-15 olivine 1core	IP-15 olivine 1c	IP-15 olivine 1e	IP-15 olivine 1rim	IP-15 olivine 2core	IP-15 olivine 2mid	IP-15 olivine 2rim	IP-15 olivine 3core	IP-15 olivine 3rim	DG-5 olivine 1	DG-5 olivine 2	DG-5 olivine 3core	DG-5 olivine 3rim	DG-11 olivine 1a
Pt#	83	84	85	86	87	88	89	90	91	46	47	48	49	2
SiO ₂	39.56	39.74	39.19	37.57	39.66	38.94	38.36	39.44	37.90	37.05	36.78	38.62	36.96	38.06
FeO	11.84	11.93	13.90	22.71	12.84	16.67	22.01	14.09	23.86	28.38	26.24	18.17	24.01	20.06
MnO	0.15	0.18	0.22	0.45	0.20	0.29	0.44	0.20	0.44	0.59	0.53	0.33	0.49	0.30
NiO	0.44	0.39	0.32	0.15	0.28	0.27	0.13	0.26	0.15	0.05	0.04	0.20	0.09	0.05
MgO	47.11	48.07	45.93	38.17	46.73	43.39	38.64	46.12	37.76	30.40	35.61	42.29	37.15	40.94
CaO	0.12	0.14	0.18	0.16	0.14	0.16	0.21	0.14	0.21	0.42	0.20	0.11	0.17	0.19
Total	99.22	100.46	99.74	99.20	99.85	99.72	99.79	100.26	100.35	96.90	99.40	99.72	98.87	99.60
Mg#	87.64	87.78	85.49	74.97	86.64	82.27	75.78	85.36	73.83	65.62	70.75	80.58	73.39	78.43

Label	DG-11 olivine 1b (core)	DG-11 olivine 1c	DG-11 olivine 1d	DG-11 olivine 2	DG-11 olivine 2rim	DG-11 olivine 3	DG-11 olivine 4core	DG-11 olivine 4mid	DG-11 olivine 4rim	DG-11 olivine 4rimb	DG-11 olivine 5core	DG-11 olivine 5mid	DG-11 olivine 5rim
Pt#	3	4	5	6	7	8	9	10	11	12	13	14	15
SiO ₂	38.33	37.66	36.83	36.55	36.52	36.37	39.06	39.87	39.22	36.73	37.35	36.79	36.53
FeO	19.95	24.41	28.13	28.06	29.63	30.79	12.87	13.17	15.40	28.08	22.67	26.06	29.18
MnO	0.32	0.39	0.51	0.49	0.52	0.53	0.19	0.19	0.21	0.48	0.35	0.37	0.49
NiO	0.03	0.07	0.03	0.03	0.04	0.01	0.20	0.21	0.13	0.08	0.04	0.04	0.00
MgO	41.02	36.97	34.16	34.19	32.84	31.82	47.11	46.78	44.52	34.13	38.81	36.02	33.46
CaO	0.19	0.18	0.21	0.17	0.25	0.26	0.19	0.19	0.20	0.20	0.15	0.13	0.21
Total	99.83	99.68	99.87	99.48	99.80	99.78	99.63	100.42	99.68	99.71	99.36	99.40	99.88
Mg#	78.57	72.97	68.40	68.47	66.39	64.81	86.71	86.36	83.75	68.41	75.32	71.13	67.15

All Fe as FeO

Samples without "core" or "rim" designations are groundmass grains

Microprobe work completed at the University of Washington, Seattle, Washington.

Table 2. Pyroxene mineral chemistry.

Label	WC-8 cpx-1	WC-8 cpx-3	WC-11 cpx-1	WC-11 cpx-2	WC-11 cpx-3	LC-4 cpx-1	LC-4 cpx-1mid	LC-4 cpx-1rim	LC-4 cpx-2core	LC-4 cpx-2rim	LC-4 cpx-3core	LC-4 cpx-3rim	LC-6 cpx 1
P#	25.00	25.00	13.00	14.00	15.00	30.00	31.00	32.00	33.00	34.00	35.00	36.00	7.00
Type	cpx	cpx	cpx	cpx	cpx	cpx	cpx	cpx	cpx	cpx	cpx	cpx	cpx
SiO ₂	51.50	52.40	49.52	50.11	51.27	52.71	51.26	50.71	52.70	51.47	51.40	50.88	52.79
TiO ₂	0.78	1.32	1.11	1.14	1.11	0.22	0.89	0.76	0.26	0.59	0.93	0.99	0.19
Al ₂ O ₃	3.21	1.62	4.08	2.92	2.16	0.94	3.55	2.60	1.28	3.44	2.60	2.96	1.04
Cr ₂ O ₃	0.23	0.10	0.40	0.01	0.01	0.00	0.12	0.00	0.00	0.52	0.01	0.13	0.00
FeO	8.40	10.10	11.57	11.33	10.66	9.23	7.50	10.35	9.20	5.27	9.74	8.15	9.00
MnO	0.22	0.42	0.28	0.29	0.33	0.14	0.20	0.33	0.13	0.13	0.26	0.21	0.34
MgO	16.03	17.83	15.56	14.89	15.85	14.95	15.95	14.32	14.83	16.91	15.25	16.50	14.87
CaO	0.39	0.15	0.47	0.47	0.44	0.31	0.42	0.42	0.40	0.31	0.32	0.31	0.39
Na ₂ O	100.21	100.45	100.22	100.53	100.83	101.68	101.08	100.97	101.51	100.76	100.61	100.76	100.53
Total	40.24	34.16	35.67	39.48	38.50	45.02	43.15	43.41	44.72	44.45	42.33	41.27	44.15
En	46.19	49.96	45.39	42.41	44.65	40.84	44.98	40.26	41.00	47.27	42.53	45.99	41.69
Fs	13.57	15.88	18.93	18.11	16.85	14.14	11.87	16.33	14.28	8.27	15.25	12.74	14.16

Label	LC-6 cpx 1 mid	LC-6 cpx 1 rim a	LC-6 cpx 1 rim b	LC-6 cpx 2 core	LC-6 cpx 2 rim	LC-6 cpx 3 core	LC-6 cpx 3 rim	LC-6 cpx 6 core	LC-6 mix 4 near rim cpx	LC-6 cpx 5	LC-6 cpx 6 rim	LC-6 cpx 7	LC-6 cpx 7 rim
P#	8.00	9.00	10.00	11.00	12.00	13.00	15.00	19.00	17.00	18.00	20.00	21.00	22.00
Type	cpx	cpx	cpx	cpx	cpx	cpx	cpx	cpx	cpx	cpx	cpx	cpx	cpx
SiO ₂	52.52	51.71	51.67	52.39	53.15	52.16	52.07	51.15	52.19	53.28	53.24	53.60	53.32
TiO ₂	0.20	0.56	0.59	0.29	0.45	0.60	0.61	0.98	0.51	0.38	0.42	0.10	0.18
Al ₂ O ₃	0.88	3.38	3.60	1.25	2.58	2.92	2.12	3.40	2.97	1.93	2.10	0.59	1.50
Cr ₂ O ₃	0.00	0.80	0.90	0.00	0.08	0.10	0.30	0.07	0.87	0.05	0.03	0.00	0.00
FeO	8.89	4.76	4.67	8.38	13.67	6.86	8.94	7.95	4.60	13.79	14.01	21.01	6.38
MnO	0.30	0.11	0.31	0.12	0.31	0.21	0.23	0.19	0.12	0.29	0.29	0.00	0.00
MgO	14.93	17.16	17.40	15.38	27.85	17.30	17.22	16.15	17.47	28.22	28.14	23.65	25.34
CaO	22.22	21.67	21.92	21.21	1.81	19.81	18.24	19.84	1.71	1.981	1.51	0.00	0.00
Na ₂ O	0.35	0.31	0.31	0.03	0.03	0.35	0.30	0.37	0.32	0.04	0.02	0.03	0.03
Total	100.29	100.46	101.28	99.71	99.93	100.30	100.01	100.10	100.65	99.76	99.76	98.98	86.76
Wo	44.51	43.99	43.92	43.15	3.54	40.24	37.10	40.89	43.63	3.32	2.92	0.00	0.00
En	41.59	48.47	48.77	43.54	75.63	48.89	48.72	46.32	49.10	75.88	75.88	66.74	87.62
Fs	13.90	7.54	7.31	13.30	20.83	10.87	14.19	12.79	7.27	20.80	21.20	33.26	12.38

Label	LC-6 opx 4 core	LC-12 cpx 1 core	LC-12 cpx 1mid-a	LC-12 cpx 1mid-b	LC-12 cpx 1rim	LC-12 cpx 2core	LC-12 cpx 2rim	LC-12 cpx 3core	LC-12 cpx 3mid	IP-3 cpx 1	IP-3 cpx 2	IP-3 cpx 3
P#	16.00	16.00	17.00	18.00	19.00	20.00	21.00	22.00	23.00	24.00	25.00	27.00
Type	opx	cpx	cpx	cpx	cpx	cpx	cpx	cpx	cpx	cpx	cpx	cpx
SiO ₂	53.10	52.02	51.92	50.07	51.18	51.46	50.77	52.06	49.59	52.00	49.57	50.29
TiO ₂	0.79	0.44	0.53	1.04	0.84	0.56	1.07	0.59	1.15	0.63	1.57	1.34
Al ₂ O ₃	1.13	2.82	2.99	5.05	5.64	2.33	4.07	3.37	5.18	2.91	3.74	3.67
Cr ₂ O ₃	0.09	0.30	0.74	0.11	0.52	0.02	0.55	0.15	0.13	0.59	0.13	0.29
FeO	16.01	4.73	4.74	6.82	5.86	8.94	6.40	6.07	6.42	6.31	9.11	8.04
MnO	0.33	0.13	0.13	0.16	0.13	0.25	0.11	0.14	0.15	0.18	0.21	0.21
MgO	26.38	17.93	17.46	16.73	15.26	14.84	16.58	17.79	15.81	17.39	15.42	15.59
CaO	2.22	21.74	22.06	20.48	19.87	22.09	21.36	21.00	21.42	21.11	20.86	21.96
Na ₂ O	0.05	0.27	0.33	0.33	0.59	0.38	0.30	0.32	0.32	0.24	0.50	0.43
Total	100.09	100.37	100.90	100.78	99.89	100.86	101.21	101.41	100.18	101.38	100.61	101.61
Wo	4.32	43.15	44.07	41.74	43.51	44.44	43.22	41.59	44.23	42.03	42.80	44.20
En	71.38	49.52	48.54	47.42	46.47	41.53	46.67	49.02	45.42	48.17	42.61	43.97
Fs	24.30	7.33	7.39	10.84	10.02	14.03	10.11	9.39	10.35	9.81	14.59	12.63

All Fe as FeO.

Samples without "core" or "rim" designations are groundmass grains

Microprobe work completed at the University of Washington, Seattle, Washington.

"Cpx" denotes clinopyroxene, "opx" denotes orthopyroxene.

Table 2 (cont.). Pyroxene mineral chemistry.

Label	IP-8 opx-1	IP-8 opx-2	IP-15 opx-1	IP-15 opx-2 ¹	IP-15 opx-3	IP-15 opx-4	DG-5 opx-1	DG-5 opx-2	DG-5 opx-3	DG-5 opx-4core	DG-5 opx-4rim	DG-8 opx-2core	DG-8 opx-2rim
P#	28.00	29.00	27.00	28.00	29.00	30.00	43.00	44.00	45.00	46.00	47.00	39.00	40.00
Type	opx	opx	opx	opx	opx	opx	opx	opx	opx	opx	opx	opx	opx
SiO ₂	50.76	52.46	51.18	44.97	50.91	51.89	49.86	51.56	52.29	52.40	51.10	50.18	51.55
TiO ₂	1.12	1.09	0.95	0.50	0.99	0.80	0.94	0.71	0.53	0.24	0.74	1.01	0.57
Al ₂ O ₃	2.94	1.62	2.61	1.68	2.66	2.09	3.50	2.59	2.22	1.01	3.67	3.24	2.89
Cr ₂ O ₃	0.26	0.03	0.42	0.06	0.24	0.28	0.01	0.00	0.13	0.00	0.20	0.12	0.10
FeO	8.25	8.09	7.47	17.42	8.18	7.00	8.57	8.16	7.55	10.23	6.94	8.56	7.51
MnO	0.24	0.28	0.20	0.40	0.33	0.20	0.24	0.25	0.25	0.33	0.17	0.18	0.18
MgO	15.88	17.23	15.78	24.98	15.86	16.75	15.25	15.75	18.60	14.52	16.37	15.42	17.41
CaO	20.85	20.34	19.98	8.32	20.38	20.38	20.92	21.87	18.57	22.02	21.55	20.80	20.23
N ₂ O	0.40	0.49	0.44	0.73	0.49	0.45	0.44	0.45	0.26	0.37	0.41	0.47	0.28
Total	100.79	101.63	99.03	99.06	99.92	99.80	99.74	101.32	100.39	101.12	101.16	99.97	100.72
Wo	42.22	40.19	42.54	27.82	41.74	41.43	42.84	43.62	36.90	43.87	43.31	42.52	40.21
En	44.74	47.34	43.47	53.26	45.19	47.32	43.46	43.69	51.39	40.22	45.79	43.83	48.15
Fs	13.04	12.47	11.99	18.92	13.07	11.20	13.70	12.70	11.71	15.90	10.89	13.65	11.65

Label	DG-8 opx-3core	DG-8 opx-3rim	DG-8 opx-1	DG-8 opx-1b	DG-11 opx-1	DG-11 opx-1rima	DG-11 opx-1rimb	DG-11 opx-2	DG-11 opx-3	DG-11 opx-4
P#	41.00	42.00	37.00	38.00	31.00	32.00	33.00	34.00	35.00	36.00
Type	opx	opx	opx	opx	opx	opx	opx	opx	opx	opx
SiO ₂	53.56	50.42	53.61	52.94	50.32	49.51	50.71	49.44	50.77	50.59
TiO ₂	0.27	0.86	0.11	0.10	0.94	1.09	0.86	1.03	1.01	0.80
Al ₂ O ₃	1.04	3.28	0.46	0.50	4.89	5.48	4.61	3.96	3.70	3.06
Cr ₂ O ₃	0.03	0.00	0.80	0.02	0.66	0.07	0.53	0.07	0.02	0.05
FeO	17.64	8.51	21.04	21.91	6.55	7.82	5.68	8.61	8.07	8.27
MnO	0.60	0.23	0.77	0.79	0.17	0.19	0.12	0.22	0.22	0.27
MgO	25.78	15.90	23.87	22.84	16.49	15.30	16.12	15.56	15.65	16.40
CaO	1.71	20.99	0.96	0.96	20.00	20.08	21.29	20.12	20.46	19.77
N ₂ O	0.03	0.41	0.03	0.42	0.46	0.46	0.39	0.43	0.42	0.40
Total	100.66	100.60	100.85	100.18	100.50	100.01	100.31	99.44	100.32	99.61
Wo	3.33	42.19	1.90	1.91	41.68	42.29	44.22	41.50	42.16	40.31
En	69.85	44.46	65.65	63.86	47.69	44.85	46.38	44.65	44.87	46.52
Fs	26.82	13.35	32.46	34.22	10.63	12.86	9.20	13.85	12.98	13.17

All Fe as FeO.

Samples without "core" or "rim" designations are groundmass grains

Microprobe work completed at the University of Washington, Seattle, Washington.

"Cpx" denotes clinopyroxene, "opx" denotes orthopyroxene.

Table 3. Plagioclase mineral chemistry.

Label	WC-8 plag 1 core micro	WC-8 plag 1 rim micro	WC-8 plag 2 micropheno	WC-11 plag 1 core	WC-11 plag 1 rim micro	WC-11 plag 2 micro	WC-11 plag 3 core	WC-11 plag 3 rim	WC-11 plag 4 resorb	WC-11 plag 4 Score	WC-11 plag 5 rim	WC-11 plag 6 resorb	WC-11 plag 6 Score	LC-4 plag 1 micro
P#	118.00	119.00	120.00	68.00	69.00	70.00	71.00	72.00	73.00	74.00	75.00	76.00	77.00	105.00
SiO ₂	49.38	53.70	49.93	46.74	51.72	49.32	46.34	49.39	48.53	46.73	48.93	50.96	48.93	52.53
Al ₂ O ₃	32.09	28.36	31.27	34.59	30.01	31.53	34.19	31.54	32.71	33.87	32.19	31.30	32.19	29.71
FeO	0.63	1.34	0.79	0.40	0.76	0.64	0.44	0.61	0.46	0.36	0.53	0.46	0.53	0.55
CaO	14.96	11.19	14.06	17.20	13.33	14.18	16.81	14.50	15.55	16.50	15.63	13.43	15.63	12.33
Na ₂ O	3.00	4.93	3.37	1.72	4.08	3.00	1.92	3.06	2.78	1.77	2.77	3.74	2.77	4.35
K ₂ O	0.05	0.13	0.09	0.03	0.20	0.07	0.05	0.10	0.05	0.00	0.05	0.06	0.05	0.18
SrO	0.09	0.08	0.08	0.13	0.07	0.11	0.12	0.11	0.12	0.11	0.13	0.12	0.12	0.17
Total	100.19	99.73	99.59	100.81	100.18	98.86	99.87	99.31	100.12	99.34	100.24	100.07	100.12	99.82
An	55.61	73.40	69.76	84.66	64.37	72.31	72.36	82.90	75.58	83.76	75.70	66.47	75.58	61.03

Label	LC-4 plag 2 core	LC-4 plag 2 rim	LC-4 plag 3 core	LC-4 plag 3 rim	LC-4 plag 4 micro	LC-4 plag 5 micro	LC-6 plag 1 core	LC-6 plag 1 rim	LC-6 plag 2 micro	LC-6 plag 3 micro	LC-6 plag 4 micro up	LC-12 plag 1 core	LC-12 plag 1 rim
P#	106.00	107.00	108.00	109.00	110.00	111.00	100.00	101.00	102.00	103.00	104.00	80.00	81.00
SiO ₂	57.24	56.03	48.28	53.71	53.54	53.50	57.06	52.45	52.42	52.61	50.05	53.97	50.95
Al ₂ O ₃	26.25	27.70	31.68	29.30	28.71	28.05	26.71	29.70	29.32	29.65	30.73	29.03	30.86
FeO	0.31	0.36	0.63	0.51	0.95	0.94	0.32	0.57	0.52	0.71	0.47	0.38	0.71
CaO	9.01	9.52	15.68	11.73	11.63	11.17	8.75	12.25	12.14	12.03	14.13	11.26	14.03
Na ₂ O	6.29	5.68	2.53	4.59	4.72	4.98	6.33	4.36	4.50	4.59	3.32	4.93	3.56
K ₂ O	0.41	0.36	0.11	0.18	0.26	0.27	0.19	0.27	0.20	0.22	0.10	0.23	0.13
SrO	0.17	0.12	0.17	0.15	0.17	0.17	0.07	0.15	0.20	0.21	0.12	0.10	0.18
Total	99.69	99.78	99.07	100.17	99.98	99.10	99.64	99.68	99.29	100.03	98.93	99.91	100.43
An	44.17	48.09	77.42	58.53	57.68	55.33	43.28	60.80	59.87	59.16	70.14	55.79	68.52

Label	LC-12 plag 2 core	LC-12 plag 2 rim	LC-12 plag 3 resorbed?	LC-12 plag 4 core	LC-12 plag 5 micro	LC-12 plag 6 micro	IP-3 plag 1 xenocryst?	IP-3 plag 2 micro	IP-3 plag 3 micro	IP-8 plag 1 xenocryst a	IP-8 plag 1 xenocryst b	IP-8 plag 2 micro a
P#	82.00	84.00	83.00	85.00	86.00	88.00	77.00	78.00	79.00	89.00	90.00	91.00
SiO ₂	57.52	55.91	53.70	58.32	56.56	51.09	55.87	51.34	51.06	54.93	51.55	52.39
Al ₂ O ₃	25.55	26.76	28.82	26.46	27.01	30.50	27.95	29.92	30.48	28.54	30.44	29.87
FeO	0.40	0.33	0.51	0.32	0.44	0.98	0.27	0.89	0.78	0.32	0.32	0.82
CaO	7.92	8.42	11.40	8.00	8.45	12.69	9.98	12.57	13.37	10.45	12.71	11.99
Na ₂ O	6.45	6.20	5.07	6.71	5.55	3.82	5.85	4.06	4.02	5.49	4.21	4.34
K ₂ O	0.46	0.39	0.22	0.42	0.37	0.20	0.32	0.20	0.11	0.27	0.16	0.25
SrO	0.13	0.09	0.13	0.08	0.13	0.19	0.13	0.26	0.26	0.14	0.09	0.21
Total	98.41	98.10	99.85	100.31	98.51	99.57	100.37	99.23	100.08	100.14	99.48	99.87
An	40.43	42.88	55.39	39.71	45.70	64.75	48.52	63.11	64.78	51.26	62.54	60.42

"Micro" denotes microphenocryst, "mid" denotes region between core and rim. Microprobe work completed at the University of Washington, Seattle, Washington.

Table 3. (cont.) Plagioclase mineral chemistry.

Label	IP-8 plag 2 micro b	DG-5 plag 1 core	DG-5 plag 1 rim	DG-5 plag 2 core	DG-5 plag 2 rim	DG-5 plag 3 microcline sp	DG-5 plag 4 core	DG-5 plag 4 rim	DG-8 plag 1 core	DG-8 plag 1 mid	DG-8 plag 1 rim	DG-8 plag 2 core	DG-8 plag 2 rim
Pt#	92.00	93.00	94.00	95.00	96.00	97.00	98.00	99.00	112.00	113.00	114.00	115.00	116.00
SiO ₂	54.30	47.11	52.48	50.71	51.62	51.70	46.02	51.69	52.51	55.94	50.51	48.78	53.43
Al ₂ O ₃	28.23	32.80	29.68	30.43	29.84	29.93	33.87	30.25	29.50	28.13	30.33	31.84	29.46
FeO	0.97	0.52	0.64	0.64	0.63	0.71	0.53	0.61	0.43	0.47	0.72	0.73	0.51
CaO	11.08	15.68	12.64	12.91	12.85	12.57	16.48	12.57	11.88	10.53	13.26	14.76	11.89
Na ₂ O	5.07	2.27	4.28	3.85	4.11	4.17	2.09	4.15	4.61	5.69	3.85	3.02	4.72
K ₂ O	0.35	0.04	0.13	0.11	0.14	0.17	0.06	0.11	0.21	0.21	0.11	0.12	0.16
SrO	0.14	0.17	0.21	0.14	0.10	0.14	0.18	0.18	0.13	0.18	0.13	0.15	0.13
Total	100.13	98.59	99.92	98.79	99.28	99.38	99.23	99.56	99.26	101.15	98.90	99.40	100.30
An	54.71	79.27	61.99	64.98	63.34	62.51	81.34	62.59	58.75	50.59	65.57	72.95	58.23

Label	DG-8 plag 3 microcline	DG-11 plag 1 core	DG-11 plag 1 rim	DG-11 plag 2 core	DG-11 plag 2 rim	DG-11 plag 3 micro	DG-11 plag 4 micro
Pt#	117.00	121.00	122.00	123.00	124.00	125.00	126.00
SiO ₂	56.36	48.13	51.37	48.81	52.34	56.07	51.45
Al ₂ O ₃	26.42	32.80	30.59	31.59	30.09	26.94	30.42
FeO	1.16	0.65	0.59	0.55	0.61	1.12	0.69
CaO	9.44	15.51	13.54	14.53	12.83	9.43	13.21
Na ₂ O	5.80	2.40	3.79	3.09	4.17	5.75	3.95
K ₂ O	0.49	0.12	0.16	0.07	0.13	0.39	0.16
SrO	0.12	0.08	0.09	0.11	0.13	0.08	0.10
Total	99.79	99.69	100.14	98.77	100.31	99.77	99.98
An	47.37	78.09	66.39	72.19	62.95	47.53	64.91

"Micro" denotes microphenocryst, "mid" denotes region between core and rim. Microprobe work completed at the University of Washington, Seattle, Washington.

Table 4. Mineral chemistry of Fe-Ti oxide pairs from Indian Pass.

Label	IP-8 fe-ti 3	IP-8 fe-ti 4	IP-8 fe-ti 4	IP-15 FeTi 1 - IP-15 FeTi 1	IP-15 FeTi 1 - IP-15 FeTi 1	IP-15 FeTi 1 - IP-15 FeTi 1	IP-15 FeTi 1 - IP-15 FeTi 1	IP-15 FeTi 1 - IP-15 FeTi 1	IP-15 FeTi 1 - IP-15 FeTi 1	IP-15 FeTi 1 - IP-15 FeTi 1	IP-15 FeTi 1 - IP-15 FeTi 1	IP-15 FeTi 1 - IP-15 FeTi 1	IP-15 FeTi 1 - IP-15 FeTi 1	IP-15 FeTi 1 - IP-15 FeTi 1	IP-15 FeTi 1 - IP-15 FeTi 1					
Pt#	3 Mag	IP-8 Ilm	Mag	24	IP-8 Ilm	Mag	25	Mag a	9	Mag b	11	- Ilm a	10	- Ilm b	12	Mag	13	Ilm	14	
SiO ₂	0.0506	0.0928	0.0553	0.0752	0.0653	0.0562	0.0309	0.0349	0.0741	0.0875										
TiO ₂	20.61	42.12	16.98	37.63	11.81	12.58	40.8	35.29	9.73	47.26										
Al ₂ O ₃	0.3451	0.4577	0.555	0.8375	0.8072	1.1343	0.1357	0.1511	1.6545	0.1521										
Cr ₂ O ₃	0.1511	0.1422	0.151	0.051	1.4622	1.3616	0.4518	0.4049	0.2905	0.0066										
FeO	67.33	45.66	69.87	49.1	71.51	71.03	42.78	49.26	79.56	45.28										
MnO	0.2403	0.1031	0.2411	0.1227	0.3995	0.3777	0.4353	0.424	0.3168	0.7382										
MgO	2.7668	3.48	1.9744	3.46	2.7354	2.532	6.57	4.53	0.8238	3.27										
Total	91.49	92.05	89.83	91.28	88.79	89.07	91.2	90.09	92.44	96.79										

Table 5. Cr-Spinel mineral chemistry.

Label	WC-8 Cr-		WC-11 Cr-		WC-11 Cr-		WC-11 Cr-		WC-11 Cr-		WC-11 Cr-		LC-12 Cr-		LC-12 Cr-		LC-12 Cr-		IP-3 Cr-		IP-3 Cr-		IP-8 Cr-	
	spinel 1	olivine	spinel 1	olivine	spinel 2	olivine	spinel 3	olivine	spinel 4	olivine	spinel 1	olivine	spinel 2	olivine	spinel 3	olivine	spinel 1	olivine	spinel 1	olivine	spinel 2	olivine	spinel 3	olivine
Pt#	28	31	31	33	33	33	34	35	35	36	37	40	40	15	16	17	15	16	17	17	16	17	17	27
SiO ₂	0.0627	0.0607	0.0607	0.0802	0.0802	0.0802	0.0618	0.0609	0.0609	0.0462	0.0822	0.0505	0.0505	0.1447	0.0625	0.086	0.1447	0.0625	0.086	0.1447	0.0625	0.086	0.0489	0.0489
TiO ₂	0.4598	0.5249	0.5249	0.6118	0.6118	0.6118	1.8711	0.5329	0.5329	0.9262	0.8088	0.7552	0.7552	0.7422	1.4244	0.7612	0.7422	1.4244	0.7612	0.7422	1.4244	0.7612	0.6605	0.6605
Al ₂ O ₃	35.33	38.86	38.86	39.19	39.19	39.19	31.64	37.35	37.35	20.26	20.46	20.67	20.67	30.06	23.82	27.05	30.06	23.82	27.05	30.06	23.82	27.05	24.3	24.3
Cr ₂ O ₃	20.44	21.77	21.77	20.18	20.18	20.18	19.63	22.91	22.91	38.59	41.75	43.3	43.3	29.62	29.32	35.62	29.62	29.32	35.62	29.62	29.32	35.62	32.56	32.56
FeO	30.38	23	23	26.54	26.54	26.54	35.95	23.83	23.83	26.81	22.74	20.72	20.72	22.34	31.28	20.4	22.34	31.28	20.4	22.34	31.28	20.4	28.68	28.68
MnO	0.2344	0.2379	0.2379	0.1965	0.1965	0.1965	0.3625	0.2627	0.2627	0.2291	0.2639	0.2643	0.2643	0.217	0.2727	0.2468	0.217	0.2727	0.2468	0.217	0.2727	0.2468	0.22	0.22
MgO	12.66	14.76	14.76	12.54	12.54	12.54	9.65	14.03	14.03	11.36	12.18	13.36	13.36	14.58	11.11	14.96	14.58	11.11	14.96	14.58	11.11	14.96	10.93	10.93
Total	99.58	99.22	99.22	99.34	99.34	99.34	99.17	98.98	98.98	98.22	98.27	99.12	99.12	97.7	97.29	99.13	97.7	97.29	99.13	97.7	97.29	99.13	97.4	97.4

Label	IP-15 Cr-		IP-15 Cr-		IP-15 Cr-		IP-15 Cr-		IP-15 Cr-		IP-15 Cr-		IP-15 Cr-		IP-15 Cr-		IP-15 Cr-		IP-15 Cr-		IP-15 Cr-		IP-15 Cr-	
	spinel 1	olivine	spinel 1b	olivine	spinel 2	olivine	spinel 3	olivine	spinel 4	olivine	spinel 5	olivine	spinel 1	olivine	spinel 2	olivine	spinel 1	olivine	spinel 1	olivine	spinel 1	olivine	spinel 2	olivine
Pt#	3	4	4	5	5	6	6	7	7	8	8	8	45	45	48	48	45	45	45	45	45	48	48	48
SiO ₂	0.0555	0.0909	0.0909	0.1452	0.1452	0.1361	0.1361	0.0801	0.0801	20.05	20.05	20.05	0.2716	0.2716	0.207	0.207	0.2716	0.2716	0.207	0.207	0.2716	0.207	0.207	0.207
TiO ₂	0.6545	0.6091	0.6091	2.2485	2.2485	0.6913	0.6913	0.8203	0.8203	0.3259	0.3259	0.3259	0.9693	0.9693	0.6943	0.6943	0.9693	0.9693	0.6943	0.6943	0.9693	0.6943	0.6943	0.6943
Al ₂ O ₃	24.99	27.54	27.54	17.95	17.95	27.55	27.55	23.78	23.78	10.63	10.63	10.63	29.49	29.49	29.28	29.28	29.49	29.49	29.28	29.28	29.49	29.28	29.28	29.28
Cr ₂ O ₃	33.34	31.78	31.78	30.87	30.87	33.6	33.6	32.72	32.72	15.1	15.1	15.1	25.37	25.37	25.67	25.67	25.37	25.37	25.67	25.67	25.37	25.67	25.67	25.67
FeO	28.37	26.86	26.86	37.07	37.07	23.27	23.27	29.01	29.01	17.55	17.55	17.55	27.39	27.39	27.7	27.7	27.39	27.39	27.7	27.7	27.39	27.7	27.7	27.7
MnO	0.3845	0.3545	0.3545	0.3492	0.3492	0.1931	0.1931	0.3063	0.3063	0.2223	0.2223	0.2223	0.1513	0.1513	0.2469	0.2469	0.1513	0.1513	0.2469	0.2469	0.1513	0.2469	0.2469	0.2469
MgO	10.92	11.65	11.65	8.59	8.59	12.61	12.61	11.1	11.1	33.96	33.96	33.96	12.7	12.7	13.04	13.04	12.7	12.7	13.04	13.04	12.7	13.04	13.04	13.04
Total	98.71	98.89	98.89	97.23	97.23	98.05	98.05	97.83	97.83	97.85	97.85	97.85	96.34	96.34	96.83	96.83	96.34	96.34	96.83	96.83	96.34	96.83	96.83	96.83

All Fe as FeO

Microprobe work completed at the University of Washington, Seattle, Washington.

Table 6. Major and Trace element data from mafic lavas and Glacier Peak dacites.

Sample:	GP-1	GP-3	GP-6	GP-7	GP-8	GP-9	GP-11	GP-12	GP-13	GP-14
Lab:	USGS	USGS	WSU	USGS	WSU	USGS	USGS	USGS	USGS	USGS
Location:	Glacier Peak	Glacier Peak	Glacier Peak	Glacier Peak	Glacier Peak	Glacier Peak	Glacier Peak	Glacier Peak	Glacier Peak	Glacier Peak
<i>wt. %</i>										
SiO ₂	64.6	62	65.34	62.8	63.06	60.2	61.8	62	62.9	62.5
TiO ₂	0.61	0.69	0.589	0.65	0.678	0.81	0.66	0.67	0.64	0.7
Al ₂ O ₃	16.3	16.8	16.55	16.5	16.9	17	16.8	16.4	16.6	16.8
FeO*	4.09	4.67	4.13	4.40	4.47	5.09	4.42	4.36	4.26	4.72
MnO	0.08	0.1	0.082	0.06	0.087	0.1	0.08	0.07	0.07	0.09
MgO	2.42	2.87	2.39	2.23	3.25	3.94	2.54	2.87	2.46	2.85
CaO	4.75	5.13	4.8	4.77	5.58	6.18	5.41	5.3	5.16	5.35
Na ₂ O	3.93	3.68	4.29	3.56	4.21	3.77	3.77	3.75	3.87	3.84
K ₂ O	2.02	1.78	2.05	1.96	1.77	1.51	1.84	1.87	1.92	1.7
P ₂ O ₅	0.2	0.23	0.152	0.18	0.154	0.23	0.24	0.23	0.22	0.24
LOI	0.06	1.14		1.75		0.33	1.39	1.15	1.04	0.34
Total	99.06	99.09	100.38	98.86	100.15	99.16	98.95	98.67	99.14	99.13
Mg#	53.93	54.90	53.38	50.09	59.04	60.51	53.24	56.62	53.37	54.49
Trace Elements (ppm):										
Ni	14	16	15	20	40	49	27	26	22	30
Cr	11	13	11	17	50	54	29	31	28	32
V	65	75	79	81	91	91	81	79	73	77
Ba	533	518	512	584	458	418	441	408	502	462
Rb	41	32	38	38	34	28	34	36	37	32
Sr	451	540	456	490	465	477	583	556	550	477
Zr	138	139	140	153	136	135	133	139	137	137
Y	15	15	15	15	17	17	18	16	16	17
Nb	6	6	6.3	6	6.4	5	6	6	6	6
Cu	12	18	9	23	20	18	23	14	13	19
Zn	55	63	59	58	57	61	64	61	57	65
Ba	480.00	468.00	501.67	473.00	459.49	387.00	436.00	436.00	459.00	437.00
Th	5.27	5.20	5.44	5.07	5.10	4.00	5.20	5.38	5.67	4.58
Hf	3.55	3.56	3.60		3.74					
Ta	0.42	0.42	0.42	0.43	0.41	0.37	0.38	0.39	0.40	0.40
U	2.18	1.95	1.86	2.16	1.78	1.48	2.03	2.04	2.18	1.77
Pb			9.11		8.66					
Rb	40.60	32.40	38.65	39.70	35.09	30.90	34.30	35.80	37.90	33.80
Cs	1.57	1.31	1.59	1.31	0.89	1.22	1.20	0.89	1.19	0.95
Sr	477.00	571.00	458.94	521.00	459.80	505.00	615.00	553.00	588.00	492.00
Sc	11.90	13.50	12.54	13.10	16.37	17.00	12.70	12.70	12.40	14.40
La	16.20	17.90	16.12	14.80	15.92	14.00	17.90	17.10	18.00	16.40
Ce	32.40	36.60	30.94	29.90	31.18	30.80	35.20	34.30	35.20	32.30
Pr			3.56		3.65					
Nd	15.60	19.00	14.13	15.70	14.89	15.40	19.60	18.10	18.80	17.70
Sm	3.47	3.81	3.20	3.49	3.50	3.60	4.12	3.84	3.91	3.89
Eu	0.87	0.95	0.91	0.92	1.00	0.97	1.00	0.95	0.96	1.01
Gd			2.87		3.29					
Tb	0.43	0.49	0.46	0.44	0.53	0.48	0.50	0.43	0.47	0.50
Dy			2.77		3.24					
Ho			0.58		0.67					
Er			1.61		1.81					
Tm			0.24		0.27					
Yb	1.70	1.73	1.56	1.74	1.77	1.85	1.77	1.65	1.68	1.82
Lu	0.25	0.26	0.25	0.26	0.28	0.27	0.27	0.25	0.26	0.29

Distinctions between Washington State University (WSU) and the U.S. Geological Survey (USGS) labs are labeled at the top.

Ni through Zn are analyzed by XRF. Ba through Lu are analyzed by ICP-MS (WSU) and INAA (USGS).

Ba, Rb, and Sr are reported for both methods of analyses. INAA (USGS) does not analyze for Pb, Dy, Ho, Er, and Tm.

USGS XRF by David Seims, INAA by James Budahn.

All Fe as FeO*.

Table 6. (cont.) Major and Trace element data from primitive lavas and Glacier Peak dacites.

Sample:	LC-1	LC-2	LC-3	LC-4	LC-5	LC-6	LC-7	LC9	LC-10	LC-11
Lab:	WSU	USGS	USGS	WSU	USGS	WSU	USGS	WSU	USGS	USGS
Location:	Lightning Creek	Lightning Creek	Lightning Creek	Lightning Creek	Lightning Creek	Lightning Creek	Lightning Creek	Lightning Creek	Lightning Creek	Lightning Creek
wt. %										
SiO ₂	55.29	54.2	55.2	55.62	56.6	55.12	56.5	57.43	57	55.5
TiO ₂	1.09	1.11	1.06	1.04	1.01	1.087	0.97	0.944	0.96	1.06
Al ₂ O ₃	16.5	16.2	16.3	16.26	16.4	16.24	16	16.24	15.9	16.3
FeO*	6.55	6.47	6.24	6.40	6.03	6.33	5.88	5.91	5.88	6.17
MnO	0.117	0.12	0.11	0.115	0.11	0.117	0.11	0.109	0.11	0.11
MgO	7.1	7.35	6.89	7.19	6.15	7.47	6.54	6.8	6.44	6.64
CaO	8.22	8.37	7.97	8.12	7.5	8.64	7.19	7.39	7.06	7.8
Na ₂ O	3.63	3.28	3.35	3.56	3.42	3.4	3.39	3.59	3.41	3.35
K ₂ O	1.05	0.93	1.07	1.07	1.22	0.87	1.2	1.19	1.28	1.1
P ₂ O ₅	0.274	0.31	0.31	0.263	0.31	0.259	0.28	0.232	0.28	0.31
LOI		0.42	0.44		0.56		0.09		0.55	0.41
Total	99.82	98.76	98.94	99.64	99.31	99.54	98.15	99.83	98.87	98.75
Mg#	68.24	69.23	68.60	68.98	66.89	70.02	68.79	69.50	68.43	68.05
Trace Elements (ppm):										
Ni	117	129	121	127	109	119	121	131	115	124
Cr	244	211	205	248	169	260	181	244	182	204
V	140	142	148	148	145	153	122	126	130	151
Ba	426	431	443	424	439	336	423	397	457	462
Rb	18	17	19	18	23	13	23	21	25	20
Sr	787	836	781	783	752	857	729	710	713	796
Zr	170	173	170	162	175	154	165	156	167	172
Y	19	19	19	19	18	20	18	19	20	19
Nb	5.7	4	6	4.8	5	5.4	6	5.4	6	5
Cu	36	47	40	38	37	32	32	35	29	45
Zn	65	65	65	64	67	59	62	58	63	67
Ba	429.27	393.00	402.00	416.66	434.00	334.78	411.00	401.97	404.00	417.00
Th	3.66	3.37	3.43	3.54	3.84	2.84	3.82	3.66	3.91	3.72
Hf	4.26	4.29	4.15	4.09	4.14	3.93	4.14	3.97	4.08	4.27
Ta	0.28	0.27	0.29	0.28	0.33	0.26	0.34	0.31	0.35	0.31
U	1.09	1.20	1.24	1.08	1.38	0.85	1.48	1.15	1.40	1.31
Pb	5.09			5.11		4.97		5.75		
Rb	17.57	18.60	19.90	18.80	25.00	13.32	24.20	20.72	25.80	22.10
Cs	0.58	0.48	0.59	0.58	0.67	1.48	0.51	1.61	0.86	0.63
Sr	831.91	912.00	874.00	829.49	788.00	823.29	801.00	669.33	774.00	872.00
Sc	26.77	24.90	22.50	25.40	20.80	22.63	21.50	19.36	20.40	22.60
La	22.28	22.80	21.70	21.22	21.30	20.21	21.10	19.44	21.00	22.40
Ce	48.91	51.20	49.30	45.84	47.90	44.84	45.90	41.94	46.50	50.70
Pr	6.04			5.65		5.61		5.19		
Nd	25.25	29.20	26.50	23.54	25.70	23.24	25.60	21.36	24.70	27.60
Sm	5.36	5.70	5.20	4.96	5.11	4.86	5.09	4.67	4.85	5.32
Eu	1.59	1.50	1.43	1.50	1.38	1.51	1.35	1.40	1.33	1.45
Gd	4.41			4.18		4.12		3.89		
Tb	0.67	0.64	0.59	0.63	0.57	0.63	0.55	0.61	0.57	0.59
Dy	4.02			3.69		3.63		3.59		
Ho	0.79			0.73		0.71		0.69		
Er	2.10			1.95		1.89		1.87		
Tm	0.29			0.28		0.27		0.27		
Yb	1.83	1.94	1.92	1.74	1.91	1.63	1.98	1.67	1.93	1.93
Lu	0.28	0.30	0.29	0.27	0.29	0.26	0.29	0.26	0.28	0.31

Distinctions between Washington State University (WSU) and the U.S. Geological Survey (USGS) labs are labeled at the top.

Ni through Zn are analyzed by XRF. Ba through Lu are analyzed by ICP-MS (WSU) and INAA (USGS).

Ba, Rb, and Sr are reported for both methods of analyses. INAA (USGS) does not analyze for Pb, Dy, Ho, Er, and Tm.

USGS XRF by David Seims, INAA by James Budahn.

All Fe as FeO*.

Table 6. (cont.) Major and Trace element data from mafic lavas and Glacier Peak dacites.

Sample:	LC-12	LC-13	WC-1	WC-4	WC-7	WC-8	WC-11	WC-12	WC-13	WC-15
Lab:	USGS	USGS	USGS	USGS	USGS	WSU	WSU	USGS	WSU	USGS
Location:	Lightning Creek	Lightning Creek	Whitechuck	Whitechuck	Whitechuck	Whitechuck	Whitechuck	Whitechuck	Whitechuck	Whitechuck
wt. %										
SiO ₂	54	57.2	50.1	50.3	50.3	50.61	51.07	50.6	51.63	50.5
TiO ₂	1.08	0.96	1.09	1.08	1.09	1.087	1.097	1.11	1.074	1.12
Al ₂ O ₃	16.4	16.2	18.1	18	18.1	18.13	17.98	18.1	17.96	17.9
FeO*	6.46	5.84	8.07	8.07	8.13	8.28	8.26	8.13	8.15	8.11
MnO	0.12	0.11	0.15	0.15	0.15	0.151	0.151	0.15	0.15	0.15
MgO	7.67	6.23	7.42	7.47	7.62	7.6	7.53	7.39	7.29	7.37
CaO	8.54	7.19	9.49	9.55	9.62	9.94	9.92	9.8	9.56	9.61
Na ₂ O	3.16	3.47	3.15	3.14	3.15	3.41	3.38	3.15	3.41	3.15
K ₂ O	0.82	1.25	0.39	0.42	0.38	0.4	0.4	0.4	0.45	0.42
P ₂ O ₅	0.3	0.28	0.22	0.22	0.23	0.174	0.174	0.22	0.177	0.23
LOI	0.15	-0.02	0.44	0.3	-0.04			0		-0.04
Total	98.70	98.71	98.62	98.70	98.73	99.78	99.97	99.05	99.85	98.52
Mg#	70.16	67.87	64.55	64.70	65.00	64.51	64.34	64.30	63.93	64.29
Trace Elements (ppm):										
Ni	140	108	62	68	71	66	59	60	57	60
Cr	244	175	169	170	179	182	181	153	176	153
V	152	129	222	217	199	182	186	176	184	182
Ba	388	417	95	92	103	101	100	100	114	103
Rb	14	22	5	5	4	3	4	4	4	5
Sr	897	728	532	537	535	534	530	546	521	543
Zr	162	169	98	97	96	95	95	96	98	102
Y	19	20	22	21	22	22	21	21	21	23
Nb	6	6	3	2	3	2.2	2.6	3	3	3
Cu	42	36	35	32	36	35	30	31	32	37
Zn	66	59	72	73	81	73	77	77	73	74
Ba	334.00	423.00	92.70	122.00	75.10	93.95	90.58	86.80	108.48	97.90
Th	2.86	3.86	0.74	0.72	0.67	0.79	0.77	0.69	0.88	0.67
Hf	4.08	4.13	2.34	2.33	2.27	2.25	2.28	2.24	2.35	2.29
Ta	0.28	0.34	0.10	0.10	0.10	0.09	0.09	0.09	0.10	0.10
U	0.98	1.40	0.26	0.19	0.22	0.21	0.20	0.29	0.24	0.22
Pb						2.35	2.32		3.11	
Rb	16.90	22.40	8.42	7.37	12.20	3.85	2.92	6.23	4.77	5.21
Cs	0.38	0.31	0.18	0.15	0.07	0.10	0.10	0.09	1.23	0.14
Sr	986.00	769.00	585.00	589.00	602.00	564.98	551.03	569.00	501.77	555.00
Sc	24.90	20.50	31.90	31.50	31.70	34.58	33.57	31.40	29.36	31.30
La	21.00	20.70	5.95	6.11	5.79	6.16	6.00	6.00	6.59	6.15
Ce	49.20	45.90	16.00	16.50	15.70	15.62	15.58	16.50	16.47	16.10
Pr						2.28	2.29		2.36	
Nd	26.60	24.90	12.40	12.80	12.20	11.28	11.44	12.50	11.61	12.10
Sm	5.09	4.89	3.64	3.59	3.41	3.26	3.29	3.35	3.37	3.44
Eu	1.45	1.34	1.19	1.18	1.20	1.22	1.27	1.18	1.27	1.18
Gd						3.63	3.65		3.63	
Tb	0.58	0.55	0.58	0.60	0.55	0.62	0.63	0.58	0.63	0.62
Dy						4.02	3.98		3.99	
Ho						0.83	0.85		0.83	
Er						2.25	2.32		2.31	
Tm						0.33	0.33		0.33	
Yb	1.83	1.90	2.35	2.28	2.38	2.08	2.05	2.28	2.07	2.39
Lu	0.29	0.29	0.35	0.35	0.36	0.33	0.32	0.34	0.33	0.35

Distinctions between Washington State University (WSU) and the U.S. Geological Survey (USGS) labs are tabulated at the top.

Ni through Zn are analyzed by XRF. Ba through Lu are analyzed by ICP-MS (WSU) and INAA (USGS).

Ba, Rb, and Sr are reported for both methods of analyses. INAA (USGS) does not analyze for Pb, Dy, Ho, Er, and Tm.

USGS XRF by David Seims, INAA by James Budahn.

All Fe as FeO*.

Table 6. (cont.) Major and Trace element data from mafic lavas and Glacier Peak dacites.

Sample:	WC-16	WC-17	IP-1	IP-2	IP-3	IP-4	IP-5	IP-7	IP-8	IP-10
Lab:	WSU	USGS	USGS	USGS	USGS	USGS	WSU	USGS	WSU	WSU
Location:	Whitechuck	Whitechuck	Indian Pass	Indian Pass	Indian Pass	Indian Pass	Indian Pass	Indian Pass	Indian Pass	Indian Pass
wt. %										
SiO ₂	50.93	50.4	51.2	52.1	50.7	51.9	52.83	52.3	52.47	52.33
TiO ₂	1.107	1.1	1.17	1.15	1.16	1.15	1.139	1.13	1.146	1.142
Al ₂ O ₃	18.29	18.1	16.6	17.1	16.5	17.1	17.17	17.1	17.08	17.14
FeO*	7.92	8.13	7.31	7.26	7.55	7.30	7.07	7.20	7.10	7.56
MnO	0.154	0.15	0.13	0.13	0.13	0.13	0.134	0.13	0.133	0.134
MgO	7.62	7.43	8.19	7.73	9.05	7.71	7.79	7.54	7.96	8.22
CaO	9.49	9.77	8.65	8.23	8.52	8.16	8.33	8.18	8.4	8.36
Na ₂ O	3.3	3.15	3.69	3.77	3.61	3.76	4.05	3.85	4.05	4.09
K ₂ O	0.42	0.39	0.92	0.86	0.82	0.87	0.89	0.88	0.89	0.88
P ₂ O ₅	0.175	0.23	0.46	0.42	0.43	0.41	0.384	0.42	0.388	0.379
LOI		-0.09	0.31	0.23	0.19	0.33		0.07		
Total	99.41	98.76	98.63	98.98	98.66	98.82	99.79	98.80	99.62	100.23
Mg#	65.57	64.43	68.94	67.83	70.36	67.66	68.56	67.47	68.95	68.30
Trace Elements (ppm):										
Ni	64	61	175	154	217	168	160	159	164	172
Cr	189	166	273	214	307	222	260	219	266	267
V	195	215	165	144	165	151	166	149	170	147
Ba	93	91	398	314	330	333	262	271	278	274
Rb	5	4	11	11	10	11	12	10	12	10
Sr	504	543	1030	871	964	858	837	866	850	859
Zr	97	99	141	144	139	143	140	144	140	138
Y	20	22	19	21	18	20	20	20	19	19
Nb	2.5	3	7	8	7	8	7.3	8	7.9	7.3
Cu	28	39	35	32	36	36	31	32	30	29
Zn	75	75	91	83	86	84	76	82	77	83
Ba	93.08	92.20	341.00	264.00	289.00	263.00	273.80	275.00	273.23	274.15
Th	0.75	0.69	2.36	1.83	2.04	1.85	1.92	1.94	1.91	1.91
Hf	2.22	2.36					3.13		3.03	3.13
Ta	0.09	0.08	0.37	0.41	0.38	0.41	0.39	0.41	0.38	0.41
U	0.20	0.22	0.82	0.71	0.71	0.69	0.59	0.72	0.59	0.56
Pb	2.59						4.71		4.80	4.53
Rb	3.71	4.63	13.40	13.30	11.00	11.90	9.92	12.00	9.86	9.69
Cs	1.17	0.10	0.30	0.23	0.28	0.22	1.28	0.13	1.17	0.13
Sr	477.91	576.00	1060.00	914.00	1040.00	902.00	807.42	906.00	817.76	883.08
Sc	27.20	31.50	23.20	22.60	23.80	22.40	21.72	22.10	21.97	24.25
La	5.47	5.90	19.70	16.80	18.50	17.00	16.91	17.00	16.87	17.09
Ce	14.59	15.70	45.00	39.40	43.10	39.50	36.59	39.10	36.54	37.19
Pr	2.15						4.69		4.62	4.75
Nd	10.61	12.50	24.90	22.70	24.80	21.80	20.14	21.60	19.95	20.20
Sm	3.18	3.46	4.98	4.60	4.87	4.62	4.47	4.58	4.48	4.51
Eu	1.25	1.17	1.46	1.41	1.45	1.37	1.48	1.39	1.48	1.52
Gd	3.57						4.11		4.07	4.08
Tb	0.60	0.59	0.59	0.58	0.60	0.58	0.64	0.59	0.63	0.64
Dy	3.90						3.85		3.78	3.74
Ho	0.80						0.77		0.74	0.77
Er	2.22						2.05		2.00	2.09
Tm	0.32						0.29		0.29	0.28
Yb	1.97	2.29	1.93	1.95	1.97	1.97	1.79	2.03	1.75	1.78
Lu	0.32	0.34	0.28	0.29	0.28	0.29	0.29	0.29	0.28	0.28

Distinctions between Washington State University (WSU) and the U.S. Geological Survey (USGS) labs are labeled at the top.

Ni through Zn are analyzed by XRF. Ba through Lu are analyzed by ICP-MS (WSU) and INAA (USGS).

Ba, Rb, and Sr are reported for both methods of analyses. INAA (USGS) does not analyze for Pb, Dy, Ho, Er, and Tm.

USGS XRF by David Seims, INAA by James Budahn.

All Fe as FeO*.

Table 6. (cont.) Major and Trace element data from mafic lavas and Glacier Peak dacites.

Sample:	IP-11	IP-12	IP-13	IP-15	DG-2	DG-3	DG4	DG-5	DG-6	DG-7
Lab:	USGS	USGS	USGS	WSU	USGS	USGS	WSU	WSU	USGS	USGS
Location:	Indian Pass	Indian Pass	Indian Pass	Indian Pass	Dishpan Gap	Dishpan Gap	Dishpan Gap	Dishpan Gap	Dishpan Gap	Dishpan Gap
wt. %										
SiO ₂	51.8	52.2	52.2	52.29	52.6	54.6	55.1	53.84	54.5	54.4
TiO ₂	1.14	1.15	1.15	1.126	1.24	1.09	1.103	1.349	1.06	1.1
Al ₂ O ₃	17.1	17.2	17.1	17.23	17.6	17.2	17.03	17.68	17.3	16.7
FeO*	7.31	7.24	7.24	7.48	7.40	6.87	6.84	7.79	6.72	6.97
MnO	0.13	0.13	0.13	0.135	0.13	0.13	0.13	0.137	0.13	0.13
MgO	7.91	7.61	7.64	7.98	5.56	5.78	5.95	4.95	5.7	5.92
CaO	8.22	8.2	8.24	8.36	8.66	8.14	8.39	8.64	8.16	8.13
Na ₂ O	3.77	3.86	3.79	4.01	3.61	3.54	3.74	4.17	3.52	3.55
K ₂ O	0.87	0.89	0.89	0.88	0.95	1.05	1.06	1.05	1.06	1.08
P ₂ O ₅	0.43	0.41	0.43	0.382	0.28	0.26	0.211	0.263	0.26	0.25
LOI	0.21	0	0		0.1	0.24			0.16	0.34
Total	98.89	98.89	98.81	99.87	98.13	98.90	99.55	99.87	98.57	98.57
Mg#	68.19	67.54	67.63	67.88	59.82	62.51	63.28	55.72	62.68	62.70
Trace Elements (ppm):										
Ni	172	156	168	165	41	56	56	24	57	61
Cr	234	216	216	260	105	123	151	67	128	131
V	150	142	146	140	191	160	167	188	156	152
Ba	288	319	322	276	353	344	325	372	318	372
Rb	11	12	11	11	16	19	17	14	19	20
Sr	874	875	867	850	696	657	634	687	661	643
Zr	140	145	143	137	144	142	136	148	139	145
Y	18	20	19	18	23	22	21	24	21	20
Nb	6	8	8	7.5	4	5	4.7	4.4	4	4
Cu	16	32	39	37	36	37	37	30	37	40
Zn	85	78	81	83	74	76	77	80	77	73
Ba	274.00	277.00	267.00	277.43	298.00	328.00	328.44	364.02	336.00	304.00
Th	1.85	1.89	1.86	1.91	3.01	3.32	3.36	3.38	3.27	3.27
Hf				3.05	3.30	3.36	3.32	3.60	3.22	3.23
Ta	0.40	0.42	0.41	0.41	0.23	0.26	0.24	0.25	0.26	0.24
U	0.69	0.70	0.69	0.57	0.87	1.05	0.95	0.83	1.09	1.06
Pb				4.59			5.58	5.06		
Rb	11.40	12.50	13.90	9.37	16.60	19.50	16.03	15.34	20.60	19.20
Cs	0.18	0.21	0.17	0.17	0.40	0.12	1.58	0.44	0.47	0.54
Sr	922.00	924.00	915.00	879.14	736.00	752.00	615.62	709.69	708.00	649.00
Sc	22.10	22.50	22.30	24.33	27.20	26.20	24.64	29.45	25.40	26.00
La	16.90	17.30	17.10	16.71	18.10	16.50	16.52	19.19	16.20	16.70
Ce	38.60	40.20	39.40	36.32	38.90	36.30	34.63	41.48	35.90	36.20
Pr				4.62			4.35	5.24		
Nd	22.10	22.20	21.90	19.95	22.60	20.70	18.62	22.65	20.80	20.00
Sm	4.56	4.66	4.60	4.44	4.84	4.42	4.34	5.23	4.44	4.37
Eu	1.37	1.41	1.39	1.48	1.43	1.34	1.43	1.67	1.36	1.29
Gd				4.07			4.16	4.82		
Tb	0.56	0.57	0.58	0.64	0.63	0.58	0.68	0.78	0.61	0.61
Dy				3.74			4.14	4.82		
Ho				0.76			0.85	0.98		
Er				2.02			2.31	2.67		
Tm				0.29			0.33	0.39		
Yb	1.95	2.01	1.97	1.75	2.39	2.22	2.03	2.35	2.22	2.23
Lu				0.28	0.37	0.34	0.33	0.37	0.34	0.34

Distinctions between Washington State University (WSU) and the U.S. Geological Survey (USGS) labs are tabled at the top.

Ni through Zn are analyzed by XRF. Ba through Lu are analyzed by ICP-MS (WSU) and INAA (USGS).

Ba, Rb, and Sr are reported for both methods of analyses. INAA (USGS) does not analyze for Pb, Dy, Ho, Er, and Tm.

USGS XRF by David Seims, INAA by James Budahn.

All Fe as FeO*.

Table 6. (cont.) Major and Trace element data from mafic lavas and Glacier Peak dacites.

Sample:	DG-8	DG-9	DG-11	DG-13	DG-14	DG-15
Lab:	WSU	USGS	WSU	USGS	USGS	USGS
Location:	Dishpan Gap	Dishpan Gap	Dishpan Gap	Dishpan Gap	Dishpan Gap	Dishpan Gap
<i>wt. %</i>						
SiO ₂	56.1	52.7	53.59	53	53.8	55.1
TiO ₂	1.047	1.32	1.331	1.25	1.26	1.11
Al ₂ O ₃	16.73	17.6	17.77	17.4	17.6	17.1
FeO*	6.37	7.66	7.77	7.44	7.25	6.74
MnO	0.125	0.14	0.14	0.14	0.13	0.13
MgO	5.64	5.51	5.17	5.79	5.02	5.47
CaO	7.91	8.88	8.74	8.78	8.37	8.06
Na ₂ O	3.78	3.72	4.17	3.65	3.81	3.66
K ₂ O	1.2	0.87	1	0.95	1.04	1.11
P ₂ O ₅	0.207	0.29	0.261	0.27	0.29	0.26
LOI		0.25		0.14	0.16	0
Total	99.11	98.94	99.94	98.81	98.73	98.74
Mg#	63.69	58.76	56.86	60.64	57.82	61.65
<i>Trace Elements (ppm):</i>						
Ni	56	33	31	47	32	50
Cr	145	86	85	105	73	97
V	158	187	189	174	173	139
Ba	345	333	358	331	402	375
Rb	21	14	14	15	17	20
Sr	614	703	694	693	699	670
Zr	138	145	146	142	148	144
Y	21	23	24	21	23	22
Nb	3.9	3	4.2	4	4	5
Cu	33	37	32	38	36	40
Zn	66	73	76	71	77	67
Ba	397.54	311.00	353.21	322.00	338.00	329.00
Th	4.28	2.90	3.21	3.01	3.27	3.28
Hf	3.94	3.27	3.51	3.37	3.27	3.20
Ta	0.30	0.21	0.24	0.22	0.23	0.25
U	1.28	0.89	0.81	0.91	1.03	1.07
Pb	7.12		5.05			
Rb	23.04	16.60	14.97	18.10	17.80	19.90
Cs	2.03	0.30	0.43	0.48	0.53	0.21
Sr	658.05	727.00	729.52	751.00	741.00	677.00
Sc	26.13	28.30	29.67	28.60	25.40	24.30
La	19.11	18.00	18.79	17.60	18.40	17.20
Ce	39.77	40.30	40.17	40.20	40.10	36.60
Pr	4.92		5.10			
Nd	21.09	22.70	21.95	22.70	22.20	19.90
Sm	4.87	5.04	5.10	4.95	4.94	4.39
Eu	1.56	1.52	1.67	1.50	1.45	1.29
Gd	4.61		4.82			
Tb	0.74	0.69	0.78	0.65	0.66	0.60
Dy	4.62		4.77			
Ho	0.94		0.95			
Er	2.55		2.60			
Tm	0.37		0.37			
Yb	2.27	2.54	2.30	2.40	2.33	2.05
Lu	0.36	0.37	0.36	0.38	0.35	0.32

Distinctions between Washington State University (WSU) and the U.S. Geological Survey (USGS) labs are labeled at the top.

Ni through Zn are analyzed by XRF. Ba through Lu are analyzed by ICP-MS (WSU) and INAA (USGS).

Ba, Rb, and Sr are reported for both methods of analyses. INAA (USGS) does not analyze for Pb, Dy, Ho, Er, and Tm.

USGS XRF by David Seims, INAA by James Budahn.

All Fe as FeO*.

RESULTS

Petrography

A brief description of the mineralogy of the Glacier Peak dacites and four nearby mafic flows is presented in Tabor and Crowder (1969). Table 7 provides a summary of important petrographic observations from each flow.

HAOT from Whitechuck are nearly aphyric (most samples have $\leq 5\%$ phenocrysts ranging from 0.2-1mm) and have sub- to euhedral olivine \pm rare plagioclase occurring in an intergranular to pilotaxitic groundmass composed of plagioclase, clinopyroxene, olivine, and Fe-Ti oxides (larger olivine phenocrysts contain inclusions of Cr-spinel). Abnormally large plagioclase megacrysts (5-7mm) and medium sized glomerocrysts (1-4mm) of olivine + plagioclase \pm rare clinopyroxene were observed in a few samples from the upper flow (WC-7, WC-12). This is an uncommon characteristic of Cascades lavas but one that is shared by other Cascades tholeiitic lavas [e.g. Indian Heaven volcanic field in southern Washington (Leeman et al. 1990) and Medicine Lake volcanic field (Bacon et al. 1997)]. No alteration was observed in any of the samples, and weathering is confined to fractures, joints, and exposed surfaces. The texture, phenocryst assemblage, and presence of glomerocrysts are all characteristics shared by primitive HAOT lavas in the Central and Southern Cascades (Leeman et al. 1990; Baker et al. 1994; Bacon et al. 1997; Clynne and Borg 1997).

Calc-alkaline lavas from Indian Pass, Lightning Creek, and Dishpan Gap can be distinguished on the basis of several textural and mineralogical differences. The least evolved flow of Indian Pass is nearly aphyric to slightly porphyritic (1-10% phenocrysts) with average groundmass size in the range of 20-100 μ m. Most Indian Pass samples are

vesicular, and contain sub- to euhedral olivine \pm subhedral clinopyroxene in a fine pilotaxitic to intergranular groundmass rich in oxides. Most olivine phenocrysts contain Cr-spinel inclusions, and make up 3-7% of the rock. In some samples, extremely rare xenocrysts of quartz and sodic plagioclase show evidence of shallow level incorporation of crustal material. In hand samples, it is apparent that most of these samples are oxidized to some degree, but no other alteration or pervasive weathering is noticeable.

Lightning Creek and Dishpan Gap samples have higher phenocryst contents (8-30%) and a generally coarser groundmass (75-400 μ m) than the Indian Pass lavas. The Lightning Creek and Dishpan Gap lavas are both massive basaltic andesites, which contain olivine + clinopyroxene + plagioclase \pm rare orthopyroxene phenocrysts in an intergranular to intersertal groundmass composed of plagioclase laths, clinopyroxene, and sparse Fe-Ti oxides. The primary mineralogical difference between the two flows is the greater amount of olivine in the Lightning Creek flow (up to \sim 10%). Clinopyroxene is more abundant at Lightning Creek and Dishpan Gap than in other localities. Both flows contain more clinopyroxene (\leq 3% of rock) than the other localities. Larger olivine phenocrysts in both flows contain Cr-spinel inclusions. Glomerocrysts (1-3 mm) composed of plagioclase \pm clinopyroxene are found in some samples from each flow. Rounded crustal xenoliths of polycrystalline equigranular feldspar (3-15 mm) are present in a small number of samples from Dishpan Gap but were not found in any of the polished sections used for microprobe analysis. One sample (LC-6) from Lightning Creek contains a fine-grained blob of basaltic material (\sim 1cm). However, it was not determined whether the blob represented a crustal xenolith or a quenched remnant of a mingling event. No alteration was present in any of the samples, and weathering was confined to

exposed faces only. Magnesian basaltic andesites with characteristics similar to the Lightning Creek flow are located elsewhere in the Cascades (Baker et al. 1994; Bacon et al. 1997).

Table 7. Petrographic characteristics of the four mafic flows.

	Whitechuck basalt	Indian Pass basaltic andesite	Lightning Creek basaltic andesite	Dishpan Gap basaltic andesite
<u>Phenocrysts</u>				
Olivine				
size	100-600 μ m	100 μ m-1.5mm	400-900 μ m	300-800 μ m
abundance	1-4%	3-7%	4-8%	2-3%
shape	resorbed (small) euhedral	sub- to euhedral	sub- to euhedral	sub- to euhedral, resorbed
<u>Plagioclase</u>				
size	1-2mm	1-2mm	0.5-2mm	0.5-2mm
abundance	0-4%	0-2%	10-20%	15-22%
shape	resorbed to euhedral	resorbed to euhedral	sub- to euhedral	sub- to euhedral
<u>Clinopyroxene</u>				
size	groundmass only	groundmass only	100 μ m-1mm	100 μ m-1mm
abundance	-	-	3-6%	1-3%
shape	-	-	sub- to anhedral	sub- to anhedral
<u>Orthopyroxene</u>				
size	not present	not present	groundmass only	200-400 μ m
abundance	-	-	trace	trace
shape	-	-	-	an- to subhedral
<u>Groundmass</u>				
size	50-150 μ m	20-100 μ m	75-400 μ m	75-400 μ m
<u>Xenoliths and xenocrysts</u>				
size	<500 μ m	<500 μ m	up to 3cm	up to 3cm
abundance	very rare	very rare	rare	rare
<u>Alteration</u>				
	Weathering on joints and exposed surfaces.	fresh to oxidized	Weathering on joints and exposed surfaces.	Weathering on joints and exposed surfaces

Mineral Chemistry

Olivine

Olivine is the most abundant phenocryst phase from the Whitechuck HAOT, with core compositions in the range of Fo₈₄₋₈₆ and rim compositions in the range of Fo₆₅₋₇₈ (Table 1). Whitechuck olivines have the highest concentration and range in Ca content (0.15-0.27 wt.% CaO) of the four chosen flows. NiO concentrations are in the range of 0-0.13wt.%, lower than any of the calc-alkaline flows except for Dishpan Gap.

The most magnesian olivine phenocrysts occur at Lightning Creek (with cores in the range of Fo₈₄₋₈₉ and rims in the range of Fo₇₅₋₈₂) and at Indian Pass (Fo₈₅₋₈₈ cores, Fo₇₅₋₈₅ rims; Table 1). Ca concentrations for both flows are similar, ranging between 0.15 and 0.20 wt.% CaO. Ni is relatively high in both flows, often exceeding 0.35 wt.% NiO in olivine cores.

Olivine phenocrysts at Dishpan Gap differ noticeably from the other flows in that the phenocrysts tend to be larger (some exceed 1 mm, see Table 6), and yet are less common (<~8% of rock) and have significantly lower Mg (Fo₆₈₋₇₈ cores and Fo₆₇₋₇₆ rims) and Ni (0-0.09 wt.% NiO; Table 1). One magnesian olivine phenocryst (Fo₈₆) was observed in sample DG-11, and could represent a xenocryst. Ca contents are similar to other chosen calc-alkaline flows, ranging from 0.1-0.2 wt.% CaO.

Pyroxene

No clinopyroxene phenocrysts were found in Whitechuck HAOT during microprobe analysis. Several groundmass pyroxenes were analyzed and have compositions averaging Wo₃₈En₄₆Fs₁₇ and Mg# values ranging from 70-77, for all Fe as Fe²⁺. These groundmass grains are lower in Ca (16-18 wt.% CaO) and Cr (0-0.4 wt.%

Cr₂O₃) than the calc-alkaline flows, and otherwise fall along similar clinopyroxene trends (Table 2).

In Indian Pass lavas, as in Whitechuck HAOT, no pyroxene phenocrysts were found. All reported analyses are of groundmass grains with average compositions ranging near Wo₄₂En₄₅Fs₁₃ (Fig. 7) and Mg# values in the range of 74-80. One groundmass grain in sample IH-15 contained orthopyroxene of composition Wo₂₈En₅₃Fs₁₉ with an Mg# of 74, which may be a microxenocryst. Clinopyroxene from Indian Pass have slightly higher Ti (0.8-1.6 wt.% TiO₂) and similar amounts of CaO (20-23 wt.%) and Cr₂O₃ (0-0.4 wt.%) as lavas from Whitechuck and Dishpan Gap.

Lightning Creek and Dishpan Gap lavas are richer in clinopyroxene phenocrysts and both have minor populations of orthopyroxene, although these are present only as microphenocrysts in the Lightning Creek rocks. Clinopyroxene compositions in the two flows are similar, approximately Wo₄₃En₄₆Fs₁₂ (Fig. 7), with Mg# values of 74-86 for Lightning Creek and 76-83 for Dishpan Gap. Orthopyroxene values differ slightly; Lightning Creek orthopyroxene average Wo₉En₇₁Fs₂₀ and Dishpan Gap orthopyroxene average Wo₂En₆₈Fs₂₅. Clinopyroxene Ti and Ca contents (0.2-1.0 wt.% TiO₂; 19-23 wt.% CaO) do not vary between the two flows. However, the Lightning Creek samples are unique in terms of Cr content and disequilibrium features. Lightning Creek clinopyroxene has 2-10 times the concentration of Cr₂O₃ (0.2-1.0 wt.%) for similar amounts of MgO. Fig. 8 shows a microprobe image of the relationship between clinopyroxene and orthopyroxene in

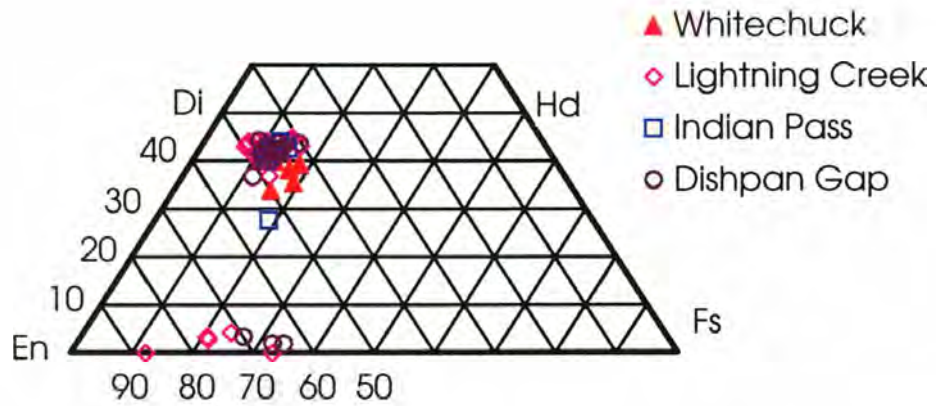


Fig. 7. Ternary plot of clinopyroxene and orthopyroxene compositions from each flow. Most of the clinopyroxenes are augite, salite, or diopside. The orthopyroxenes are hypersthene. Some orthopyroxenes from Lightning Creek may represent xenocrysts.

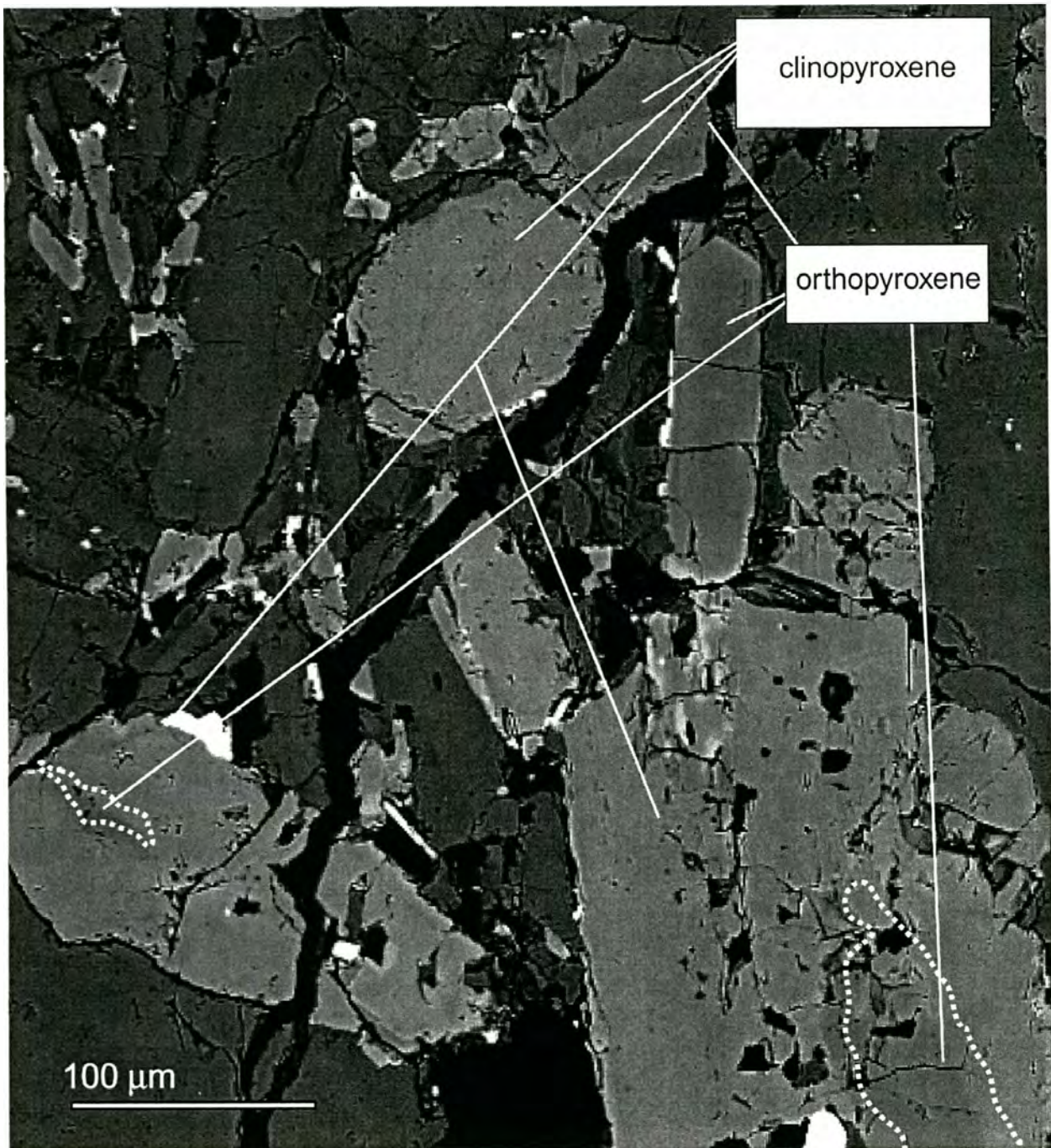


Fig. 8. Electron microprobe image of complex orthopyroxene-clinopyroxene relationships in the Lightning Creek basaltic andesite (Sample LC-6). Orthopyroxene is represented by the darker shades of gray within the larger phenocrysts (within dotted line in larger crystals). Clinopyroxene is represented by the lighter gray and usually, but not always, comprises the outer crystal. These features do not represent two-pyroxene exsolution. It is possible that the orthopyroxenes are xenocrystic and are altering to clinopyroxene. The darker interstitial crystals are laths of plagioclase.

Lightning Creek sample LC-6. The crystallization sequence is hard to ascertain. In one crystal, a “core” of clinopyroxene is apparently mantled by a “rim” of orthopyroxene. In another crystal lower in the photo-micrograph, the opposite relationship can be observed. The boundaries are rounded between the two phases, straight boundaries commonly associated with exsolution or coexisting adjacent mineral phases are not observed. The disequilibrium features observed between the two pyroxene phases at Dishpan Gap suggest that orthopyroxene is probably xenocrystic in origin.

Plagioclase

Plagioclase occurs rarely in the Whitechuck HAOT as weakly zoned phenocrysts, and has the highest Ca content (13.5-17 wt.% CaO; Table 2) among the four flows. Phenocrysts typically have An₈₂₋₈₅ cores and An₆₄₋₇₅ rims. Groundmass laths have compositions similar to phenocryst rims. K₂O and SrO wt.% in plagioclase are lowest at Whitechuck, and there is a perceptible increase in SrO content with increasing CaO.

Plagioclase in the Indian Pass samples is extremely rare, and occurs as large (1-3mm), zoned, resorbed phenocrysts with compositions in the range of An₄₈₋₆₂. Several microlites were analyzed to test for equilibrium; these were in the range of An₆₃₋₆₄. Because the phenocryst phases display resorbed features and have lower Ca and higher Na, K, and Sr than the groundmass or other flows (Table 3), it is inferred that these represent xenocrystic material incorporated from the upper crust.

Plagioclase is ubiquitous in the Lightning Creek and Dishpan Gap lavas, making up a continuum of phenocryst sizes from groundmass (50-100µm) to larger phenocrysts (2-3cm). About 25-40% of the plagioclase phenocrysts from each flow are resorbed and

could represent xenocrystic material (as low as An₃₉). The majority of the larger phenocrysts are reversely-zoned at Lightning Creek and have weak normal zoning at Dishpan Gap. Compositions are in the range of An₄₂₋₆₈ at Lightning Creek and An₆₀₋₈₀ at Dishpan Gap (Table 3). Both flows commonly contain phenocrysts with sieved cores of quenched glass or clinopyroxene. When CaO is plotted against an incompatible plagioclase component such as K₂O (Fig. 9), a bimodal distribution of analyses from Lightning Creek becomes apparent: one population is above 0.35 wt.% K₂O and below 10.5 wt.% CaO, the other population is the inverse. The high-K, low-Ca analyses represent phenocryst cores, while the low-K, high Ca analyses are taken from rims and groundmass laths. One further notable observation is that there seems to be a correlation between the magnitude of resorption and K₂O content of Lightning Creek lavas. Lightning Creek plagioclase phenocrysts either began crystallization in a separate magma or have undergone a complex fractionation scheme. Nevertheless, many phenocrysts do not meet chemical criteria (*e.g.* Clyne, 1993) for being in equilibrium with their host magma.

Oxides

Chromium spinel occurs in the cores of olivine phenocrysts in all flows. Coexisting Fe and Ti oxides (magnetite-ulvöspinel and hematite-ilmenite) only occur in the groundmass of Indian Pass lavas. The groundmass of the other flows contains titaniferrous magnetite as the only oxide phase. Representative analyses for all oxide phases are shown in Tables 4 and 5. Recalculation techniques from Spencer and Lindsley

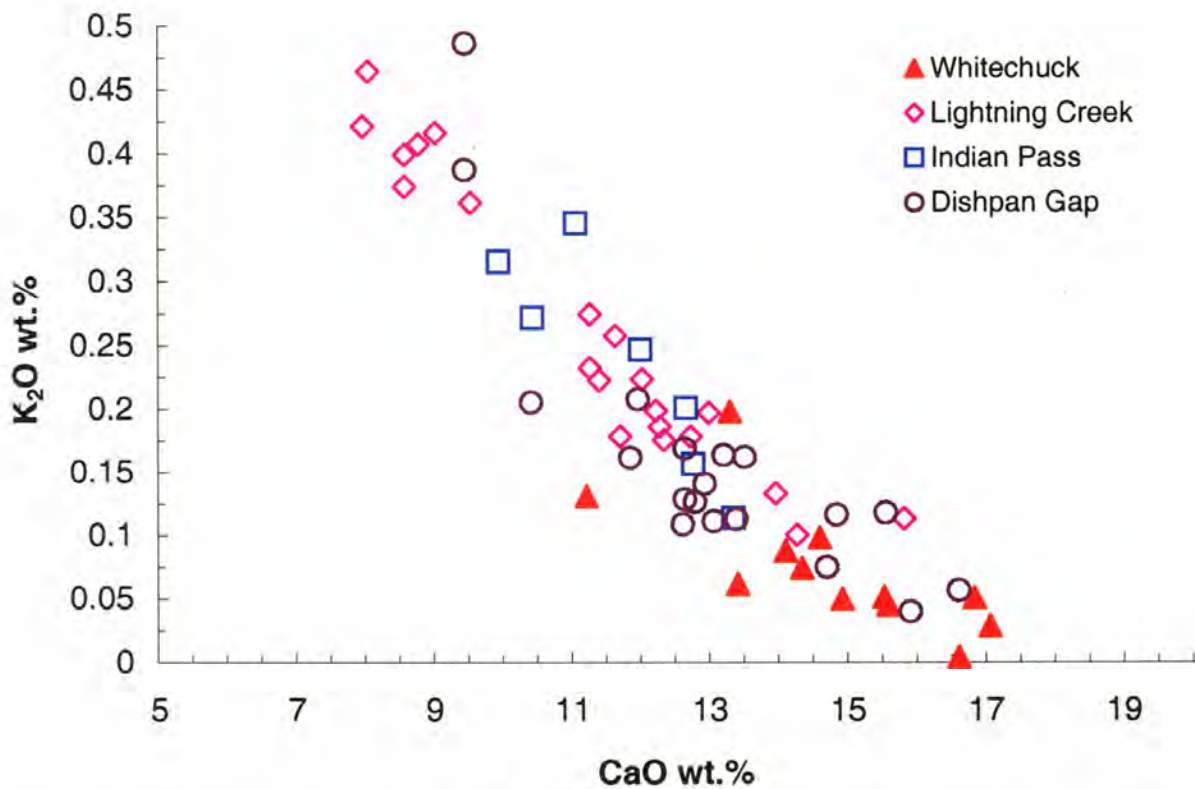


Fig. 9. Variation of K₂O vs CaO (wt.%) for plagioclase phenocrysts. The Lightning Creek flow follows a bimodal trend, with potentially xenocrystic plagioclase having higher K₂O than plagioclase more in equilibrium with bulk-rock values.

(1981) and the QUILF software of Anderson et al. (1993) were used to determine concentrations of Fe^{3+} for geothermometry.

Whole Rock Geochemistry

Major elements

According to the criteria of Tatsumi and Eggins (1995) and Gill (1981), the Whitechuck lavas belong to the low-K basalt suite while the other three flows form a continuous array in the medium-K field (Fig. 10). Using the FeO^*/MgO vs SiO_2 diagram of Miyashiro (1974) (Fig. 11) and the AFM diagram of Irvine and Baragar (1971) (not shown), the four lava flows plot in the calc-alkaline field, with the Whitechuck basalt plotting near the tholeiitic boundary.

Major-element compositions from each locality are plotted on SiO_2 variation diagrams in Figure 12. The lowest SiO_2 lavas are found at Whitechuck, where basalt is universally present. Some basalt can be found at Indian Pass, but most of the samples have $\text{SiO}_2 > 52$ wt.% and fall in the basaltic andesite field. At Lightning Creek, most samples are basaltic andesites, but a few of the most fractionated samples are andesitic and have SiO_2 ranging from 56-57 wt.%. This thesis focuses mainly on the least fractionated members of each suite, therefore the Lightning Creek lavas are referred to as basaltic andesites. Basaltic andesites are the only rocks present at Dishpan Gap.

Figure 12 also shows several other noteworthy distinctions between the four flows. Whitechuck HAOT are predictably enriched in Al_2O_3 (~18-18.5 wt.%) and are comparable to HAOT from Lassen and Medicine lake (Bacon et al. 1997). Indian Pass

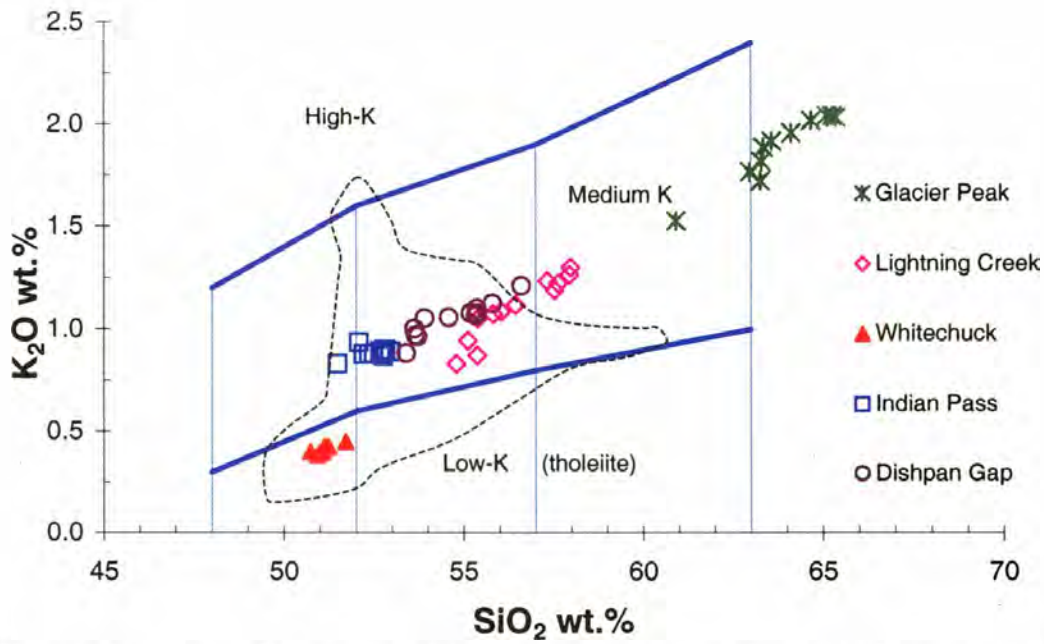


Fig. 10. Lavas from Whitechuck, Lightning Creek, Indian Pass, and Dishpan Gap plotted on a K_2O vs. SiO_2 diagram. Glacier Peak dacites are plotted for reference. Vertical lines at 52%, 57%, and 63% delineate basalt, basaltic andesite, andesite, and dacite. The classification fields are from Gill (1981). The dashed field encloses primitive lavas from the southern Washington, Oregon, and northern California Cascades (from Bacon et al. 1997).

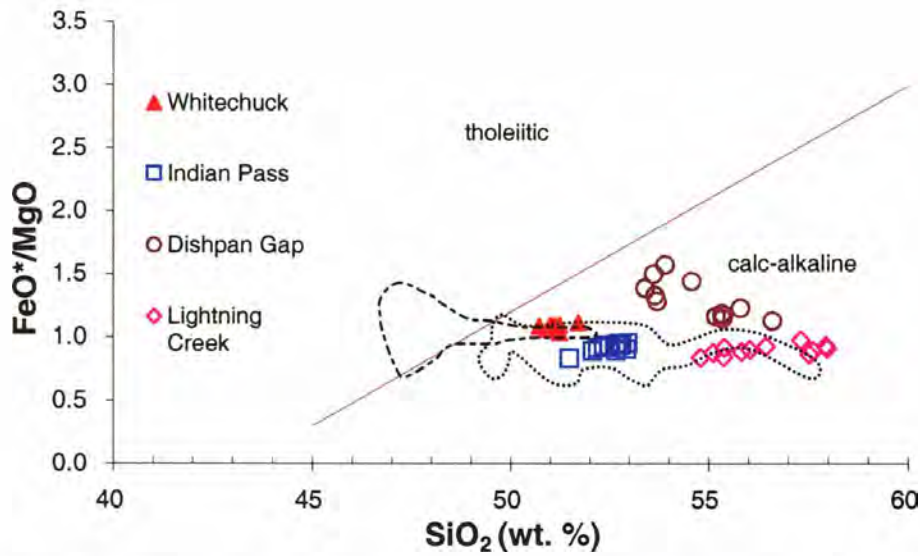


Fig. 11. FeO*/MgO vs. SiO₂ variation diagram of Miyashiro (1974) showing the tholeiitic and calc-alkaline series. Dashed field represents HAOT samples from Central and Southern Cascades primitive lavas, dotted field represents calc-alkaline Cascades lavas. Published data from Bacon et al. (1997). Note that the Whitechuck basalts plot in the calc-alkaline field but are referred to in this thesis as fractionated HAOT due to chemical similarities with other published HAOT in the Cascades.

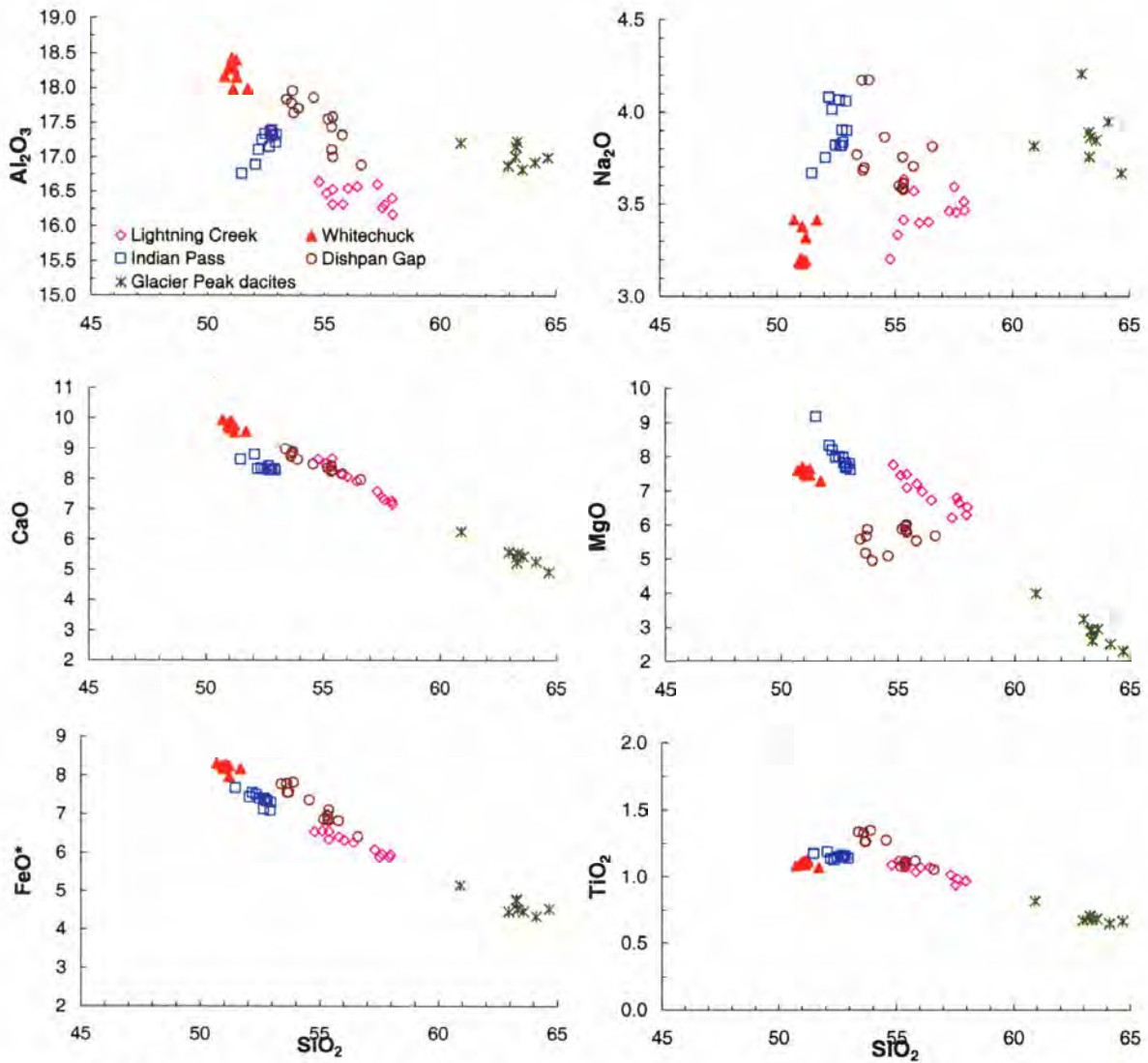


Fig. 12. Major element vs. SiO_2 variation diagrams for mafic lavas near Glacier Peak. Dacite lavas from Glacier Peak are plotted for reference.

has lower Al concentrations for given silica content, while Dishpan Gap and Lightning Creek occupy a steeply descending trend. There is no systematic variation between Na₂O and SiO₂ for the sample group as a whole. However, Indian Pass and Whitechuck plot as high-Na (~3.7-4.2 wt.%) and low-Na lavas, respectively. Samples from all flows form a descending linear trend on a plot of SiO₂ vs. FeO* and CaO. MgO concentrations for Indian Pass lavas form a tight trend from 7.5-8.5 wt.% and comprise the most magnesian rocks in the field area. One Mg-rich basalt sample (IH-3) has >9 wt.% MgO and represents the most primitive member of the suite. Mg# at Whitechuck are lower for a given SiO₂ content, forming a tight cluster at 7.3-7.6 wt.% MgO. Lightning Creek samples form a coherent trend extending towards the dacites of Glacier Peak, and have the highest concentrations of MgO (~6-8 wt.%) but have relatively high SiO₂ as well. Dishpan Gap lavas form a loose trend showing a slight increase in MgO (~4.8-6.4 wt.%) with increasing SiO₂. There is little variation in TiO₂ (~0.9-1.4 wt.%) between the four suites of mafic magmas, although a small population of Dishpan Gap samples plot with slightly higher amounts of TiO₂.

In Figure 13, Mg# [$100 * \text{Mg} / (\text{Mg} + \text{Fe}^{2+})$] is plotted against SiO₂ to provide an index of Mg enrichment and fractionation. The Whitechuck samples form a tight group of basalts with Mg# values near ~65. Indian Pass forms a typical trend in which Mg# decreases with increasing SiO₂. Lightning Creek is odd in that it has Mg# values near 70 for samples with SiO₂ ≥ 57 wt.%. The Dishpan Gap lavas have the greatest range in Mg# for given SiO₂. However, Mg# seems to increase proportionally with SiO₂.

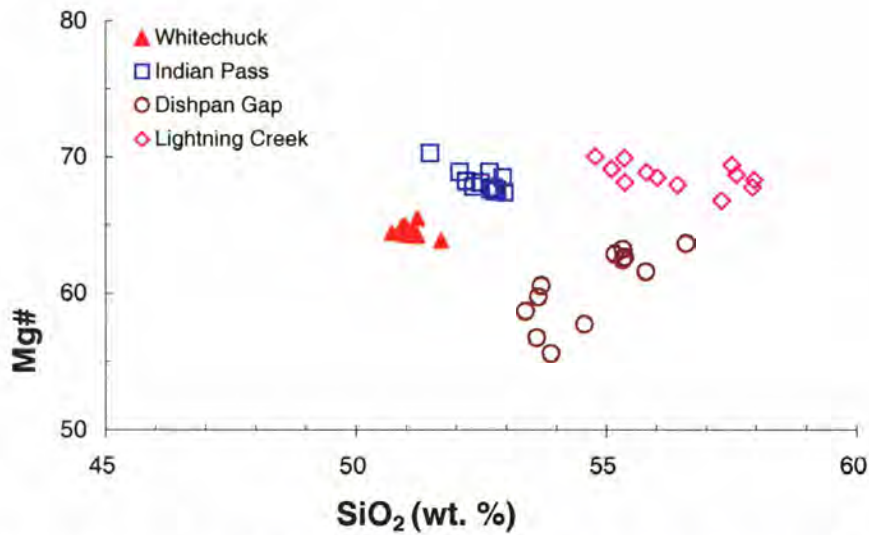


Fig. 13 Mg# vs. SiO₂ variation diagram. Mg# = 100*Mg/(Mg+Fe) at FMQ. Indian Pass and Whitechuck samples generally do not have significant variation in Mg#. The Lightning Creek basaltic andesites follow a trend from a more mafic parent composition to slightly more fractionated derivatives. Mg# generally decreases with increasing SiO₂ for all flows, except for the Dishpan Gap samples.

Trace elements

Compatible element concentrations reflect variable degrees of oxide fractionation or diverse source characteristics for the four flows, as there are significant variations in Ni and Cr content at given SiO₂ (Fig. 14). The Whitechuck HAOT is comparably low in Ni (55-75 ppm) and Cr (150-175 ppm) but is also low in SiO₂. Indian Pass lavas contain the most primitive concentrations of Ni (>150 ppm) and Cr (>200 ppm), and form a trend extending towards the Lightning Creek compositions. Dishpan Gap samples reflect higher degrees of fractionation and have <60 ppm Ni and ≤150ppm Cr.

Variations in incompatible trace elements offer further insight into the processes affecting arc magma compositions. Whitechuck has low concentrations of the lithophile elements Rb (<6 ppm) and Sr (<550 ppm), as well as low concentrations of the HFSE Zr (≤150 ppm). These values from Whitechuck are similar to published values of HAOT from the central and southern Cascades (Bacon et al. 1997) (Fig. 15). For Rb and Zr, the calc-alkaline lavas fall along the arc trend, although Zr decreases in Dishpan Gap. However, for Sr, which is influenced by fractionation of plagioclase and assimilation of crustal material, there is a systematic decrease with increasing SiO₂ in Lightning Creek and Dishpan Gap samples, which form converging trends towards the Glacier Peak dacite. Sr behaves differently with regard to other incompatible elements such as La and Zr. Sr increases with increasing La and Zr (not shown; Table 6.), which makes the inverse correlation between Sr and SiO₂ hard to explain by plagioclase fractionation alone.

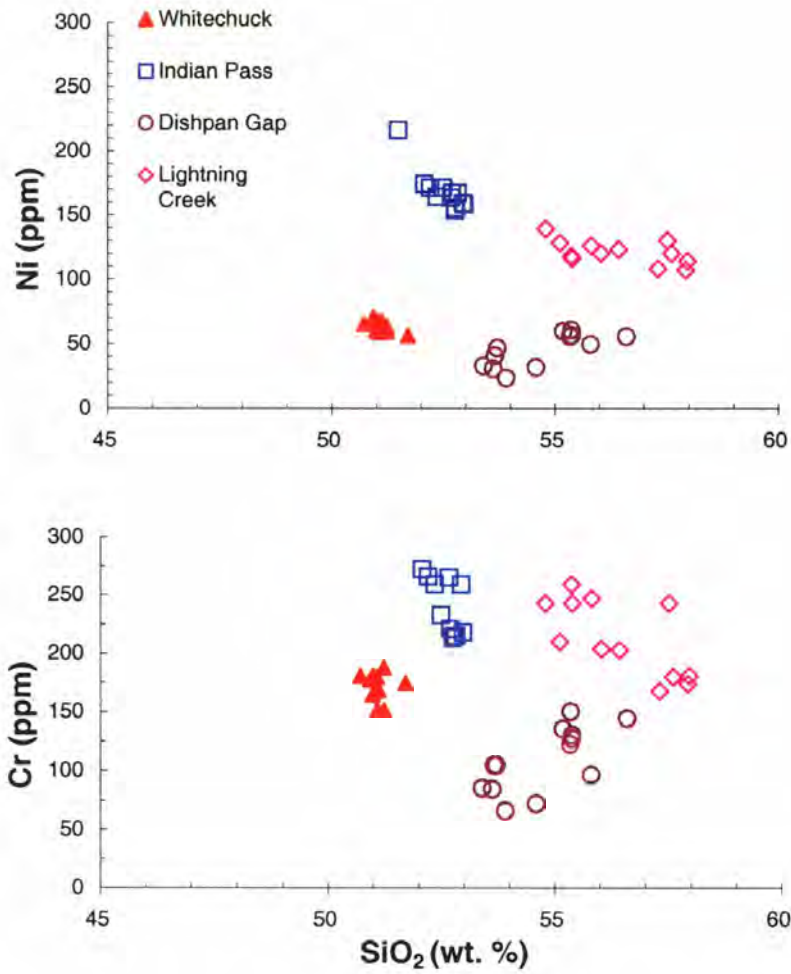


Fig. 14. Variation diagrams of Ni and Cr vs. SiO₂. Ni and Cr behavior is similar in both diagrams, but there is more range in Cr composition. The most mafic suite, Whitechuck, is depleted in Ni and Cr, as is Dishpan Gap.

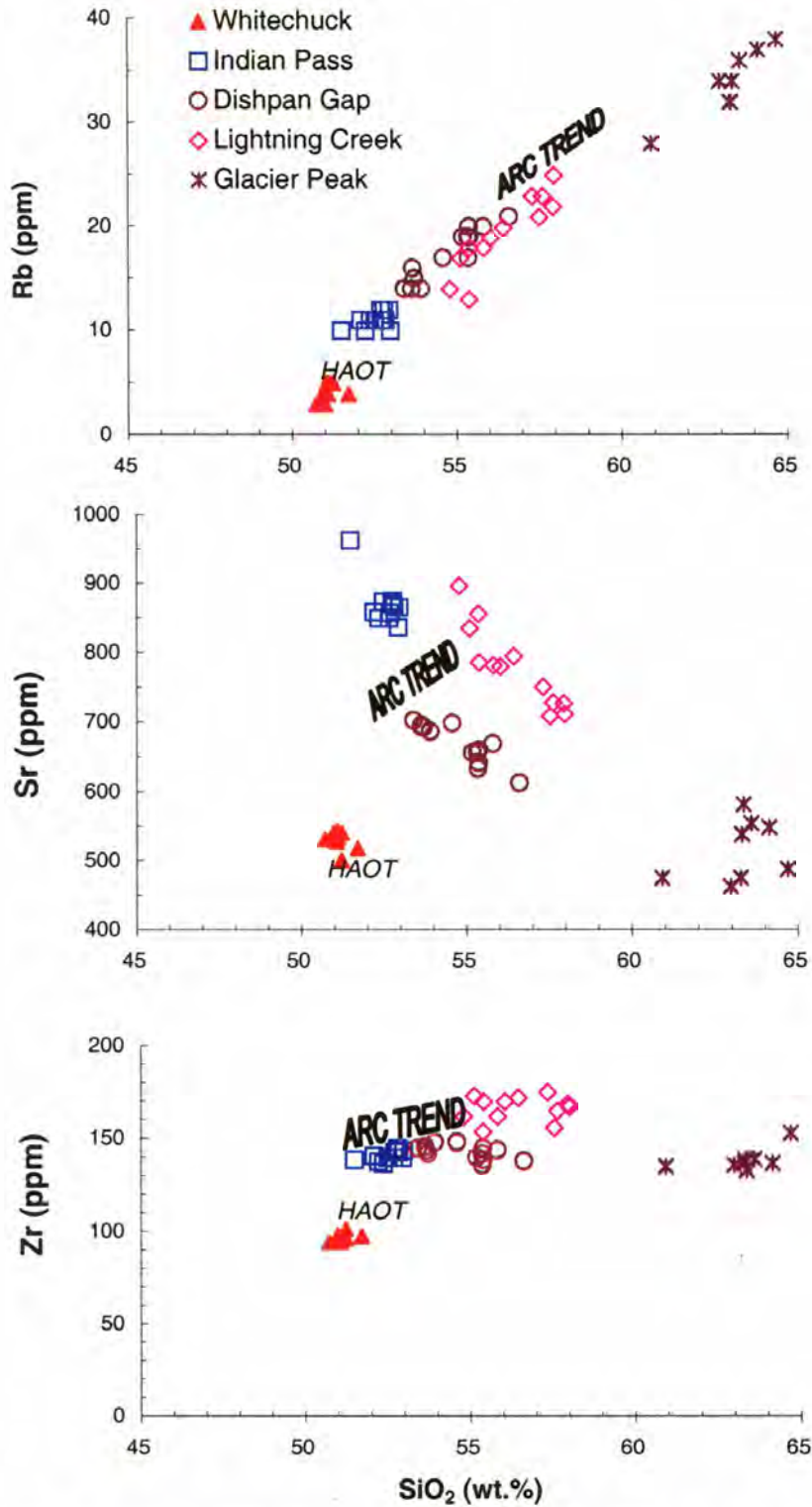


Fig. 15. Variation of Rb, Sr, and Zr vs SiO₂. The Whitechuck lavas fall near HAOT from the central and southern Cascades. Rb behaves incompatibly in all flows. Sr behaves compatibly in the basaltic andesites, which form separate trends converging towards the Glacier Peak dacites. Zr increases with increasing SiO₂ in all flows except for Dishpan Gap. The HAOT and arc trend regions are from Bacon et al. (1997)

Concentrations of LILE (Cs, Rb, Ba, Th, Sr, K, U, LREE), and HFSE (Nb, Ta, Hf, Zr, Ti) are strongly influenced by most processes in arc magmatism. LILE and HFSE are nearly equally incompatible and generally do not decouple from each other during partial melting or fractional crystallization. Magmas typically become enriched in LILE relative to HFSE when slab-derived fluids infiltrate and enrich the mantle wedge beneath the volcanic front with fluid-mobile elements (Tatsumi et al. 1986, Hawksworth et al. 1991; Stolper and Newman 1994).

Representative samples from each flow are plotted on a primitive mantle-normalized multi-element diagram in Figure 16. All samples have the characteristic LILE enrichment and negative Nb and Ta anomalies typical of arc magmas enriched by a subduction component. The Whitechuck flow samples are the least enriched, with most elements ≤ 10 times primitive mantle values of Sun and McDonough (1989). For the most part, the calc-alkaline lavas are equally enriched across the diagram. Indian Pass, however, is distinctive in that it is more enriched in Ta and Nb relative to the other flows, but is less enriched in LILE. Dishpan Gap and Lightning Creek have an almost indistinguishable pattern, with both plotting along a typical arc trend. It is interesting to note that while no samples show characteristic HFSE enrichment of OIB-like lavas, the Whitechuck basalt displays HFSE concentrations similar to or below N-MORB values, and is comparable to HAOT from elsewhere in the Cascades (Leeman et al. 1990; Bacon et al. 1997). Intraflow comparisons of incompatible elements (Table 6) show that there is negligible variability between sample patterns from the same flow, thus necessitating only one representative sample from each flow in Figure 16.

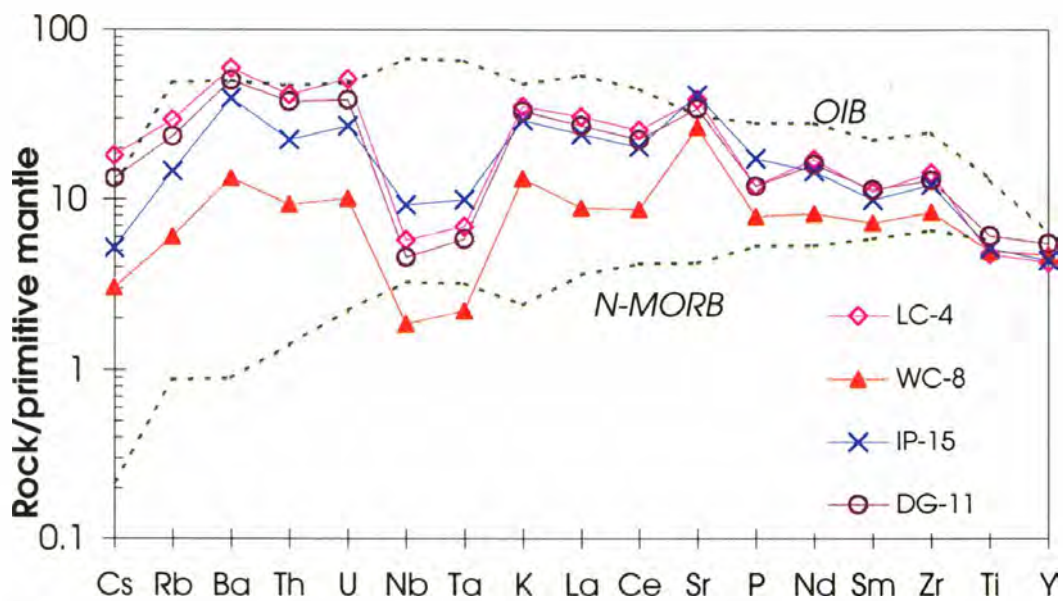


Fig. 16. Primitive mantle normalized incompatible element diagrams for representative samples from each flow. Note typical arc signature (enrichment in Ba, Th, U, and Sr; and depletion in Ta, Nb, and Zr). The sample from Indian Pass has the lowest enrichment in LILE relative to Nb and Ta and the highest abundance of fluid-immobile elements. LC: Lightning Creek; WC: Whitechuck; IP: Indian Pass; DG: Dishpan Gap. OIB, N-MORB, and primitive mantle values from Sun and McDonough (1989).

While Figure 16 shows relative magnitude of enrichment vs. primitive mantle, plots of LILE/HFSE ratios (Fig. 17) are useful in highlighting the compositional distinction between calc-alkaline, OIB-like, and HAOT or MORB-like lavas. Bacon et al (1997), Borg et al. (1997) and Reiners et al. (2000) associate higher Ba, Th, Ba/Nb (≥ 40), and Ba/Zr (≥ 1) and lower Ta, Nb, and Nb/Zr (≤ 0.075) with calc-alkaline magmatism involving a subduction component. The calc-alkaline basalts and basaltic andesites from this study lie along the lower end of this field, while the Whitechuck HAOT lie close to the MORB field (Sun and McDonough 1989) near the origin. Lower concentrations and ratios of these elements coupled with higher proportions of HFSE define a trend extending towards OIB-like magmas (e.g. Simcoe volcanic field; Bacon et al. 1997). No magmas from this study lie along the OIB trend. It is rare to find arc magmas between the two trends, a characteristic that usually implies contamination by crustal material rather than an origin by a different source material or process (Borg et al. 1997; Reiners et al. 2000).

Representative REE patterns for each flow are shown in Figure 18. The Whitechuck lavas are easily distinguished from the other three flows on the basis of very little LREE enrichment (REE abundances < 20 -30 times chondrite), a nearly flat pattern, and a very slight positive Eu anomaly. The calc-alkaline flows show a typical arc pattern of LREE enrichment (70-100 times chondrite) with barely perceptible positive Eu anomalies at Dishpan Gap and Indian Pass. Lightning Creek is the most LREE enriched and HREE depleted, with some fractionation evidenced by $(La/Sm)_N$ ratios > 2.5 (Fig. 19). Dishpan Gap and Indian Pass have similar patterns, and have $(La/Sm)_N \sim 2.5$, but Dishpan Gap is more HREE enriched. Intraflow comparisons of REE data show that

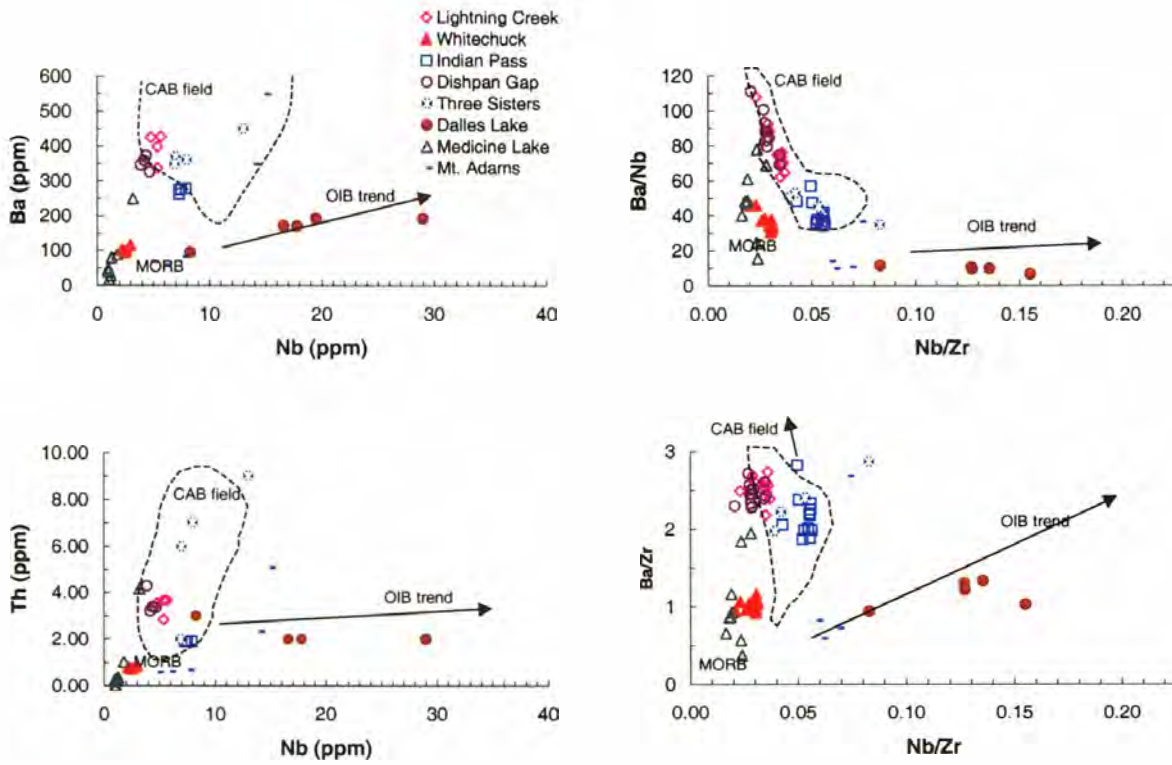


Fig. 17. Concentrations and ratios of LILE and HFSE for the four mafic flows near Glacier Peak, as well as basalts from Dalles Lake and Three Sisters (Reiners et al. 2000), and Mt. Adams and Medicine Lake (Bacon et al., 1997). Note that no samples from this study fall along the OIB trend, or in between the diverging trends. Whitechuck basalts plot near the Medicine Lake basalts, a representative HAOT from the southern Cascades, and above the N-MORB value of Sun and McDonough (1989). Calc-alkaline basalt (CAB) field and OIB trend are adapted from Reiners et al. (2000).

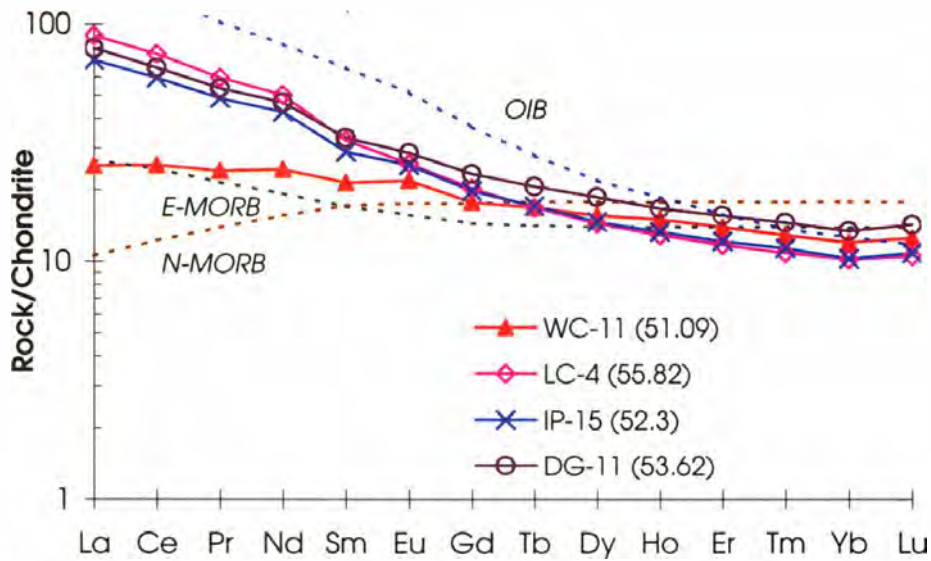


Figure 18. REE abundances from each flow normalized to the chondrite values of Sun and McDonough (1989). The Whitechuck basalts are significantly less enriched in LREE than the calc-alkaline basalts and basaltic andesites, and plot near E-MORB. Wt.% SiO₂ for each sample is shown in parentheses. Representative OIB, E-MORB, and N-MORB values are from Sun and McDonough (1989).

porphyritic flows (Dishpan Gap and Lightning Creek) have a greater range in REE abundances, which correlate positively with SiO₂ content. For all flows, REE abundances increase proportionately with increasing SiO₂ (in parenthesis in Fig. 18 legend). However, the most fractionated and highest SiO₂ calc-alkaline flows are progressively more enriched in LREE, with concave-down patterns for LREE and concave-up patterns for HREE. These patterns are consistent with other Cascades primitive lavas reported by Bacon et al. (1997) for lavas derived by hydrous partial melting of the lower garnet-bearing mantle wedge.

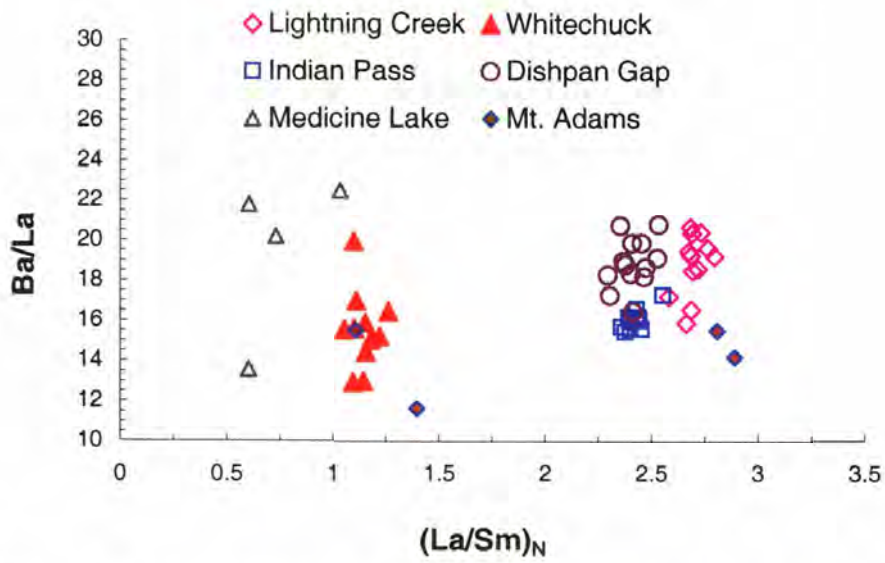


Figure 19. Variation diagram of Ba/La vs. $(La/Sm)_N$. Representative HAOT from Medicine lake and Mt. Adams (Bacon et al. 1997) have a range of Ba/La and low $(La/Sm)_N$, and are similar to Whitechuck. The arc basalts of Mt. Adams share similar $(La/Sm)_N$ with calc-alkaline basaltic andesites from Indian Pass, Lightning Creek, and Dishpan Gap.

DISCUSSION

Geothermometry of Mafic Lavas

Sub-liquidus magmatic temperatures were calculated for the Indian Pass basaltic andesites using the Fe-Ti oxide thermometer equations and QUILF software of Anderson et al. (1993) which follows the methods of Spencer and Lindsley (1981). Coexisting ilmenite-hematite and magnetite-ulvöspinel were only observed at Indian Pass. The mineral chemistry of oxide pairs from these lavas are shown in Table 4, calculated temperatures and $f(\text{O}_2)$ are shown in Table 8a. Calculated temperatures range from 656-1139° C, $-\log f(\text{O}_2)$ ranges from -13.79 to -8.73, falling near the nickel-nickel-oxide (NNO) curve of Spencer and Lindsley (1981). Calculated uncertainties of $\pm 160^\circ\text{C}$ and $\pm 2.3 -\log f(\text{O}_2)$ are due to uncertainties in the role of Mg and Mn in Fe-Ti partitioning. Low calculated temperatures probably represent late-stage (near-solidus) Fe-Ti oxide re-equilibration or analytical error in microprobe analyses. Accuracy of microprobe analyses is compromised due to the small size ($\leq 10\text{-}15\mu\text{m}$) of oxides in the groundmass. Exsolution bands of ilmenite in magnetite approach minimum probe beam-width ($< 5\mu\text{m}$), thus the likelihood of obtaining accurate analyses for each phase is low.

Magmatic temperatures were also calculated using the olivine-melt geothermometer of Roeder and Emslie (1970). The most forsteritic olivine cores were compared with bulk rock compositions to calculate temperatures averaging near 1240° C for Indian Pass, 1214° C for Lightning Creek, 1226° C for Whitechuck, and 1157° C for Dishpan Gap (Table 8b). Melting experiments could provide a higher degree of accuracy in which to check this data. However, the calculated temperatures agree with the geochemical

Table 8a. Geothermometry of mafic lavas from the Indian Pass basaltic andesite.

Sample:	IP-8 ox-2	Uncertainty	IP-8 ox-3	Uncertainty	IP-8 ox-4a	Uncertainty	IP-15 ox-2	Uncertainty	IP-15 ox-1a	Uncertainty	IP-15 ox-1b	Uncertainty
T(°C)	656	121	1139	160	1031	278	759	51.43	904	105	1003	117
log _f (O ₂)	-13.79	2.301	-8.475	1.193	-8.736	2.477	-14.56	0.6149	-10.85	1.132	-8.906	1.142
N _{Ti} ¹	0.041		0.6076		0.5189		0.2389		0.36		0.3822	
N _{Mg}	0.0905		0.1606		0.1167		0.0462		0.1628		0.1524	
N _{Mn}	0.008		0.008		0.0082		0.0104		0.0137		0.0129	
X _{Hem} ²	0.3827		0.1559		0.2383		0.099		0.1988		0.2901	
X _{Gk}	0.1184		0.1233		0.1364		0.1233		0.2553		0.1797	
X _{py}	0.0103		0.0158		0.0027		0.0158		0.0096		0.0096	

Temperature calculations for the coexisting ilmenite-hematite and magnetite-ulvospinel geothermometer using the QUILF software developed by Anderson et al. (1993) which is adapted from the equations of Spencer and Lindsley (1981). Table 6 shows chemical data for each oxide pair used in the calculations.

¹N_{Ti}, N_{Mg}, and N_{Mn} are the proportions of Ti, Mg, and Mn in the spinel end-member.

²X_{Hem}, X_{Gk}, and X_{py} are for the molar proportions of the rhombohedral oxide phased of hematite, Geikielite, and Pyrophanite in the ilmenite end-member.

Table 8b. Olivine-liquid geothermometry using the methods of Roeder and Emslie (1970).

Sample:	Whole rock		Olivine		Log Mg ^{ol} /Mg ^{liq}	Temp (°C)	Average T (°C)
	molar Mg	Whole rock molar Fe	molar Mg	molar Mg			
LC-4	0.179	0.080	1.812	1.005	1.005	1207	1214
LC-6	0.186	0.080	1.795	0.984	0.984	1216	
LC-12	0.193	0.082	1.818	0.974	0.974	1220	
WC-8	0.189	0.104	1.736	0.963	0.963	1225	1226
WC-11	0.190	0.104	1.717	0.956	0.956	1228	
IH-3	0.228	0.096	1.752	0.886	0.886	1259	1240
IH-8	0.198	0.089	1.771	0.951	0.951	1230	
IH-15	0.198	0.094	1.772	0.951	0.951	1230	
DG-5	0.123	0.098	1.616	1.119	1.119	1161	1157
DG-11	0.128	0.097	1.760	1.137	1.137	1154	
DG-11	1.128	0.097	1.578	0.146	0.146	1722	

characteristics of each flow: i.e., Indian Pass has the highest temperature and the highest Mg and lowest phenocryst content; Dishpan Gap is coolest, with the lowest Mg and highest phenocryst content.

Evaluation of Primitive Characteristics

Primitive magmas are the most useful lavas for determining the nature of processes and components active in arc magmatism. These magmas represent the least fractionated end-members of their suite, and in rare cases, approach primary magmas, or magmas that are in equilibrium with mantle compositions. There are many published criteria for the evaluation of primitive magmas (*e.g.* BVSP 1981; Bacon et al. 1997; Nixon and Johnston 1997). This thesis uses the minimum limiting criteria of BVSP (1981), in which primitive magmas are defined as those having $Mg\# [100 * Mg / (Mg + Fe^{2+})] > 55$, $MgO > \sim 6$ wt.%, $Ni > 100$ ppm, and $Cr > 200$ ppm. $Mg\#$'s are not well constrained because the Fe^{2+}/Fe^{3+} ratio and $f(O_2)$ are unknown for the chosen samples. The Fe^{2+}/Fe^{3+} ratio of these samples are assumed to be consistent with $f(O_2)$ at the FMQ (fayalite-magnetite-quartz) buffer (*e.g.* Kress and Carmichael 1991) of $FeO/FeO^* = 0.9$. However, more oxidizing conditions consistent with the NNO (nickel-nickel-oxide) buffer cannot be ruled out. Even more oxidizing conditions (FeO/FeO^* as low as 0.6) have been reported for arc basalts in the central and southern Cascades by Bacon et al. (1997).

According to the above criteria for primitive magma evaluation, lavas from Indian Pass and Lightning Creek are primitive, while Whitechuck and Dishpan Gap lavas are insufficiently enriched in compatible elements (Ni and Cr: Fig. 14) and are too fractionated to be considered primitive. $Mg\#$ values for the Indian Pass and Lightning

Creek lavas are generally ~70-72 (Fig. 13) and MgO at Lightning Creek ranges from 6.5 to 7.5 wt.% (Fig. 12) while MgO at Indian Pass often exceeds 8 wt.%. While the Lightning Creek flow exhibits primitive magma characteristics, it should be noted that the flow is higher in SiO₂ than any of the other mafic flows in this study.

The Whitechuck lavas, based on their lower Ni (<100ppm), and Cr (<200 ppm) are assumed to have fractionated from a more primitive basalt parent, or to have lost Ni and Cr-phases (*e.g.* chromite). Dishpan Gap lavas have Mg# values <65, MgO <6 wt.%, and Ni and Cr concentrations <100 ppm. Furthermore, they are generally rich in zoned and reversely zoned phenocrysts (most notably plagioclase) as well as xenocrystic material and are therefore considered to be evolved descendants of more primitive parent magma.

Other criteria are also important for evaluating primitive magmas. In most studies, the most phenocryst-poor samples are chosen for primitive magma evaluation (*e.g.* Baker et al. 1994; Bacon et al. 1997; Conrey et al. 1997). This usually assures that the samples represent liquid compositions. However, some authors (*e.g.* Della-Pasqua and Varne 1997; Sunda and Vanuatu arcs) report that phenocryst-rich lavas (~50% phenocrysts) can also represent liquid compositions, as long as there is evidence to show that the magma has not lost any mineral phases to settling. In the case of mafic magmas in this study area, 11 samples representing the four flows were chosen for microprobe analysis based on contrasting SiO₂ and MgO wt.%. As shown in Table 2, samples from Lightning Creek and Dishpan Gap are the most phenocryst rich, while lavas from Whitechuck and Indian Pass are generally phenocryst-poor.

In order to test for equilibrium liquid compositions, the most forsteritic olivine phenocryst compositions are compared with calculated liquidus olivine compositions

using the relationship $K_D = (\text{Fe}/\text{Mg})^{\text{olivine}} / (\text{Fe}/\text{Mg})^{\text{liquid}} = 0.3$ (Roeder and Emslie 1970). Figure 20 shows the relationship of the olivine rims and cores with calculated equilibrium olivine compositions. Most rims plot well above the equilibrium line, showing significant late-stage Fe enrichment and equilibration with the groundmass. Most cores plot at or just above the equilibrium line, and likely became slightly more enriched with Fe over time through rapid diffusion of Fe from rims to cores (Misener, 1974). Figure 21 shows variation of olivine Mg# vs. bulk rock MgO wt.%. Observed olivine Mg# values plot at or just below the expected range of calculated olivine compositions that would have crystallized from a magma with the given wt.% MgO. Calculations utilized the NNO (above) and FMQ (below) buffers. Lavas with calculated olivine Mg#'s higher than observed olivine Mg#'s are inferred to have accumulated olivine (Baker et al. 1994). The more primitive Indian Pass and Lightning Creek basaltic andesites both show evidence of minor olivine accumulation, and likely represent near-liquid to liquid compositions. If a higher K_D is used (*e.g.* 0.31 from Baker et al. 1994), many observed olivines plot between FMQ and NNO conditions.

One sample each from the Dishpan Gap and Whitechuck flows (DG-11 and WC-11) shows olivine with a significantly low Mg# (higher olivine FeO). However, this is not interpreted solely as a sign of olivine accumulation. The higher Fe is more likely due to analyses of microphenocrysts, or analyses of areas not representing core compositions. The low phenocryst contents in Whitechuck lavas suggest that they may represent near-liquid compositions. Most Dishpan Gap lavas do contain olivine in equilibrium with bulk rock compositions (Figs. 20 & 21), and these may represent near-liquid compositions.

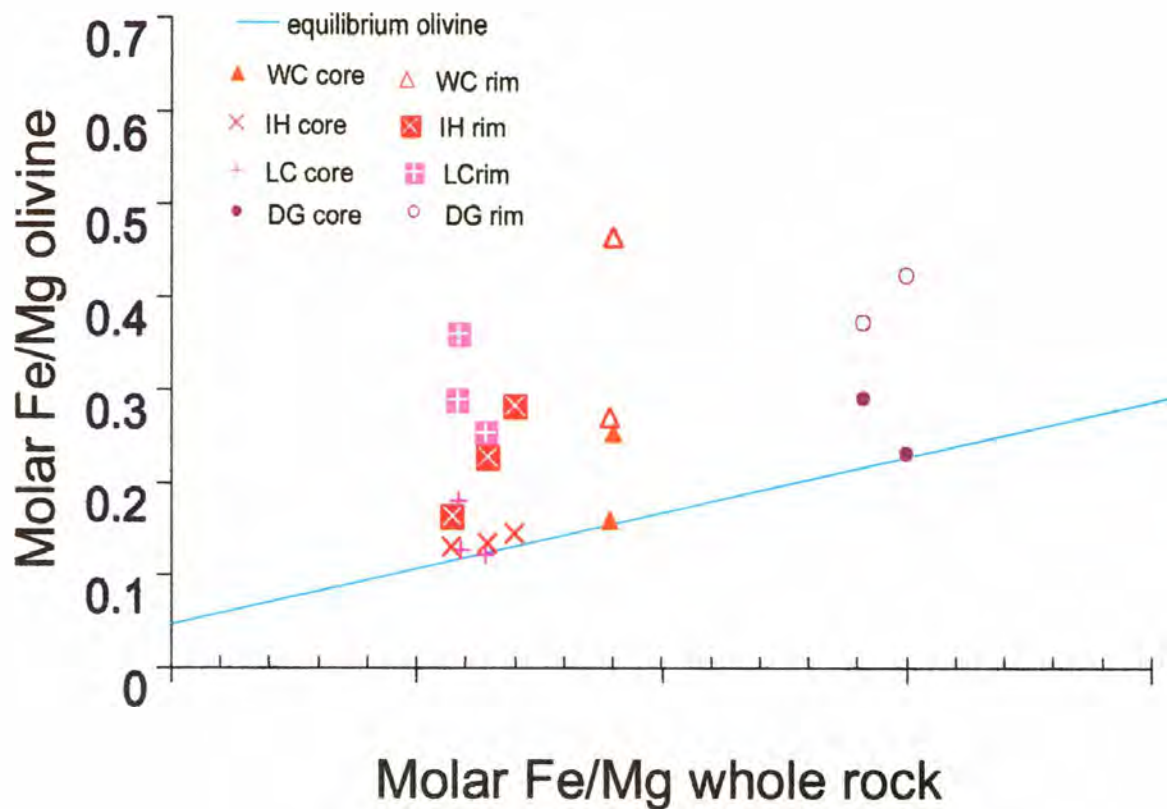


Fig. 20. Molar Fe/Mg olivine plotted against molar Fe/Mg whole rock, with Fe^{2+} calculated at QFM. The line represents the equilibrium concentration of olivine vs. liquid using the relationship, $KD = \text{Fe/Mg}_{\text{olivine}} / \text{Fe/Mg}_{\text{liquid}} = 0.3$ (Roeder and Emslie 1970). Liquid or near-liquid compositions are represented when olivine core compositions plot on or just above the olivine equilibrium line. The rims become more enriched in Fe as the magma crystallizes.

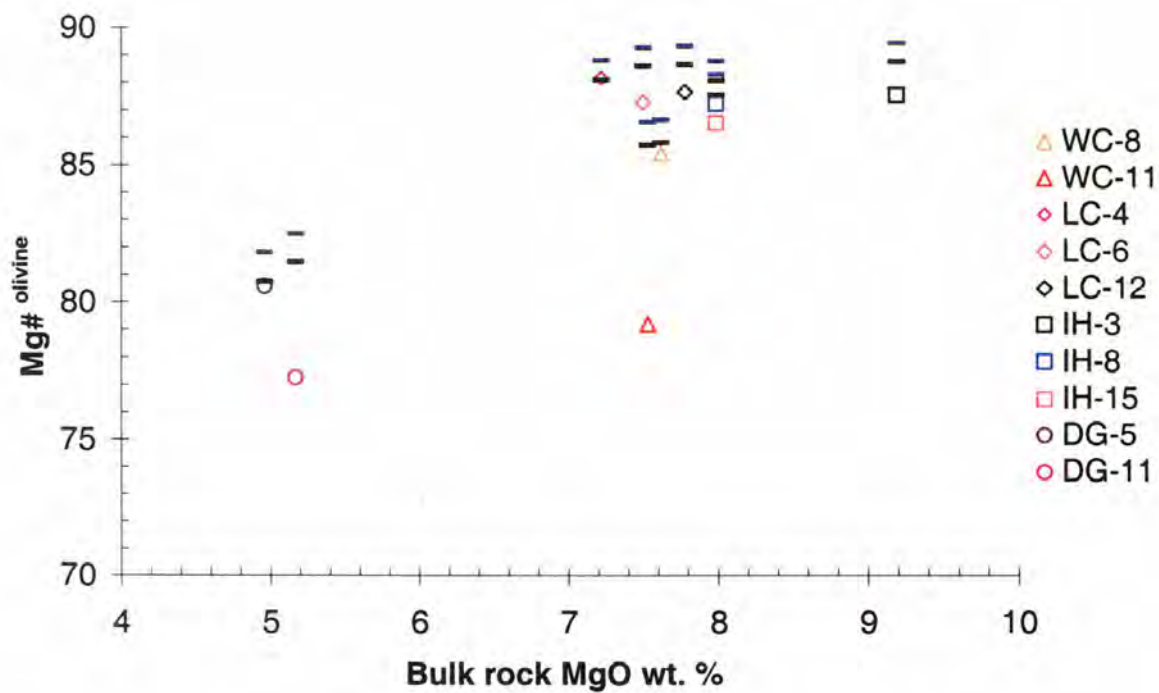


Fig. 21. Mg# of olivine vs. bulk rock MgO (wt.%). Horizontal lines bracket the range of calculated olivine concentrations from liquids with the given wt.% MgO between NNO (top) and FMQ conditions (bottom) for $K_D = 3.0$. Observed olivines represent the most forsteritic olivines from each sample. The observed olivine compositions fall below the calculated olivine compositions, which indicates only a small degree of olivine accumulation. See text for discussion.

In summary, primitiveness provides a measure of how much a magma can be trusted to accurately reveal equilibria with the mantle source. The Indian Pass and Lightning Creek lavas both exhibit primitive characteristics, especially in the least evolved samples. Lightning Creek deserves special attention, however, because it has such primitive compositions at such high concentrations of SiO₂. The role of the crust in influencing the composition of Lightning Creek will be discussed in a later section. Whitechuck and Dishpan Gap lavas are not primitive due to fractionation of compatible element-rich phases. However, most olivine in Whitechuck samples, and some olivine in Dishpan Gap samples are in equilibrium with whole rock compositions. Therefore, the Whitechuck basalt, though fractionated, still offers some insight into the characteristics of the mantle which produced it.

Crustal Effects on Lava Chemistry

A key observation of this study is that the four mafic flows, which are spatially and chronologically erupted in close proximity to one another, are compositionally diverse in both major and trace-element concentrations. Conrey et al. (1997) state that equally primitive lavas with different geochemical signatures must be derived from separate sources or processes. Although there is a continuum of primitiveness shown by the four lavas, there is ample evidence to suggest that differentiation alone can not account for the chemical variation between them. This section reviews observations of possible contributions from the crust that can be correlated with geochemical characteristics.

Essentially, magmas can be modified by the crust in three ways: 1) assimilation of exotic wallrock material during ascent to the surface; 2) fractionation of various mineral

phases due to changing P-T conditions as the magma ascends; and 3) mixing or mingling with other magmas.

Xenoliths and/or xenocrysts are observed in at least some samples from each locality (Table 2). The largest xenoliths (<2-3 cm in Dishpan Gap and Lightning Creek) contain felsic crustal lithologies. However, most of the xenoliths have sharp boundaries and show little interaction with the magma. Exceptions include microscopic quartz xenocrysts found in Indian Pass sample IH-2 (not analyzed) and Whitechuck sample WC-11, which are resorbed and rimmed by orthopyroxene; and rare, resorbed sodic plagioclase phenocrysts occurring in Whitechuck, Indian Pass, and Lightning Creek samples.

The Rb and Sr concentrations (Table 6, Fig. 15) are higher in the more primitive Indian Pass and Lightning Creek Lavas than in Whitechuck or Dishpan Gap, but are still within the range of primitive arc basalt and basaltic andesite lavas found in the central and southern Cascades (Bacon et al. 1997). Compatible behavior of Sr in the basaltic andesites (especially Dishpan Gap and Lightning Creek) could in part reflect plagioclase fractionation, but could also reflect mixing with a felsic component. Both Indian Pass and Lightning Creek magmas have higher SiO₂ than the Whitechuck basalts, which have significantly less enrichment in compatible elements.

There is little evidence that fractionation could have produced the differences observed between the Indian Pass and Lightning Creek primitive basaltic andesites. Indian Pass is nearly aphyric, has the lowest SiO₂ and the highest Ni and Cr concentrations (Table 6, Fig 13), and was likely derived from a basaltic primary magma. Lightning Creek samples have higher SiO₂, slightly lower compatible element

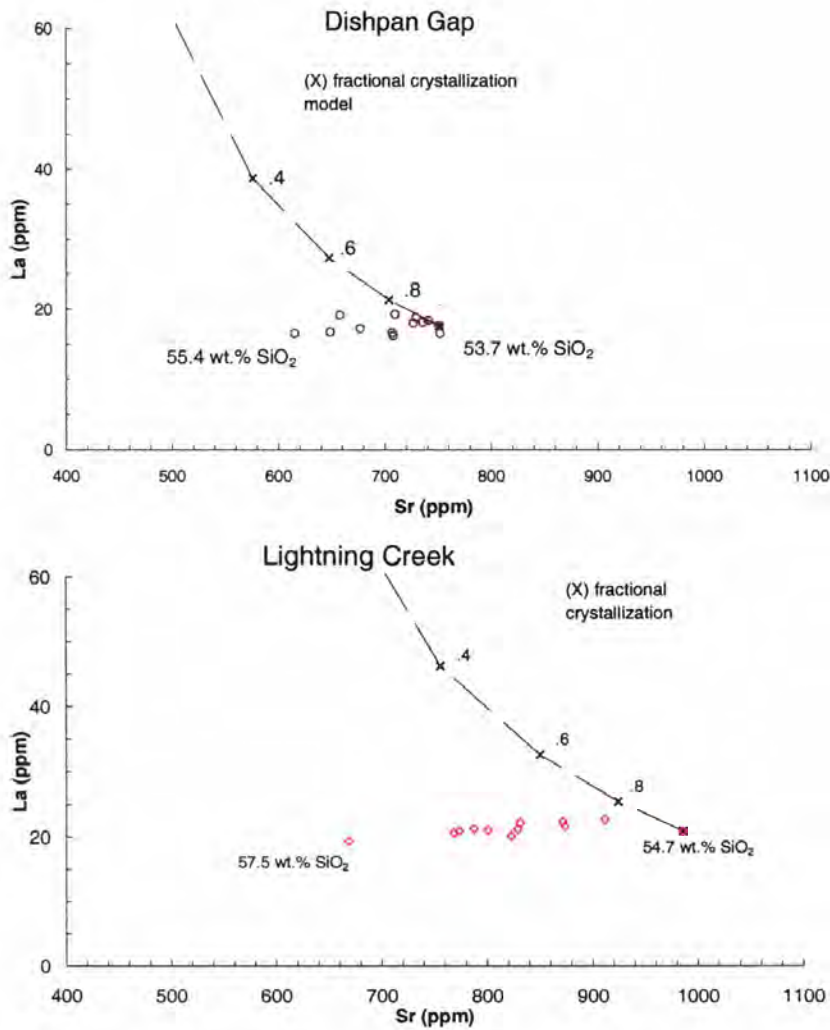
concentrations, but similar to higher MgO content and olivine Mg# values (Figs. 13, 14, and 20). Baker et al. (1994) and Borg et al. (1997) describe primitive basaltic andesites in the southern Cascades (e.g. Lassen and Shasta region) derived by low degrees of hydrous melting of the mantle wedge. This explanation of magma petrogenesis may apply to the Lightning Creek basaltic andesite as well. The Whitechuck HAOT has probably fractionated some compatible element-rich phases (e.g. olivine, spinel, and/or chromite) due to its lower Mg# and lower Ni and Cr concentrations, and therefore is not considered to be very primitive. However, low Rb and Sr concentrations in Whitechuck lavas (Fig. 15) are representative of other HAOT in the Cascades (Bacon et al. 1997) and strongly suggest that they have undergone little crustal contamination. The least primitive flow, Dishpan Gap, has similar Rb and Sr concentrations as the other basaltic andesites, but it also has the lowest Ni and Cr concentrations (Fig. 14) along with the most complex phenocryst assemblage (which includes xenoliths and strongly zoned olivine, plagioclase, and clinopyroxene). It is thus inferred to have experienced crustal contamination or magma mixing.

Figure 15 shows that the Lightning Creek and Dishpan Gap (and to some degree Indian Pass) trends for the trace elements converge towards Glacier Peak dacites. Sr is compatible in plagioclase (K_{plag} of 1.83 from Rollinson 1993), but a decrease from ~900 ppm to ~700 ppm for an increase of 4 wt.% SiO₂ is hard to explain by plagioclase fractionation alone. Furthermore, Sr correlates positively with certain incompatible elements, such as La and Zr (Table 6 & Fig. 22), indicative of another process in addition to, or in lieu of, normal fractionation processes. The following discussion evaluates the possibility that magma mixing between a felsic Glacier Peak dacite-like component and a

mafic representative of Dishpan Gap and Lightning Creek could have produced the more evolved members of these two calc-alkaline flows.

A simple fractionation model was used to rule out plagioclase fractionation as a cause for the anomalous Sr and La behavior in Dishpan Gap and Lightning Creek (Fig. 22). Partition coefficients for Sr and La (from Rollinson 1993) for each mineral in the phenocryst assemblage are shown in Figure 22. Crystallizing proportions for cpx:opx:ol:plag are an average of all samples from Dishpan Gap and Lightning Creek, and are also shown in Figure 22. Manipulation of the crystallizing proportions of clinopyroxene, orthopyroxene, and olivine does not significantly change the shape of the modeled fractionation trend. For both flows, La increases slightly with increasing Sr (and decreasing SiO₂, as shown for most evolved and least evolved samples). The model predicts that under normal crystallizing conditions, La should increase rapidly with decreasing Sr. If the crystallizing proportion of plagioclase is increased, La increases less rapidly with decreasing Sr, depressing the model curve in Figure 22. However, both Dishpan Gap and Lightning Creek have La values decreasing with Sr and increasing SiO₂. Therefore, closed system fractionation of plagioclase can not explain the behavior of Sr and La.

A simple least squares regression analysis (Fig. 23) of major elements from the Glacier Peak dacite, and the Lightning Creek and Dishpan Gap basaltic andesite shows that the most evolved members of the basaltic andesites can be modeled as mixes between a felsic and mafic end-member (represented by Glacier Peak sample GP-6 and the most primitive member of the Lightning Creek and Dishpan Gap suites, LC-12 and DG-9, respectively).



assemblage	cpx	opx	olivine	plag
Crystallizing proportions:	8%	2%	20%	70%
La	0.06	0.01	0.01	0.19
Sr	0.06	0.04	0.01	1.83

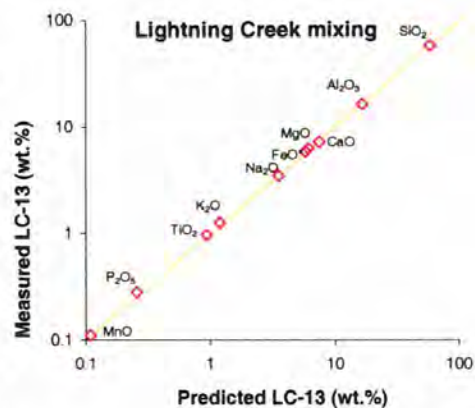
Figure 22. Fractional crystallization model for Dishpan Gap and Lightning Creek samples. Sr-La data sets for each flow are shown for comparison (from Table 7). Under normal fractional crystallization conditions, La should increase rapidly with decreasing Sr from the least evolved sample (SiO₂ shown) to the most evolved sample. However, in the case of Dishpan Gap and Lightning Creek, Sr is highest in the least evolved sample. Observed La either does not change or increases slightly with increasing Sr (or decreases with increasing SiO₂). Numbers on the model curve indicate proportion of melt remaining. Partition coefficients for crystallizing assemblage from Rollinson (1993) are shown in the table below plots.

Plots of the measured hybrid magmas (LC-13 and DG-8) vs. predicted concentrations are shown in Figure 23, as are the raw data used for the modeling. R^2 for both models is ~ 0.999 . Oxides with the most % error (calculated as the difference between measured and predicted values / predicted values) from the trend are K_2O and P_2O_5 in Lightning Creek, and TiO_2 , MgO , and P_2O_5 in Dishpan Gap. The log scale magnifies the effect of error for low concentrations and minimizes the effect at higher concentrations. However, error for low concentrations (*e.g.* P_2O_5) is less significant because the original concentrations are so low. The most evolved Lightning Creek sample, LC-13, can be reproduced by mixing 31% of GP-6 and 69% of LC-12, while the most evolved Dishpan Gap sample, DG-8, can be reproduced by mixing 27% of GP-6 and 73% of DG-9. Because the end-member compositions are assumed, it must be stressed that this is only one of many possible explanations for producing hybrid magmas by mixing of mafic and felsic end-members.

The model was further tested for trace elements using these same mixing proportions. Representative trace element concentrations from GP-6 and LC-12 (for Lightning Creek) and GP-6 and DG-9 (for Dishpan Gap) were mixed and compared to their more evolved magma compositions. Figure 24 shows data for the felsic and mafic end-members, and the measured and predicted hybrid compositions. Measured trace-element concentrations (in ppm) for the evolved compositions are plotted against their respective predicted compositions on the far right of Figure 24. Most elements strongly correlate. The elements with the highest error (on the x-axis) are shown in the furthest right column. All elements in Lightning Creek have $<10\%$ error. Hf, Th, Ta, and La have the highest error in Dishpan Gap. It must be noted that the error shown by some elements

Sample #	Most evolved felsic end-member	Least evolved mafic end-member	Most evolved mafic sample	Predicted most evolved hybrid	error (x-axis)
GP-6	GP-6	LC-12	LC-13	LC-13	
Mixing proportions					
	31%	69%			
SiO ₂	65.09	54.79	57.94	57.89	0%
TiO ₂	0.59	1.10	0.97	0.94	3%
Al ₂ O ₃	16.49	16.64	16.41	16.58	1%
FeO*	4.12	6.56	5.91	5.81	2%
MnO	0.08	0.12	0.11	0.11	2%
MgO	2.38	7.78	6.31	6.13	3%
CaO	4.78	8.67	7.28	7.47	3%
Na ₂ O	4.27	3.21	3.51	3.53	0%
K ₂ O	2.04	0.83	1.27	1.20	5%
P ₂ O ₅	0.15	0.30	0.28	0.26	10%

R²=0.999



Sample #	Most evolved felsic end-member	Least evolved mafic end-member	Most evolved mafic sample	Predicted most evolved hybrid	error (x-axis)
GP-6	GP-6	DG-9	DG-8	DG-8	
Mixing proportions					
	27%	73%			
SiO ₂	65.09	53.40	56.61	56.48	0%
TiO ₂	0.59	1.34	1.06	1.14	7%
Al ₂ O ₃	16.49	17.83	16.88	17.46	3%
FeO*	4.12	7.76	6.42	6.78	5%
MnO	0.08	0.14	0.13	0.13	0%
MgO	2.38	5.58	5.69	4.72	21%
CaO	4.78	9.00	7.98	7.86	2%
K ₂ O	2.04	0.88	1.21	1.19	2%
Na ₂ O	4.27	3.77	3.81	3.90	2%
P ₂ O ₅	0.15	0.29	0.21	0.26	18%

R²=0.999

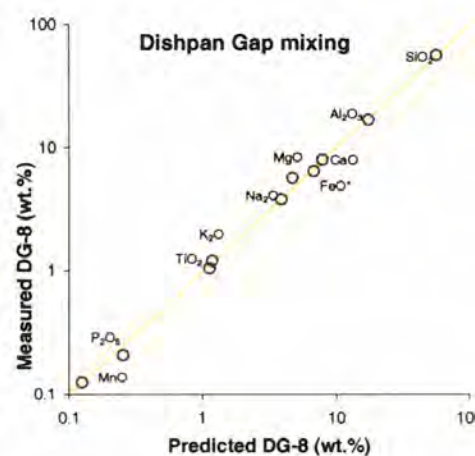
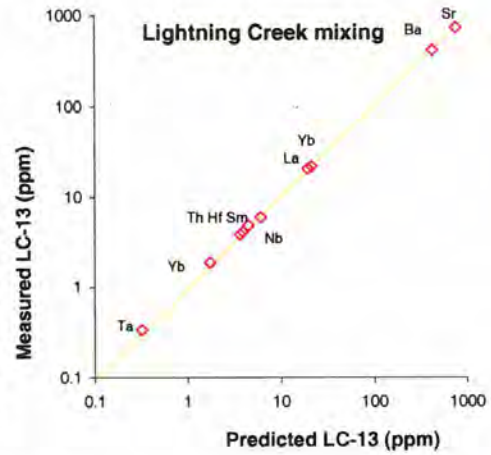


Figure 23. Results of Regression Analysis of major elements from mixing felsic end-member GP-6 (Glacier Peak) with end-members from Lightning Creek (LC-12), and Dishpan Gap (DG-9). Major element concentrations for the end-members are shown in the columns at left. Major element concentrations and predicted concentrations for the most evolved (hybrid) sample from Lightning Creek and Dishpan Gap are shown at right. On the far right, the predicted hybrid concentration is plotted vs. the measured evolved concentration. Results show that a proportion of 31% Glacier Peak sample GP-6 and 69% Lightning Creek LC-12 can mix to produce sample LC-13, while GP-6 and Dishpan Gap sample DG-9 can mix in the proportions 27%:73% to produce sample DG-8. R² values for both models are ~0.99. The error column shows the % error (the difference between the measured and produced divided by the predicted values). For Lightning Creek, Ca and Mg have the greatest deviation, but K₂O and P₂O₅ have the greatest % error. For Dishpan Gap, MgO and P₂O₅ have the greatest % error.

Sample #	Most evolved felsic end-member	Least evolved mafic end-member	Most evolved mafic sample	Predicted most evolved hybrid	error (x-axis)
	GP-6	LC-12	LC-13	LC-13	
Mixing proportions	31%	69%			
Ba (ppm)	512	388	417	426.44	2%
Sr	456	897	728	760.29	4%
Rb	38	14	22	21.44	3%
Nb	6.3	6	6	6.09	2%
Th	5.44	2.86	3.86	3.66	5%
Ta	0.42	0.28	0.34	0.32	6%
Hf	3.60	4.08	4.13	3.93	5%
La	16.1	21.0	20.7	19.5	6%
Sm	3.2	5.1	4.9	4.5	9%
Yb	1.6	1.8	1.9	1.7	9%



Sample #	Most evolved felsic end-member	Least evolved mafic end-member	Most evolved mafic sample	Predicted most evolved hybrid	error (x-axis)
	GP-6	DG-9	DG-8	DG-8	
Mixing proportions	27%	73%			
Ba (ppm)	512	333	345	381.33	10%
Sr	456	703	614	636.31	4%
Rb	38	14	21	20.48	3%
Nb	6.3	3	3.9	3.89	0%
Th	5.44	2.90	4.28	3.59	19%
Ta	0.42	0.21	0.30	0.27	13%
Hf	3.60	3.27	3.94	3.36	17%
La	16.1	18.0	19.1	17.5	9%
Sm	3.2	5.0	4.9	4.5	7%
Yb	1.6	2.5	2.3	2.3	0%

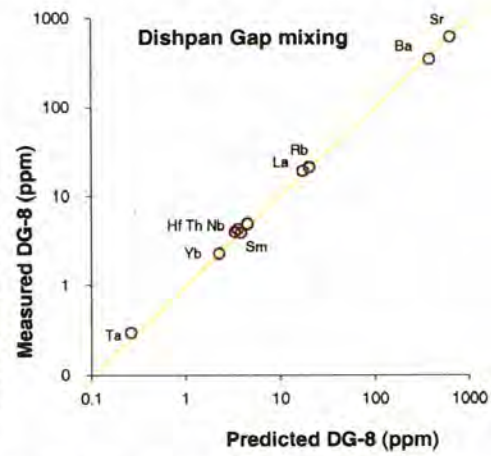


Figure 24. Results of regression analysis of trace elements using the same samples as Figure 23. Mixing proportions are from regression analysis of major elements. The mixing proportions are shown in the table on the left, as are selected trace elements from each end-member. On the right, the data (from Table 1.) is shown for the hybrids LC-13 and DG-8. The predicted trace elements for the samples are shown on the far right column. Predicted and measured concentrations are plotted for each hybrid sample on the right. The concentrations for each representative element fall along a very straight line (R^2 for both is ~ 0.999). The model works most poorly for the elements Hf, Th, Nb, and Sm from DG-8, where deviations can be seen in the right two columns and in the plot. Nevertheless, these results do provide a viable explanation for trace-element behavior in the two calc-alkaline flows as a result of mixing.

is actually within the expected deviation due to uncertainty in chemical analysis. Nevertheless, the results show that mixing in these proportions with these or similar end-members is a viable explanation for the later-stage petrogenesis of Lightning Creek and Dishpan Gap Lavas. Disequilibrium features in Lightning Creek and Dishpan Gap lavas, also support the premise that mixing took place between a primitive parent to Lightning Creek and Dishpan Gap, and a felsic magma similar to the dacites at Glacier Peak. It is impressive that both major and trace element variation can be explained so well by this mixing model.

In conclusion, crust contamination by AFC processes is unlikely given the relatively low concentrations of crustal contaminants such as Rb and Sr, especially in the Whitechuck flow. Additionally, with the exception of Dishpan Gap, higher compatible element concentrations are present in the flows with higher SiO₂. AFC processes generally require a simultaneous increase in SiO₂ and incompatible elements, and a decrease in compatible elements (Clynne, 1993); making it unlikely that the higher SiO₂ lavas could be evolved from a Whitechuck parent. Xenocryst and xenolith contents and other disequilibrium features are observed to be minor in all flows except for Lightning Creek and Dishpan Gap. Mixing of a felsic crustal derived component (*e.g.* Glacier Peak dacites) with magmas parental to Lightning Creek and Dishpan Gap could account for the linear trends in observed in Figure 15 and the disequilibrium textures observed in thin sections. Fractional crystallization modeling shows that Sr and La behavior can not be explained by closed-system crystallization of plagioclase. Regression analysis supports the inference that the two lavas could represent hybrids of mixing. Although insight into the mantle characteristics leading to the generation of Dishpan Gap and Lightning Creek

lavas have been obscured, trace-element characteristics in Figure 16 and 17 presumably still offer some insight into the mantle beneath Glacier Peak, especially if the least evolved samples are used for comparison. The Whitechuck and Indian Pass lavas are inferred to have received negligible input from crustal materials and therefore still likely record incompatible trace-element signatures representative of the mantle source and melting characteristics.

Mantle Characteristics beneath the Glacier Peak Region

Determining the mantle source and melting processes active in the generation of primitive magmas in the Cascades has been the focus of many authors (e.g. Leeman et al. 1990; Bacon et al. 1997; Conrey et al. 1997; and Reiners et al. 2000). As mentioned previously, three types of mantle domains are proposed to coexist beneath the Cascades arc (Bacon et al. 1997; Borg et al. 1997; Conrey et al. 1997): depleted sub-arc mantle; mantle enriched by a modern subduction component; and OIB-source-like mantle. The size and distribution of these mantle domains beneath the arc are unknown. Moreover, it is not known whether the continuum of diverse primitive magmas erupted in the Cascades is produced by mixing of source domains or by mixing of the three magma end-members (Bacon et al. 1997). Many studies in the Cascades (Leeman et al. 1990; Bacon 1990; Baker et al. 1994; Bacon et al. 1997; Conrey et al. 1997) would seem to indicate that large volcanic centers (e.g. Adams, Medicine Lake, Lassen, Shasta, and others) are underlain by more than one type of mantle domain, or are fed by more than one type of end-member magma. In contrast, the model proposed by Reiners et al. (2000) assumes

that a more homogeneous mantle underlies certain volcanic centers (*e.g.* the Dalles Lake and Three Sisters basalts north of Mt. Rainier), and that it is the processes (melt fraction and added subduction component) rather than the mantle source that leads to compositional distinctions between proximally located arc lavas.

Compositions of arc magmas are inextricably linked to varying degrees of melting of mantle peridotite in response to fluxing by fluids derived from the subducting slab. Assessing the role of subduction fluxes and the degree of partial melting are the goals of many authors in the Cascades (Baker et al. 1994; Bacon et al. 1997; Borg et al. 1997; Reiners et al. 2000), Central America (Reagan and Gill 1989; Patino et al. 2000), and the Western Pacific (Stolper and Newman 1994; Smith et al. 1997). Determining the amount of sediment added to arc magmas is also a primary goal of research, but requires an extensive data set of primitive magma compositions in order to interpret slab tracers such as Cs, Rb, Ba, ^{10}Be , Boron, and isotopic data (*e.g.* Plank and Langmuir 1993; Leeman 1996; Borg et al. 1997; Patino et al. 2000).

Comparisons of LILE and HFSE are a useful tool in assessing the role of subduction fluxes in arc settings. The primitive mantle-normalized incompatible element diagram (Fig. 16) shows that the Whitechuck HAOT and the three calc-alkaline flows have similarly shaped patterns of incompatible element enrichment with varying degrees of Nb and Ta depletion. Influence from a hydrous subduction component is illustrated by the strong negative Nb and Ta anomalies and the large $(\text{Sr}/\text{P})_{\text{N}}$ ratio, or “Sr spike” (explained by Borg et al. 1997). These anomalies arise because the LILE are fluid-mobile and are transported by a hydrous phase from the slab, while the HFSE are not fluid-mobile and are left behind (Hawthorn et al. 1991; Tatsumi and Eggins 1993; Stolper

and Newman 1994; Bacon et al. 1997; Borg et al. 1997; Reiners et al. 2000; and others). Thus, the relative enrichment of Nb and Ta in Figure 16 corresponds with the relative fertility of the source; or with the degree of partial melting.

The Whitechuck lavas are more depleted in Nb and Ta than the N-MORB values of Sun and McDonough (1989), which suggests that they are likely to have been derived from a more primitive (MORB-like) mantle source, and/or by higher degrees of melting. This relationship is in contrast to what Baker et al. (1994) and Bacon et al. (1997) have reported for HAOT. These lavas do share similar LILE/HFSE characteristics with HAOT from the Medicine Lake volcanic field and other centers of primitive centers of mafic magmatism in the central and southern Cascades. There is no consensus between authors as whether to recognize Medicine Lake, which is east of the volcanic front, as a true Cascades volcano. However it is useful as a comparison to other HAOT because of its low LILE/HFSE and low water content (Sisson and Layne; 1993; Bacon et al. 1997). HAOT from the southern Cascades (Bacon et al. 1997; Borg et al. 1997) have inconsistent enrichment of LILE relative to HFSE. This reportedly results from melting of heterogeneously distributed parcels of mantle peridotite that record previous episodes of metasomatism from a subduction component, rather than enrichment from a modern subduction component.

The Indian Pass basaltic andesites lie on the opposite end of the spectrum from Whitechuck, and have the greatest enrichment in Nb and Ta and the lowest relative enrichment of LILE. Dishpan Gap and Lightning Creek lavas are intermediate between the two previously mentioned flows. All three calc-alkaline flows share LILE/HFSE

characteristics with basaltic andesites from the Shasta, Lassen, and Crater Lake regions reported by Baker et al. (1994) and Bacon et al. (1997).

Similar LILE/HFSE relationships can also be seen in Figure 25, where the Lightning Creek, Indian Pass, and Dishpan Gap samples are normalized to the average Whitechuck composition. Using the Whitechuck lavas for normalization values allows relative differences in LILE and HFSE abundances to stand out more prominently. Indian Pass lavas have twice the LILE enrichment of Whitechuck, and nearly four times the enrichment of Nb and Ta. The opposite relationship is true for the Dishpan Gap and Lightning Creek lavas. Based on this diagram and on Figure 16, the Dishpan Gap and Lightning Creek lavas record the largest contribution from a subduction component, while Indian Pass lavas were produced by the lowest degree of melting or melting of the most enriched source.

Concentrations and ratios of LILE (Cs, Rb, Ba, Th, Sr, K, U, LREE) and HFSE (Nb, Ta, Ti, Zr) were modeled by Reiners et al. (2000) for young primitive magmas north of Mt. Rainier. An isenthalpic melting model was used to show that a composite peridotite composition (spinel lherzolite with ~2.5% garnet; modified from the OIB and MORB sources of Borg et al. 1997) could melt to produce calc-alkaline, OIB-like, or under special circumstances, MORB-like lavas when fluxed by a hydrous subduction component. Isenthalpic melting refers to the decreased efficiency of melting (lower ΔF) due to the cooling effects of an increased subduction component. A fundamental point of this model is that only one peridotite source domain is required to produce the three end-member magmas under varying degrees of melting and varying contributions from a subduction component (from Borg et al. 1997 and Stolper and Newman 1994).

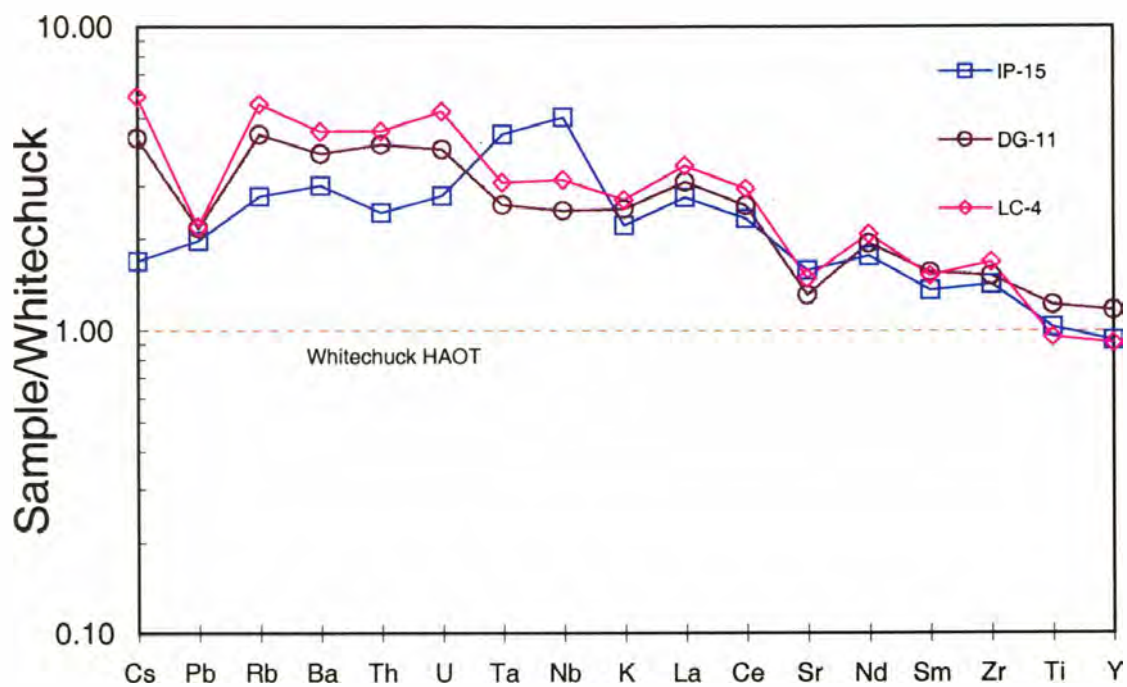


Fig. 25. Incompatible elements from Indian Pass, Dishpan Gap, and Lightning Creek normalized to the average Whitechuck composition to better show subtle differences between similar patterns in Figure 16. The same samples from Figure 16 are used. The relative enrichment of LILE vs. HFSE is prominent. Indian Pass is opposite of the other two calc-alkaline flows in that it is twice as enriched in Nb and Ta and half as enriched in Rb, Ba, and Th.

The model uses the elements Ba, Th, Nb, and Zr, which are plotted in Figure 17. The origin of OIB, MORB-like, and calc-alkaline lavas is shown to be a function of mantle temperature, degree of melting, and addition of a subduction component. OIB melts may result from low degree melts of hot or cold mantle. Even if slight amounts of subduction flux are present in the OIB source, it does not provide enough LILE to keep pace with Nb and Ta partitioning into the melt. MORB-like magmas (HAOT) can be produced by 1) low-degree melts [melt fraction (F) =5-15%] of cold (~1225° C), depleted mantle or 2) high degree ($F > 15\%$) melts of hot (~1375° C) mantle. In both scenarios, LILE/HFSE ratios are kept low because Nb and Ta supplied by lower degree melts keep pace with LILE supplied by the subduction component. Finally, calc-alkaline lavas can be produced by high degrees of melting ($F > 15\%$) of cooler, variably depleted peridotite with a significant added subduction component.

The model of Reiners et al. (1997) assumes that the melts contain significant H₂O released from the slab. Mafic lavas in the Cascades and other arcs have recorded pre-eruptive H₂O contents ranging from nearly 0% for some HAOT to >8% for basalts and basaltic andesites with lower (<5 wt.%) MgO (Sisson and Grove 1993; Sisson and Layne 1993; Baker et al. 1994; Borg et al. 1997).

The four flows, along with the Dalles Lake and Three Sisters basalt (Reiners et al. 2000), are plotted in Figure 17 to show whether the model of Reiners et al. is applicable to the mantle beneath the Glacier Peak region. The HAOT of Medicine Lake and Mt. Adams (data from Bacon et al. 1997) are also shown for comparison. According to the model, and assuming that the peridotite source is similar for the four flows, the Whitechuck lavas would either represent 1) higher amounts of partial melting ($F \geq 15\%$)

of hotter ($\sim 1375^\circ\text{C}$) mantle peridotite enriched by moderate amounts of subduction component, or 2) low to moderate degree melts (5-15%) of strongly incompatible-element depleted mantle with an added subduction component. More enriched mantle melted under the conditions of 2) would produce higher Nb concentrations, higher Nb/Zr ratios, and lower Ba/Nb ratios, similar to OIB-like compositions.

The Indian Pass basaltic andesites have similar Ba/Nb, Ba/Zr, and Nb/Zr ratios to the Three Sisters basalt of Reiners et al. (2000), but lower Ba and Th (Fig. 17). If the Indian Pass lavas were produced from a peridotite source similar to that of the Three Sisters basalts, they would represent fractionated higher degree melts ($F=15-25\%$) of mantle peridotite with a significant subduction component ($\sim 4.0\%$ from Reiners et al. 2000). Following this rationale, the Lightning Creek, and potentially the fractionated Dishpan Gap, lavas would represent higher degree melts ($>\sim 20\%$) of a similar mantle source with a large extent of subduction component metasomatism ($>4\%$). Alternatively, high Ba/Nb ratios can be produced by moderate amounts of melting of a previously depleted mantle source.

Observations from Figures 16 and 25 are reconciled with comparisons of the mafic lavas with the Reiners et al. (2000) model to show that the model is not entirely applicable to the mantle beneath the Glacier Peak region. As stated earlier, the Whitechuck HAOT has the lowest enrichment of Nb and Ta, and therefore represents either the most depleted source or the highest degree of melting. The opposite is true for the Indian Pass basaltic andesite. According to the Reiners et al. (2000) model, the calc-alkaline lavas would have a higher degree of melting if they were derived from the same source as Whitechuck. Thus, the observations from Figures 16 and 25 contradict this

model. There must be at least two mantle sources present below Glacier Peak: a depleted mantle that produced the Whitechuck lavas, and a slightly more enriched mantle that produced the calc-alkaline basaltic andesites. Both sources probably received significant fluxing from a hydrous subduction component. However, primitive basaltic andesites are typically derived by low degree melts with significant H₂O (~6%) present in the source (Sisson and Grove 1993; Baker et al. 1994; Borg et al. 1997). The depleted Nb and Ta in the Whitechuck HAOT may also have resulted from nearly anhydrous melting of mantle previously enriched by a subduction component (Bacon et al. 1997; Borg et al. 1997). The Reiners et al. (2000) model may hold true for the melting relationships between the calc-alkaline lavas, as the Dishpan Gap and Lightning Creek lavas have a higher Ba/Nb and lower Nb (Fig. 17) than the Indian Pass lavas, and could have been produced by higher degree melts. However, effects from the crust obscure subtle trace-element differences in the more evolved calc-alkaline lavas. Finally, no OIB-like signature can be observed in any of the lavas. The addition of these lavas to the data set of primitive and near-primitive lavas from the Cascades shows that, as of yet, no OIB-like mantle exists north of the southern Washington Cascades.

CONCLUSIONS

Four young, petrologically distinct lava flows were erupted between five and ten km south of Glacier Peak during the late Pleistocene and/or early Holocene. The four flows include the Whitechuck fractionated high alumina olivine tholeiite (HAOT), and the calc-alkaline Indian Pass, Lightning Creek, and Dishpan Gap basaltic andesites. Indian Pass and Lightning Creek are primitive on the basis of their high MgO and other compatible element concentrations. As indicated by olivine-liquid equilibria, none of the four flows has experienced significant olivine accumulation. All four lavas have been influenced by the crust to different degrees, but they cannot be related to one another by fractional crystallization; nor can the most mafic and most felsic member of each suite be related by fractional crystallization. However, there is evidence to show that the more evolved members of these mafic magmas were formed as a result of mixing with more felsic compositions similar to evolved Glacier Peak dacites.

The Whitechuck and Indian Pass lavas, and to some extent the Lightning Creek and Dishpan Gap lavas, each record characteristics of the mantle beneath the Glacier Peak region and provide insight into the processes and components of magma genesis beneath the Glacier Peak region. All four lavas exhibit the characteristic Nb and Ta depletion exhibited by arc magmas that have been enriched by a slab-derived fluid contribution to the mantle wedge. The Whitechuck lavas show olivine-liquid temperatures at $\sim 1200^{\circ}\text{C}$, have the lowest Nb and Ta enrichment, and were likely derived by higher degrees of nearly anhydrous melting of depleted (MORB-like) peridotite in the upper mantle wedge, similar to HAOT occurring elsewhere in the Cascades as described by Bacon et al. (1997) and Conrey et al. (1997). In contrast, the three calc-alkaline lavas were derived from

lower degree melts of more enriched mantle peridotite. Olivine in the calc-alkaline flows equilibrated with melt at temperatures ranging from 1147° C for Dishpan Gap, to 1240° C for Indian Pass, reflecting a trend of decreasing subduction component. The geochemical characteristics of each flow show that the mantle beneath the Glacier Peak region is represented by two source domains: a depleted (MORB-like) mantle receiving very little subduction component, and a slightly less-depleted mantle that is being fluxed by significantly more subduction component. No OIB-like mantle domain is represented by the lavas analyzed.

REFERENCES

- ANDERSEN, D.J., LINDSLEY, D.H., & DAVIDSON, P.M. (1993): QUILF: a PASCAL program to assess equilibria among Fe-Mg-Mn-Ti oxides, pyroxenes, olivine, and quartz. *Computers & Geosciences*, **19**, 1333-1350, 1993.
- ARMSTRONG, J.T. (1988): Quantitative analysis of silicate and oxide minerals: comparison of Monte Carlo, ZAF and phi - rho - z procedures. In: Newbury, D.E. (ed) *Microprobe analysis*, San Francisco Press, 239-246.
- BACON, C.R. (1990): Calc-alkaline, shoshonitic, and primitive tholeiitic lavas from monogenetic volcanoes near Crater Lake, Oregon. *J. Petrol.* **31**(1), 135-166.
- _____, BRUGGMAN, P.E., CHRISTIANSEN, R.L., CLYNNE, M.A., DONNELLY-NOLAN, J.M., & HILDRETH, W. (1997): Primitive Magmas at five Cascade volcanic fields: Melts from hot, heterogeneous sub-arc mantle. *Can. Mineral.* **35**, 397-423.
- BAEDECKER, P.A., & MCKOWN D.M. (1987): Instrumental neutron activation analysis of geochemical samples. In: P.A. Baedecker (ed.), *Methods for geochemical analysis. U.S. Geol. Surv. Prof. Paper*, **1770**, H1-H14, 1987.
- BAKER, M.B., GROVE, T.L., & PRICE, R. (1994): Primitive basalts and andesites from the Mt. Shasta region, N. California: Products of varying melt fraction and water content. *Contrib. Mineral. Petrol.* **118**, 111-129.
- BASALTIC VOLCANISM STUDY PROJECT (1981): *Basaltic Volcanism on the terrestrial planets*. Pergamon, New York, N.Y.
- BENCE, A.E., & ALBEE, A.L. (1968): Empirical correction factors for the electron microanalysis of silicates and oxides. *J. Geol.*, **V76**, 382-403.
- BEGET, J.E. (1981): Early Holocene glacial advance in the North Cascade Range, Washington. *Geology*, **9**, 409-413.
- _____(1982): Recent activity at Glacier Peak. *Science*, **215**, 1389-1390.
- _____(1983): Glacier Peak, Washington: A potentially hazardous Cascade volcano. *Environ. Geol.* **5**, 83-92.
- BORG, L.E., CLYNNE, M.A., & BULLEN, T.D., (1997): The variable role of slab derived fluids in the generation of a suite of primitive calc-alkaline lavas from the southernmost Cascades, California. *Can. Mineral.* **35**, 425-452
- CLYNNE, M.A. (1993): Geologic Studies of the Lassen Volcanic Center, Cascade Range, California: Ph.D. thesis, Univ. of California at Santa Cruz, Santa Cruz, California.

- _____, & BORG, L.E. (1997): Olivine and Chromium Spinel in Primitive Calc-alkaline and Tholeiitic Lavas from the Southernmost Cascade Range, California: A reflection of relative fertility of the source. *Can. Mineral.* **35**, 453-471.
- CONREY, R.M., SHERROD, D.R., HOOPER, P.R., & SWANSON, D.A., (1997): Diverse primitive magmas in the Cascade arc, Northern Oregon and Southern Washington. *Can. Mineral.* **35**, 367-396.
- CROWDER, D.F., TABOR, R.W., & FORD, A.B. (1966): Geologic Map of the Glacier Peak Quadrangle, Snohomish and Chelan Counties, Washington. *U.S. Geol. Surv. Geologic Quadrangle Map GQ-473*, Scale 1:62,500.
- DELLA-PASQUA, FN, & VARNE, R. (1997): Primitive ankaramitic magmas in volcanic arcs: A melt-inclusion approach. *Can. Mineral.* **35**, 291-312
- FORD, A.B. (1959): Geology and Petrology of the Glacier Peak quadrangle, northern Cascades, Washington. Seattle, Washington Univ., Ph. D. thesis, 374 p.
- GILL, J.B. (1981): *Orogenic andesites and Plate Tectonics*. Springer-Verlag, New York. 390 p.
- GREEN, N. & HARRY, D.L. (1999): On the Relationship between subducted slab age and arc basalt petrogenesis, Cascadia subduction system, North America. *Earth Planet. Sci. Lett.* **171**, 367-381.
- HAWKSWORTH, C.J., HERGT, J.M., ELLAM, R.M., & MCDERMOTT, F. (1991): Element fluxes associated with subduction related magmatism. *Philosoph. Trans. R. Soc. Lond.* **A335**, 393-405.
- IRVINE, T.N., & BARAGAR, W.R.A. (1971): A guide to the chemical classification of the common rocks. *Can. J. Earth Sci.* **8**, 523-548.
- JOHNSON, D. M., HOOPER, P.R., & CONREY, R. M. (1999): XRF Analysis of Rocks and Minerals for Major and Trace Elements on a Single Low Dilution Li-tetraborate Fused Bead. *Advances in X-ray Analysis.* **41**, 843-867.
- KRESS, V.C., & CARMICHAEL, I.S.E. (1991): The compressibility of silicate liquids containing Fe₂O₃ and the effect of composition, temperature, oxygen fugacity and pressure on their redox states. *Contrib. Mineral. Petrol.* **108**, 82-92.
- LUEDKE, R.G., & SMITH, R. L. (1982): Map (1:1,000,000) showing the distribution, composition, and age of late Cenozoic volcanic centers of Oregon and Washington: *U.S. Geol. Surv. Map I-1091-D*.
- LEEMAN, W.P., SMITH, D.R., HILDRETH, W., PALACZ, Z., & ROGERS, N. (1990): Compositional Diversity of Late Cenozoic Basalts in a Transect Across the Southern Washington

- Cascades: Implications for Subduction Zone Magmatism. *J. Geophys. Res.* **95**, B12, 19,561-19,582.
- _____ (1996): Boron and other fluid-mobile elements in volcanic arc lavas: Implications for subduction processes. In: Bebout, G.E., Scholl, D., Kirby, S., and Platt, J.P. (eds.), *Subduction Top to Bottom*. AGU Monograph **96**, 269-276.
- LESCINSKY, D.T., & SISSON T.W. (1998): Ridge-forming, ice-bounded lava flows at Mount Rainier, Washington. *Geology*, **26**, 351.
- MCBIRNEY, A.R. (1968): Petrochemistry of the Cascade andesite volcanoes. *Oregon Dept. of Geol. Min. Indust. Bull.* **62**, 101-107.
- MICHAELSON, C.A., & WEAVER, C.S. (1986): Upper mantle structure from teleseismic P wave arrivals in Washington and northern Oregon. *J. Geophys. Res.* **91**, 2, 2077-2094.
- MISENER, D.J. (1974): Cationic diffusion in olivine to 1400° C and 35 kbar. In: A.W. Hofmann et al. (eds), *Geochemical transport and kinetics*, Carnegie Inst. Washington Publ. **634**, 117-129.
- MOONEY, W. D. & WEAVER, C. S. (1989): Regional crustal structure and tectonics of the Pacific coastal states; California, Oregon, and Washington: Pakiser, Louis C.; Mooney, Walter D., eds., *Geophysical framework of the continental United States*, *Geol. Soc. Am. Mem.* **172**, p. 129-161.
- MIYASHIRO, A. (1974): Volcanic Rock series in island arcs and active continental margins. *Am. J. Sci.* **274**, 321-355.
- NIXON, G., & JOHNSTON, A.D. (1997): Nature and Origin of Primitive Magmas at Subduction Zones. Preface: *Can. Mineral.* **35**, 253-256.
- PATINO, L.C., CARR, M.J., & FEIGENSON, M.D. (2000): Local and regional variations in Central American arc lavas controlled by variations in subducted sediment input. *Contrib. Mineral. Petrol.* **138**: 265-283.
- PLANK, T., & LANGMUIR, C.H. (1993): Tracing trace elements from sediment input to volcanic output at subduction zones. *Nature*, **362**, 739-742.
- REAGAN, M.K., & GILL, J.B. (1989): Coexisting Calc-alkaline and High-Niobium Basalts from Turrialba Volcano, Costa Rica: Implications for residual titanites in arc magma sources. *J. Geophys. Res.* **94**, B4, 4619-4633.
- REINERS, P.W., HAMMOND, P.E., MCKENNA, J.M., & DUNCAN, R.A. (2000): Young basalts of the central Washington Cascades, flux melting of the mantle, and trace element signatures of primary arc magmas. *Contrib. Mineral. Petrol.* **138**: 249-264.

- RIDDIHOUGH, R.P. (1984): Recent movements of the Juan de Fuca Plate system. *J. Geophys. Res.* **89**, 6980-6994.
- ROEDER, P.L., & EMSLIE, R.F. (1970): Olivine-Liquid Equilibrium. *Contrib. Mineral. Petrol.* **29**, 275-289.
- ROLLINSON, H.R. (1993): *Using geochemical data: evaluation, presentation, interpretation*. J. Wiley & Sons, New York.
- SISSON, T.W. & GROVE, T.L. (1993): Temperature and H₂O contents of low-MgO, high-Al₂O₃ basalts. *Contrib. Mineral. Petrol.* **113**, 167-184.
- _____, & LAYNE, G.D. (1993): H₂O in basalt and basaltic andesite glass inclusions from four subduction-related volcanoes. *Earth Planet. Sci. Lett.* **117**, 619-635.
- SMITH, I.E.M., WORTHINGTON, T.J., PRICE, R.C., & GAMBLE, J.A. (1997): Primitive Magmas in Arc-type Volcanic Associations: Examples from the Southwest Pacific. *Can. Mineral.* **35**, 257-273.
- SPENCER, K.J., & LINDSLEY, D.H. (1981): A solution model for coexisting iron-titanium oxides: *Am. Mineral.* **66**, 1189-1201.
- STOLPER, E., & NEWMAN, S. (1994): The role of water in the petrogenesis of Mariana trough magmas: *Earth Planet. Sci. Lett.* **121**, 293-325.
- SUN, SHEN-SU, & MCDONOUGH, W.F. (1989): Chemical and isotopic systematics of oceanic basalts: implications for mantle composition and processes. In: (A.D., Saunders, and M.J. Norry, eds.), *Magmatism in the Ocean Basins*, Geological Society Special Publications. **42**, 313-346.
- TABOR, R.W., & CROWDER, D. F. (1969): On Batholiths and Volcanoes- Intrusion and Eruption of Late Cenozoic Magmas in the Glacier Peak Area, North Cascades, Washington. *U. S. Geol. Surv. Prof. Paper* 604.
- _____, FRIZZELL, V.A., BOOTH, J.R., WAITT, D.B., WHETTEN, R.B., & ZARTMAN, R.E. (1993): Geologic Map of the Skykomish River 30- By 60-Minute Quadrangle, Washington. *U.S. Geol. Surv. Misc. Investigations*, Map I-1963, Scale 1:100,000.
- TATSUMI, Y., HAMILTON, D.L., & NESBITT, R.W. (1986): Chemical characteristics of fluid phases released from a subducted lithosphere and origin of arc magmas: evidence from a high-pressure experiments and natural rocks: *J. Volc. Geophys. Res.* **29**, 293-309.
- TATSUMI, Y. & EGGINS, S. (1995): *Subduction Zone Magmatism*. Blackwell Science, Cambridge. 211 p.

Appendix 1: Sample locations from the Glacier Peak region

Glacier Peak dacite

General location information	Sample #	Location (Lat/Long nearest 1/10 second):
GLACIER PEAK SAMPLES, JULY 1999, FROSTBITE RIDGE AND SITKUM GLACIER, SNOHOMISH AND CHELAN COUNTIES, WASHINGTON.	99-DDT-GP-1	48°07'04"/121°06'38"
	GP-2	04"/39"
	GP-3	06'41"/06'46"
	GP-4	43"/51"
	GP-5	43"/55"
	GP-6	40"/07'03" (FLOAT)
	GP-7	45"/07'28"
	GP-8	34"/45"
	GP-9	34"/45"
	GP-10	32"/51"
	GP-11	34"/56"
	GP-12	34"/56"
	GP-13	38"/08'01"
	GP-14	43"/08'55"

Whitechuck basalt

General location information	Sample #:	Location (Lat/Long nearest 1/10 second):
WHITECHUCK CINDER CONE AND FLOW SAMPLES, JULY, 1999, SNOHOMISH COUNTY, WASHINGTON	99-DDT-WC-1	48°03'25"/121°09'31"
	WC-2	3'25"/9'31"
	WC-3	3'26"/9'42"
	WC-4	3'28"/9'39"
	WC-5	3'28"/9'39"
	WC-6	3'28"/9'39"
	WC-7	3'30"/9'39"
	WC-8	3'33"/9'40"
	WC-9	3'29"/9'33"
	WC-10	3'28"/9'28"
	WC-11	3'28"/9'31"
	WC-12	3'28"/9'31"
	WC-13	3'13"/9'39"
	WC-14	3'04"/9'53"
	WC-15	3'26"/9'52"
	WC-16	3'27"/9'49"
	WC-17	3'33"/9'42"

Lightning Creek basaltic andesite

General location information	Sample #:	Location (Lat/Long nearest 1/10 second):
LIGHTNING CREEK FLOW SAMPLES, JULY 1999, CHELAN COUNTY, WASHINGTON	99-DDT-LC-1	48°01'58"/121°03'14"
	LC-2	48°01'58"/121°03'14"
	LC-3	48°01'58"/121°03'14"
	LC-4	48°01'58"/121°03'14"
	LC-5	48°01'58"/121°03'14"
	LC-6	48°02'/121°03'09"
	LC-7	48°02'/121°03'09"
	LC-8	48°02'/121°03'09"
	LC-9	48°02'/121°03'09"
	LC-10	48°01'54"/121°03'15"
	LC-11	48°01'54"/121°03'15"
	LC-12	48°01'54"/121°03'15"
	LC-13	48°01'54"/121°03'15"

Indian Pass basaltic andesite

General location information	Sample #:	Location (Lat/Long nearest 1/10 second):
INDIAN HEAD FLOW OR FEEDER DIKE SAMPLES, SEPTEMBER, 1999, SNOHOMISH AND CHELAN COUNTIES, WASHINGTON	99-DDT-IP-1	48°00'00"/121°07'04"
	IP-2	47°59'58"/06'56"
	IP-3	47°59'58"/06'56"
	IP-4	47°59'58"/06'56"
	IP-5	47°59'58"/06'56"
	IP-6	59'57"/06'51"
	IP-7	59'56"/06'47"
	IP-8	59'54"/6'43"
	IP-9	59'54"/6'43"
	IP-10	59'53"/6'39"
	IP-11	59'53"/06'37"
	IP-12	59'53"/06'37"
	IP-13	59'53"/06'37"
	IP-14	59'53"/06'37"
	IP-15	59'53"/06'37"

Appendix 1. (cont.) Sample locations from the Glacier Peak region

Dishpan Gap basaltic andesite

General location information	Sample #:	Location (Lat/Long nearest 1/10 second):
<i>DISHPAN GAP FLOW SAMPLES, SEPTEMBER, 1999, SKYKOMISH COUNTY, WASHINGTON</i>	99-DDT-DG-1	47°58'/121°11'42"
	DG-2	47°58'/121°11'42"
	DG-3	47°58'/121°11'42"
	DG-4	47°58'/121°11'42"
	DG-5	47°58'/121°11'42"
	DG-6	47°57'58"/121°11'34"
	DG-7	47°57'56"/121°11'26"
	DG-8	47°57'55"/121°11'21"
	DG-9	47°57'56"/121°11'14"
	DG-10	47°57'56"/121°11'08"
	DG-11	47°57'56"/121°11'08"
	DG-12	47°57'58"/121°11'42"
	DG-13	47°57'58"/121°11'42"
	DG-14	47°57'58"/121°11'42"
	DG-15	47°57'58"/121°11'42"